UNIVERSITÀ DEGLI STUDI DI TRIESTE

XXXI CICLO DEL DOTTORATO DI RICERCA IN

BIOMEDICINA MOLECOLARE

UNDERSTANDING THE MOLECULAR MECHANISMS UNDERLYING THE PATHOGENESIS OF OPITZ G/BBB SYNDROME EXPLOITING THE *Mid1* KNOCK-OUT MOUSE MODEL

Settore scientifico-disciplinare: BIO/18

Dottoranda
Rossella Baldini

Coordinatore
Prof. Germana Meroni

Supervisore di tesi
Prof. Germana Meroni

ANNO ACCADEMICO 2017/2018

UNIVERSITÀ DEGLI STUDI DI TRIESTE

XXXI CICLO DEL DOTTORATO DI RICERCA IN

BIOMEDICINA MOLECOLARE

UNDERSTANDING THE MOLECULAR MECHANISMS UNDERLYING THE PATHOGENESIS OF OPITZ G/BBB SYNDROME EXPLOITING THE *Mid1* KNOCK-OUT MOUSE MODEL

Settore scientifico-disciplinare: BIO/18

Dottoranda
Rossella Baldini

Coordinatore
Prof. Germana Meroni

Supervisore di tesi
Prof. Germana Meroni

ANNO ACCADEMICO 2017/2018

TABLE OF CONTENTS

ABSTRACT

Opitz G/BBB syndrome (OS) is a multiple congenital anomaly disorder characterised by developmental defects of midline structures. Mutations in the *MID1* gene are responsible of the X-linked form of the syndrome and lead to loss-of-function of the protein. MID1 is an E3 ubiquitin ligase of the tripartite motif (TRIM) subfamily of RING proteins and associates with microtubules. The mouse line carrying a nonfunctional ortholog of the human *MID1* gene, *Mid1*, (*Mid1*$^{-/Y}$) recapitulates the brain morphological abnormalities observed in patients, i.e. hypoplasia of the anterior cerebellar vermis, although the role of *Mid1* in cerebellar development is still unclear. Previous analysis demonstrated that the alteration of the cerebellum in *Mid1*$^{-/Y}$ mice originates prenatally, delineating the embryonic day (E) 13.5 as the time of the first sign of the cerebellar defect. We started to explore the molecular pathways affected by the lack of *Mid1* at E13, thus placing immediately before the appearance of the defect. Differential proteomic analysis indicated some proteins presenting quantitative unbalance in *Mid1*$^{-/Y}$ embryonic brains. In particular, two RNA exosome components, Exosc8 and Exosc10, displayed increased protein levels in *Mid1*$^{-/Y}$ cerebella and the MID1-associated regulation of these two proteins has been further confirmed in HEK293T cells. The exosome components modulation is presumably driven through an indirect interaction, as neither Exosc10 nor Exosc8 directly binds Mid1. Interestingly, the subcellular distribution of Exosc8 was found affected by MID1 overexpression in hTERT-RPE cells and by *Mid1* depletion in primary mouse fibroblasts, disclosing an involvement of the E3 ligase in regulating exosome core nuclear localisation.

In addition, the network analysis has suggested that *Mid1*$^{-/Y}$ cerebella might present impairment in vesicular trafficking. In particular, *Mid1* depletion causes a decrease in SNARE (soluble N-ethylmaleimide-sensitive factor attachment protein receptors) proteins (i.e. Snap25 and Vamp2) and SNARE complex assembly, implying that SNARE-mediated release of different type of vesicles (e.g. synaptic vesicles, exosomes, or other cellular trafficking components) might be altered in *Mid1*$^{-/Y}$ embryos.

SNARE complexes are found decreased specifically in the cerebellar territory of E13 *Mid1*$^{-/Y}$ embryonic brains and the reduction is maintained through adulthood.

Thus, the increased level of RNA exosome components, concomitantly with altered subcellular core distribution, along with the reduction of SNARE complex assembly, responsible for defective intra- and extra-cellular vesicles release, in the *Mid1*$^{-/Y}$

developing cerebellum might affect RNA stability in developing neurons and also the proper cells distribution, neuronal maturation and signal transmission, affecting the intercellular communication during embryogenesis.

Further investigations are required to provide new evidence confirming our data and the results may be helpful to unravel the OS pathogenesis not only in the cerebellar compartments but also in the other midline-affected structures.

1. INTRODUCTION

1.1 X-linked form of Opitz G/BBB syndrome

Opitz G/BBB Syndrome (OS) is a multiple congenital anomaly disorder characterised by developmental defects of midline structures. OS was first reported as two separate entities, BBB syndrome (Opitz et al., 1969a) and G syndrome (Opitz et al., 1969b). Subsequently, it has become apparent that the two syndromes identified in 1969 are in fact a single entity, now named Opitz G/BBB syndrome. The most characteristic manifestations of OS are facial abnormalities, which include ocular hypertelorism, broad nasal bridge and cleft lip and/or palate. Laryngo-tracheo-esophageal (LTE) anomalies, congenital heart defects, as well as genitourinary abnormalities are also present (Opitz, 1987). Wide clinical variability occurs even within the same family and the syndrome is usually diagnosed on the basis of clinical findings (Fig. 1.1).

OS is genetically heterogeneous, presenting an autosomal dominant form (ADOS) and an X-linked form (XLOS) that cannot be distinguished based on the clinical phenotype (Robin et al., 1995) and in both cases male patients exhibit a more complex and more severe phenotype than female patients (Robin et al., 1996). The autosomal dominant form is linked to a large region in chromosome 22 (22q11.2) and mutations in the *SPECC1L* gene on 22q11.2 have been recently reported to be likely associated with ADOS (Kruszka et al., 2015). Moreover, the gene implicated in the XLOS is *MID1*, which has been identified on the X chromosome (Quaderi et al., 1997). OS patients carrying mutations in the *MID1* gene always present a typical facial appearance, possibly as the result of incorrect morphogenetic processes during the formation, definition and closure of embryonic ventral midline, usually determining hypertelorism, prominent forehead, broad nasal bridge, frontal bossing, anteverted nares, abnormal position of the ears and defects in the oral cavity (cleft lip/palate, bifid uvula, tooth abnormalities). Likewise, LTE anomalies may present different severity, clinically resulting in swallowing and respiratory dysfunctions. In addition, cardiac malformations, mainly represented by ventricular and/or atrial septal defects, anal abnormalities (imperforate or anteriorly positioned anus), hypospadias and other urogenital defects, as well as anatomical and functional abnormalities in bladder and kidney are often reported (Fontanella et al., 2008). In XLOS, male patients manifest the clinical signs with variable expressivity, whereas female carriers only show hypertelorism (Robin et al., 1995). Moreover, a high percentage of XLOS patients

presents cognitive disabilities and developmental delay associated with anatomical brain abnormalities. Approximately one-third of the patients subjected to magnetic resonance imaging (MRI) show defects in midline structure, which mainly consist of hypoplasia of the anterior cerebellar vermis, along with agenesis or hypoplasia of the corpus callosum. Other mild or severe neurological signs in OS patients carrying *MID1* mutations may be present, such as Dandy-Walker malformation and impaired cognition and psychomotor development (Fontanella et al., 2008).

Fig. 1.1: Pictures of OS patient. The frontal (left panel) and lateral (right panel) views show the typical OS facial anomalies (adapted from De Falco et al., 2003).

1.2 *MID1* mutations in X-linked Opitz syndrome patients

Since its discovery as the causative gene for X-linked Opitz syndrome, several mutations have been identified along the *MID1* gene in OS patients (Fig. 1.2). Analysis of isolated and familial cases of OS revealed more than 80 different pathogenetic mutations in the gene, that are scattered along the entire length of the *MID1* gene and include missense and nonsense mutations, insertions and deletions, either inframe or causing frameshifts, splice site changes and small intragenic as well as entire MID1 coding region deletion (De Falco et al., 2003; Fontanella et al., 2008). The majority of the mutations is described in the 3' region, although all the protein domains are affected, with the exception of the RING domain (Fontanella et al., 2008). The presence of several types and the distribution of mutations, along with the poor association with the expressivity of the clinical signs indicate the loss-of-function as the mechanism underlying the pathogenesis of OS (Cox et al., 2000). Importantly, both the type of mutation and the domain of the protein involved are not sufficient to predict the presence and/or the severity of specific clinical features, thus underlining the importance of the genetic background and the environment and indicating the difficulty in assessing possible genotype/phenotype correlations (Migliore et al., 2013).

Few recurrent mutations lead to substitution of a coding triplet with a stop codon, therefore causing premature truncation of the MID1 protein (Fontanella et al., 2008). Some of them produce a very short N-terminal portions of truncated protein bringing to a truncated tripartite motif, others are more distal and may cause the loss of MID1 crucial domains, as those responsible for microtubule binding (Short and Cox, 2006). Moreover, most of the missense mutations affect the overall protein structure and activity due to a dramatic amino acid charge change (Massiah et al., 2006). In addition, many of the insertions are actually duplications and the majority of them fall within exon 8, suggesting the presence of repeated sequences in the surrounding genomic region that may favor genomic rearrangements (Fontanella et al., 2008). Insertion/deletions that are relatively small often result in in-frame mutations, whereas the other larger rearrangements mainly lead to premature truncation of the protein. The large rearrangements that involve entire exons very likely affect the general transcription and translation of MID1 gene (Winter et al., 2003). Furthermore, nucleotide changes that occur in splice site consensus acceptor or donor sequences result in *MID1* splicing aberrations (Fontanella et al., 2008).

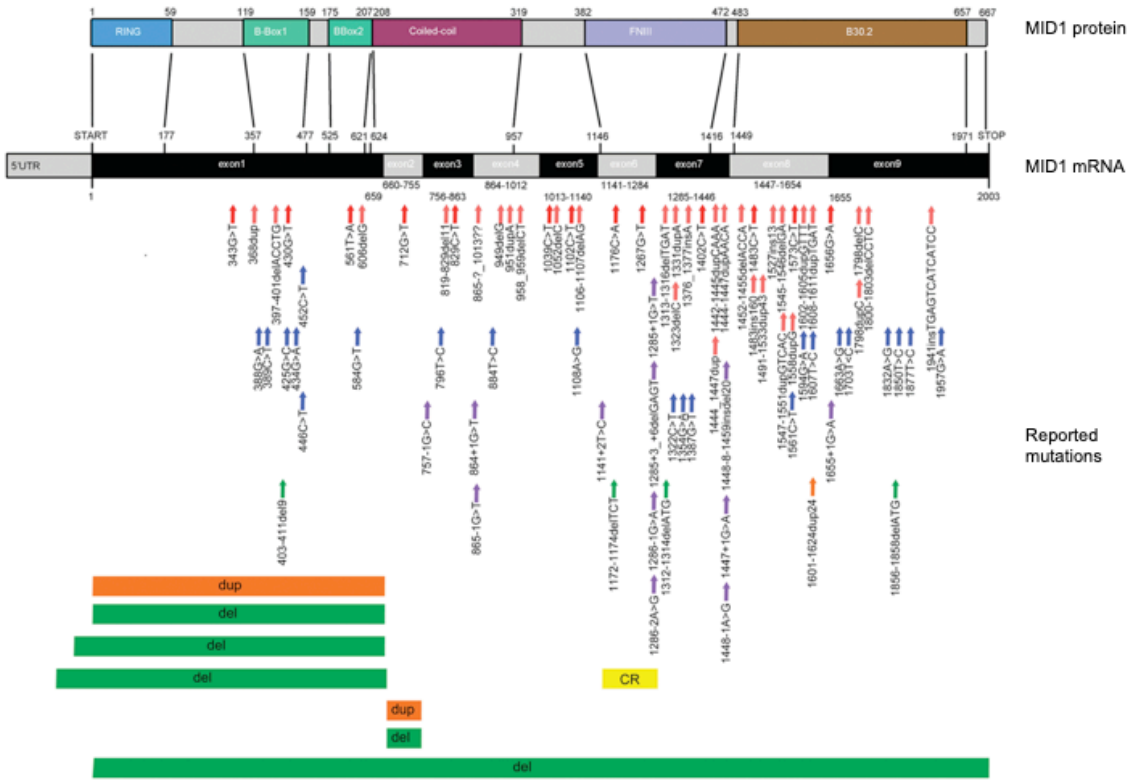

Fig 1.2: The MID1 gene product. Schematic showing the MID1 mRNA and its protein product. Mutations that have been reported in OS patients are indicated, along with their localisation. RING, RING finger domain; FNIII, fibronectin type III repeat; B30.2 indicates PRY-SPRY domain of the RFP-like domain. Colors indicate the different effect of the mutations, as follow: red arrows show mutations that lead to premature stop; blue arrows show point mutations leading amino acid exchanges; orange bars or arrows indicate deletion; green bars or arrows visualize insertions; violet arrows show mutation affecting the splice-site mutations; yellow bar indicates a complex rearrangement that includes four breakpoints (adapted from Winter et al., 2016).

1.3 *MID1* gene and protein structure

The *MID1* gene is located on the short arm of the X chromosome (Xp22.2) and consists of nine coding exons with several alternatively spliced exons, spanning approximately 400 kb of genomic sequence (Quaderi et al., 1997) (Fig. 1.2). The *MID1* gene encodes the 667 amino acid protein MID1 that belongs to the tripartite motif (TRIM/RBCC) family. As the other TRIM proteins, MID1 consists of a RING (Really Interesting New Gene) domain, followed by two B-box zinc-binding domains and an alpha-helical coiled-coil region (RBCC), forming the tripartite motif at the N-terminus of the protein (Quaderi et al., 1997; Cainarca et al., 1999; Reymond et al., 2001) (Fig 1.2). The RING domain is defined by a regular arrangement of cysteine and histidine residues that coordinate two atoms of zinc (Freemont, 1993). Both the RING domain and B-boxes play a role in protein-protein interactions. The coiled-coil region of MID1 is confined within 120 residues from the end of the B-box2 and mediates MID1 homodimerisation, as well as hetero-interaction with other TRIM family members such as MID2 and TRIM16 (Meroni and Diez-Roux, 2005; Short and Cox, 2006; Sardiello et al., 2008; Bell et al., 2012). The C-terminal region of MID1 is represented by an RFP-like domain, also known as B30.2 domain, consisting of a COS domain, a Fibronectin type III (FN3) repeat and a PRY-SPRY domain. Through its C-terminal domain, MID1 can associate with and stabilize microtubules, along which the protein is actively bi-directionally transported (Schweiger et al., 1999; Aranda-Orgillés et al., 2008a). The 67-amino acid COS domain, in particular, is constituted by two alpha-helices and its association with the coiled-coil domain is essential for proper microtubule association. MID1 binding with microtubules throughout the cell cycle is regulated by phosphorylation (Cainarca et al., 1999; Liu et al., 2001; Short and Cox, 2006). Interestingly, this association is not static but allows anterograde and retrograde transport of MID1 along the microtubules, depending also on microtubule integrity and on kinesin and dynein motor proteins. This mechanism is finely regulated by MID1 phosphorylation and dephosphorylation via mitogen activated protein kinase (MAPK) and protein phosphatase 2A (PP2A) (Aranda-Orgillés et al., 2008a). B-box1 domain, in fact, is known to mediate MID1 interaction with the rapamycin-sensitive regulatory subunit of PP2A, the alpha4 protein, thus recruiting the phosphatase to microtubules and mediating the ubiquitin-specific and proteasomal degradation of the microtubule-associated catalytic subunit of PP2A (PP2Ac) (Trockenbacher et al., 2001; Short et al., 2002).

1.4 MID1 protein functions

Functionally, MID1 protein acts as an E3 ubiquitin ligase, responsible for mediating the transfer of the ubiquitin moiety to the specific target (Han et al., 2011; Napolitano et al., 2011). In fact the RING domain is mainly responsible for the interaction with the ubiquitin conjugating enzymes (E2) in the ubiquitination cascade process (Meroni and Diez-Roux, 2005).

Ubiquitination is a post-translational modification that involves three sequential steps catalysed by different enzymes. The first step consists in the binding between ubiquitin and a ubiquitin-activating enzyme (E1). Next, the ubiquitin is transferred to a ubiquitin conjugating enzyme (E2) and, lastly, the transfer of ubiquitin from the E2 enzyme to its target protein is catalysed by a ligase (E3) enzyme, resulting in the formation of an isopeptide linkage between the C-terminus of ubiquitin and the ε-amino group of the target lysine (Fig. 1.3) (Pickart and Eddins, 2004). Protein ubiquitination can either target a substrate for degradation by the proteasome or mediate other functional changes, such as modify protein cellular localisation, modulate its activity, alter its interaction with other proteins (Komander and Rape, 2012).

The E3 ubiquitin ligase activity of MID1 was first described for the catalytic subunit of PP2A. Interestingly, through the binding with alpha4 protein, MID1 catalyzes the ubiquitination and proteasomal degradation of PP2Ac (Trockenbacher et al., 2001). In particular, polyubiquitination of alpha4 protein, which mechanistically requires both the RING and B-box1 domains, leads to protein degradation via the proteasome (Du et al., 2013). In addition, monoubiquitination of alpha4 promotes calpain-mediated cleavage and degradation of its C-terminal domain that contains the MID1 binding region. Furthermore, alpha4 cleavage disrupts the MID1-mediated association of alpha4/PP2A complex to microtubules thus influencing PP2Ac stability and phosphatase activity on microtubule-associated proteins (MAPs) such as Tau (Liu et al., 2001; Short et al., 2002; Watkins et al., 2012).

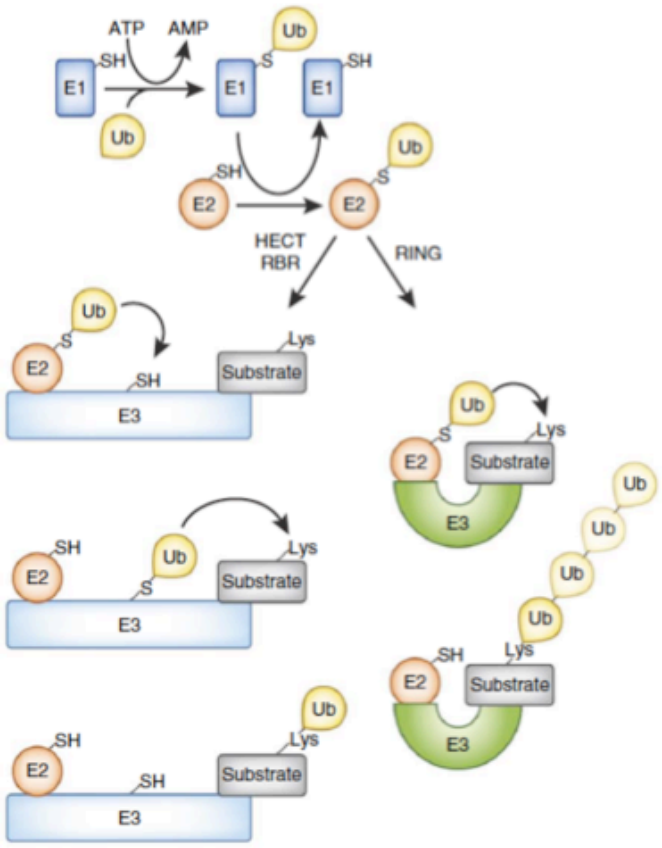

Fig 1.3: The ubiquitination cascade. Ubiquitination is initiated by the formation of a thiolester bond between the C-terminus of ubiquitin and the active-site of the ubiquitin-activating enzyme (E1). Next, the ubiquitin is transferred to the ubiquitin conjugating enzyme (E2) active site cysteine in a transthioesterification reaction. The third step is catalysed by an ubiquitin ligase enzyme (E3), which transfers the ubiquitin from the E2 enzyme to its target protein. This step may vary dependently on the nature of the E3 ligase (adapted from Berndsen and Wolberger, 2014).

Interestingly, PP2A is an important player in mTOR/TORC1 pathway. The TORC1 complex consists of the mTOR kinase, mLST8 and Raptor, which have a scaffolding role in the complex leading to recruitment of the substrates for phosphorylation through the kinase domain of mTOR. Eukaryotic translation initiation factor 4E-binding protein 1 (4E-BP1) and the 40S ribosomal S6 kinase (S6K), that represents two substrates of mTOR, both control translation initiation. By opposing mTOR kinase, PP2A dephosphorylates 4E-BP1 and S6K, and thereby down-regulates translation of several mRNAs (Aranda-Orgillés et al., 2008b). It has been also reported that the MID1/alpha4

complex interacts through the PRY-SPRY domain with S6K and with the elongation factor-1α (EF-1α), another important regulatory factor of protein translation. Therefore MID1, alpha4 and EF-1α are described to be at the core of a large microtubule-bound multiprotein complex that is able to bind RNA, along with other mRNA transport and translational control factors, thus forming a ribonucleoprotein (RNP) complex. Together with PP2Ac, RNP complex controls the activity of mTOR kinase (Aranda-Orgillés et al., 2008b). Furthermore, increased level of PP2A, resulting from depletion of MID1, abolishes the interaction between mTOR and Raptor, thus downregulating mTORC1 signaling (Liu et al., 2011). In this respect MID1 acts as a positive translational regulator of those mRNA that are associated with RNP complex (Fig. 1.4).

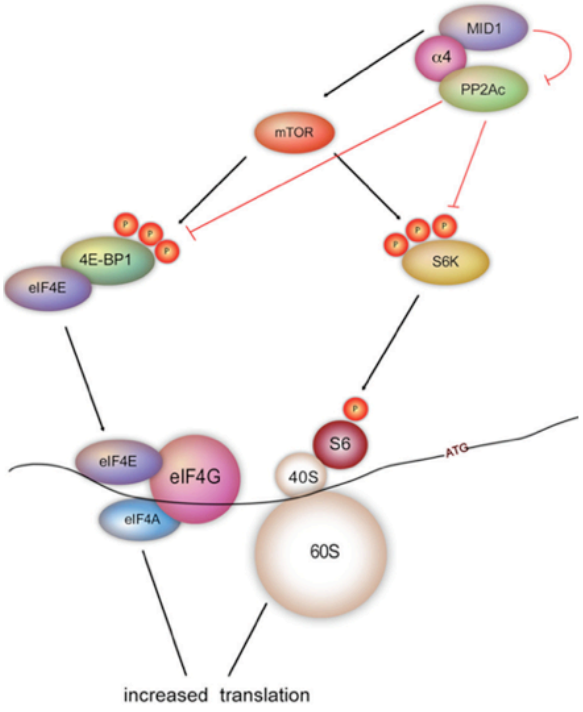

Fig 1.4: MID1 regulates mTOR/PP2A-dependent translation. MID1 is a positive regulator of mTOR and a negative regulator of PP2A, that both control the phosphorylation status and the activity of their downstream targets S6K and 4E-BP1. By regulating the composition of the eukaryotic translation initiation factor (eIF) complex and through the phosphorylation-dependent activation of eIF4B and ribosomal protein S6, 4E-BP1 and S6K mediate the unwinding and the linearizing of the 5'UTR of those mRNA that are associated with RNP complex, finally promoting the translation initiation (from Winter et al., 2016).

Given its broad function, MID1 is implicated in a wide variety of cellular mechanisms, via selective regulating proteins involved in several pathways. Physiological roles of MID1 include emerging participation of the E3 ubiquitin ligase in cytokinesis (Zanchetta and Meroni, 2019) and embryonic development (Dal Zotto et al., 1998; Pinson et al., 2004). As a consequence of its large connection to such biological processes, alterations in MID1 are associated with pathological conditions, like cancer and neurodegeneration (Fig 1.5).

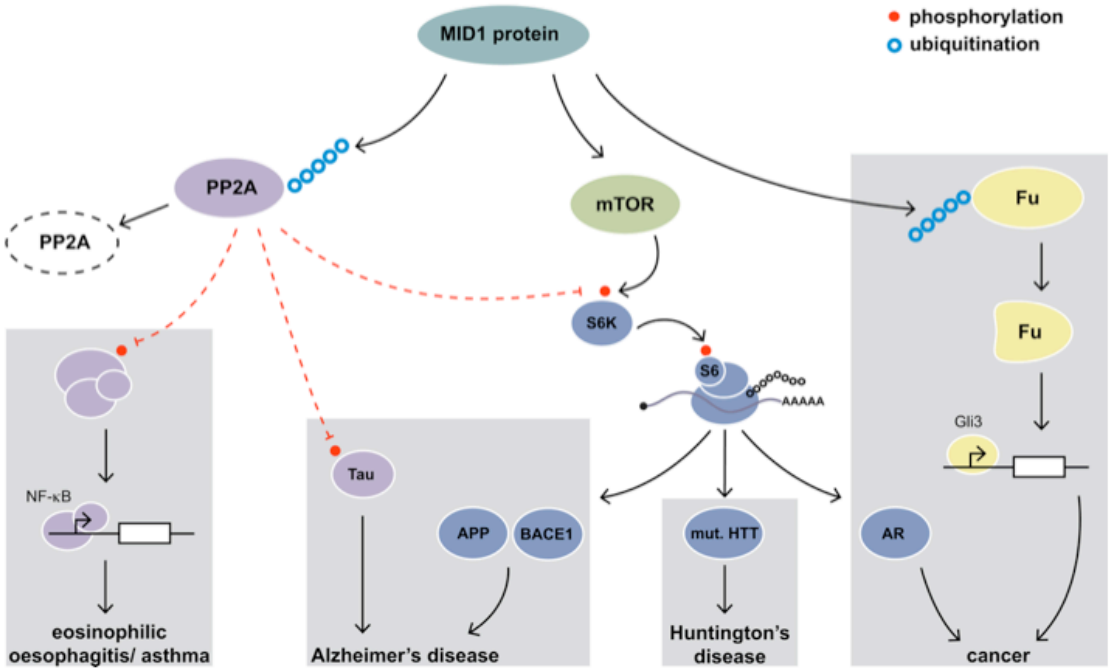

Fig 1.5: Schematic showing the MID1 functions in different pathological conditions. Box on the right shows the role of MID1 in cancerogenesis: on one hand MID1 regulates the activity of an effector of mammalian Sonic Hedgehog (SHH) pathway, GLI3 transcription factor, by ubiquitinating Fu. On the other hand MID1 binds to and induces the translation of the AR mRNA, which is involved in prostate tumor progression. The two boxes in the middle show how MID1 is involved in neurodegenerative diseases: MID1 regulates the pathological hallmarks of Alzheimer's disease by influencing the translation and the activity of the BACE1 secretase and mediating the hyperphosphorylation of Tau protein. MID1 is also involved in Huntington's disease, through the binding and the further stimulation of mutant HTT mRNA translation. The box on the left shows the MID1 role as transcriptional regulator of inflammatory genes via NF-κB signaling, which are essentially involved in inflammatory diseases such as asthma, eosinophilic oesophagitis, or in rhinovirus-induced exacerbations, by limiting PP2A activity through its ubiquitination (adapted from Unterbruner et al., 2018).

1.4.1 Role of MID1 in pathologies

Together with mTOR, the MID1/alpha4/PP2A complex controls the subcellular localisation and the transcriptional activity of the activator form of the GLI3 transcription factor, which is one of the three transcriptional effector molecules of mammalian Sonic Hedgehog (SHH) signaling. SHH pathway not only plays an important role during embryogenesis, but is also widely involved in carcinogenesis. It was demonstrated that inhibition of the MID1 complex and mTOR activity results in cytosolic retention and decreased transcriptional activity of GLI3, while inhibition of PP2A mediates its nuclear localisation (Krauss et al., 2008). However, MID1/alpha4/PP2A complex does not directly affect GLI3, but the modification of the transcription factor is instead mediated by interaction of MID1 with GLI3-interacting protein Fu. Ubiquitination of Fu, mediated by MID1, leads to its proteasome-dependent cleavage, through which the kinase domain of Fu is cleaved off, stimulating the GLI3 nuclear translocation and transcriptional activity (Schweiger et al., 2014). Therefore, MID1-dependent activation of GLI3 might be one of the mechanisms involved in the regulation of SHH signaling in some cancer types.

Moreover, recent works indicate an involvement of MID1 also in prostate cancer. In particular, it was demonstrated that the androgen receptor (AR) mRNA, which is a ligand-activated transcription factor able to trigger several intracellular processes upon androgen binding, is bound by MID1. Binding of the MID1 complex to AR mRNA induces its translation. In turn, AR also regulates MID1 transcription in response to androgen stimulation, suppressing it. AR transcription factor physiologically regulates androgen-dependent gene expression during prostate development, but is found aberrantly activated in prostate cancer. Similarly, subtypes of prostate cancer characterised by a more aggressive phenotype, show high level of MID1 protein, delineating a role as tumour progressing and metastasis promoting factor (Demir et al., 2014).

The ubiquitin system has been linked also to infection and inflammation. MID1 has been identified as a regulator of allergic airway inflammation in the bronchial epithelium in asthma and rhinovirus-induced exacerbations by limiting PP2A activity (Collison et al., 2013). Furthermore, MID1 expression in cytotoxic lymphocytes (CTLs) is reported, where it controls TCR signaling, microtubule-organizing center (MTOC) organisation and exocytosis of lytic granules, responsible for the release of cytolytic mediators (Boding et al., 2014a). By localising to the uropod of migrating CTLs, MID1

has been shown to control lymphocytic polarisation and migration in forming the immunological synapse. Directional cell migration and secretion of perforin- and granzymes-containing lytic granules, both essential for proper defense against infections, are two mechanism mediated by microtubule cytoskeleton. Therefore, through the association with the cytoskeleton, MID1 controls these mechanisms probably by affecting microtubule dynamic (Boding et al., 2014b).

Interestingly, several studies have reported the implication of MID1 in different neurological diseases.

In Huntington's disease, for example, MID1 is involved in stimulating the translation of the mutant Huntingtin (HTT) protein. More in detail, some genes, such as *HTT*, present nucleotide expansions in their sequence, leading to the formation of stable double-stranded RNA structures that are prone to be bound by proteins in RNP complex. Expanded CAG repeats in *HTT*, in fact, are described to trigger translation in a MID1/PP2A/mTOR dependent manner, thus enhancing translation of mutant HTT mRNA (Krauss et al., 2013).

Moreover, the MID1 protein has a role also in the pathogenesis of Alzheimer's disease (AD). The two pathological hallmarks of this type of dementia are extracellular amyloid plaques, which contain A-beta, and intracellular neurofibrillary tangles, which are composed of hyperphosphorylated Tau (Alzheimer et al., 1995). The A-beta peptides are generated by two sequential cleavages of the Amyloid Precursor Protein (APP), the first of them is performed by the beta-site APP-cleaving enzyme BACE1 (Zhang et al., 2011). Different levels of regulation connect MID1 to AD. First, it is extensively demonstrated that phosphorylation status of both Tau and BACE1 is crucially important for determining either the physiological or the pathological role of these proteins. MID1/PP2A complex is able to bind BACE1 and Tau, regulating their phosphorylation and translation. It was proved that disassembly of the MID1-PP2A complex by specific drugs may target both pathological hallmarks of AD (Hettich et al., 2014; Schweiger et al., 2017). Second, the protein synthesis of APP is controlled by MID1 through the modulation of mTOR-eIF signaling (Matthes et al., 2018). Lastly, APP mRNA has been identified as a binding partner of MID1, indicating that the MID1 complex can also induce its translation (Matthes et al., 2018).

1.5 *MID1* embryonic expression and role of MID1 in nervous system development

The role of MID1 during embryonic development has been investigated through expression studies conducted in mouse (Dal Zotto et al., 1998), chicken (Richman et al., 2002) and human (Pinson et al., 2004). In mouse and chicken expression of *MID1* is very similar. Although it is nearly ubiquitously expressed in all embryonic tissues, the highest levels of *MID1* transcript are observed in the undifferentiated progenitor cells of the central nervous system, in the developing branchial arches and in the gastrointestinal and urogenital systems, that correlates with the organs affected in OS patients (Dal Zotto et al., 1998). In human embryos, *MID1* is strongly expressed in the developing central nervous system, from the prosencephalon to the spinal cord, and also in the optic vesicle, in the pharyngeal arches, in the gastrointestinal tract, and in the mesonephros. *MID1* transcript is also detected in the respiratory and digestive tract epithelium and in vertebra. In addition, *MID1* expression in heart interventricular septum correlates with conotruncal lesions commonly seen in OS patients. Importantly, *MID1* is also expressed in the cerebellum anlage, reflecting the cerebellar hypoplasia or agenesis observed in OS (Pinson et al., 2004) (Fig. 1.6).

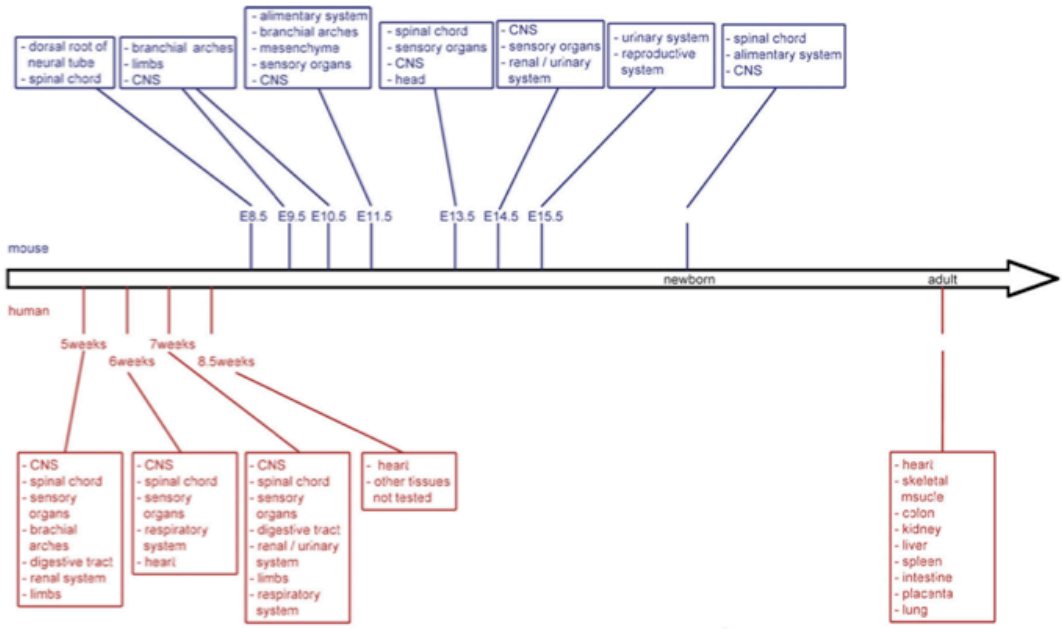

Fig. 1.6: Developmental stage specific expression pattern of MID1 in human and murine tissues (adapted from Winter et al., 2016).

During embryogenesis MID1 interacts with transcription factors, regulating their expression and functionality. Pax6 is one of the most important regulators of eye and brain development and its function is critically dependent on a temporarily and quantitatively defined expression level (Shaham et al., 2012). In *Xenopus*, the expression of *mid1* overlaps with those of *pax6* in the optic vesicle during early embryogenesis and it was described that mid1 mediates pax6 proteasomal degradation, as the two proteins physically interact. When Mid1 levels were reduced, Pax6 expression was expanded and eyes are enlarged (Pfirrmann et al., 2016). By precisely regulating temporal and spatial expression of Pax6, Mid1 exerts a pivotal role during the formation of the visual system.

Furthermore, several studies have reported an implication of Mid1 particularly in neural development (Alexander et al., 2010; Suzuki et al., 2010). A detailed analysis of Mid1 function in mouse has revealed an essential role for the E3 ligase in axon development. It is reported, in fact, that Mid1 is highly expressed in the brain during development and enriched in the axon segment of developing neurons. The depletion of Mid1 in cultured neurons results in the disrupted turnover of PP2Ac in the axons. Accumulation of PP2Ac mediates abnormal axonal growth and branch formation, as well as accelerated axonal growth and altered projection pattern in corpus callosum of mouse embryos (Lu et al., 2013). Therefore, Mid1-dependent PP2Ac turnover is required for proper axon development, indicating that Mid1 acts as an inhibitory factor to regulate axon growth to ensure precise structural and functional patterning, which is crucial for proper circuit formation.

Moreover, Mid1 regulates the levels and the activity of several factors involved in neurodevelopment, such as GLI3, which has been described as a mediator of Wnt/beta-catenin signaling axis during hippocampal development (Hasenpusch-Theil et al., 2012). In addition, Mid1 contributes to the development of the cerebellum and other craniofacial structures that are commonly found altered in OS patients (Lancioni et al., 2010; Dierssen et al., 2012; Nakamura et al., 2017). Downregulation of Mid1 has been reported in cerebellum and hippocampus of transgenic mice expressing a dominant active downstream regulatory element antagonist modulator (DREAM) mutant. At the same time, those mice exhibit a significant shortening of the rostro-caudal axis of the cerebellum, along with a severe delay in neuromotor development early after birth (Dierssen et al., 2012), delineating a role for Mid1 in contributing to cerebellar functions.

In particular, migration of immature neurons from germinal zones towards their final destination is an essential process during cerebellar development. Tangential and radial migrations are required for the establishment of proper circuitry, mediated both by Rac proteins, that belong to the Rho family of small GTPases. Rac1 and Rac3 are known to play important roles during embryogenesis in regulating transcription of genes (Govek et al., 2005), in fact axonogenesis, dendritogenesis, tangential and radial migrations are impaired in transgenic mice depleted for Rac1 and Rac3. Interestingly, Rac-knockout mice exhibited higher levels of *Mid1* transcripts, suggesting that the upregulation of Mid1 expression, together with the deregulation of mTORC1 signaling pathway, is responsible for the defective processes observed in these mice (Nakamura et al., 2017). Therefore, the role of Mid1 in brain and, in particular, in cerebellar development has been defined.

1.6 Cerebellar development in mouse

The cerebellum is a structure of central nervous system with a well-defined anatomy and physiology that can be morphologically divided into a central vermis flanked by lateral hemispheres. Both the vermis and hemispheres are subdivided by parallel fissures in a reproducible series of anteroposterior folds, called lobules, defining a conserved pattern of folia (Fig. 1.7) (Larsell, 1971).

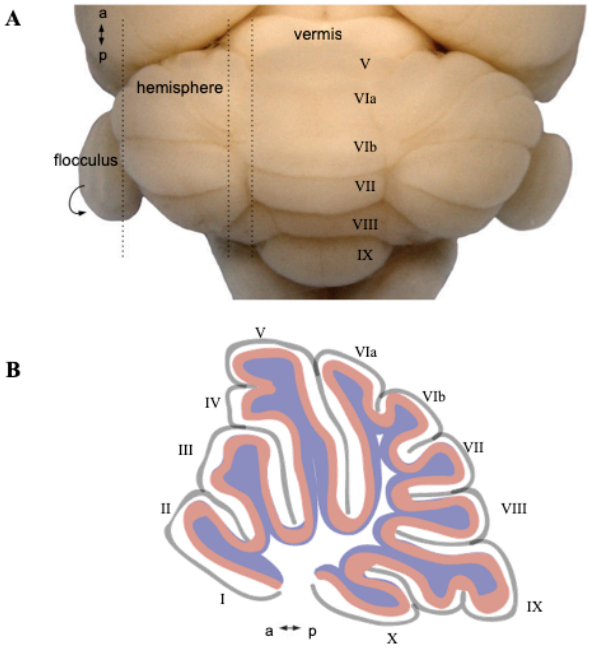

Fig. 1.7: Morphology of the adult cerebellum. A) Dorsal view of whole mount cerebellum shows the three medio-lateral major regions: vermis, hemispheres and flocculi. Conserved foliation patterns divide the cerebellum into lobules, typically identified with Roman numerals (adapted from White and Sillitoe, 2013). B) A sagittal section of the cerebellar vermis revealing the stereotypical foliation pattern, which consists of 10 lobules (a, anterior; p, posterior) (adapted from Corrales et al., 2006).

As in other mammals, mouse cerebellum starts developing early during embryogenesis from the neuroepithelium. Although it is one of the first structure of the brain to differentiate, the transformation of the initially smooth embryonic cerebellum into mature configuration of lobules occurs through a series of dramatic cellular movements that are largely complete by two weeks after birth (reviewed in Chizhikov and Millen,

2003; Apps and Garwicz, 2005; Sillitoe and Joyner, 2007; White and Sillitoe, 2013; Leto et al, 2016). In the adult cerebellum, the precise neuronal functioning requires an elaborate interplay between intrinsic and cell extrinsic events controlled by multiple genetic cascades, guiding morphogenesis and establishing the circuit connections. Cerebellar development occurs in several stages, aimed to define the cerebellar territory along anterior-posterior and dorsal-ventral axes of the neural tube, the specification and subsequent differentiation of cells and neuronal migration (Zervas et al., 2004) (Fig. 1.8).

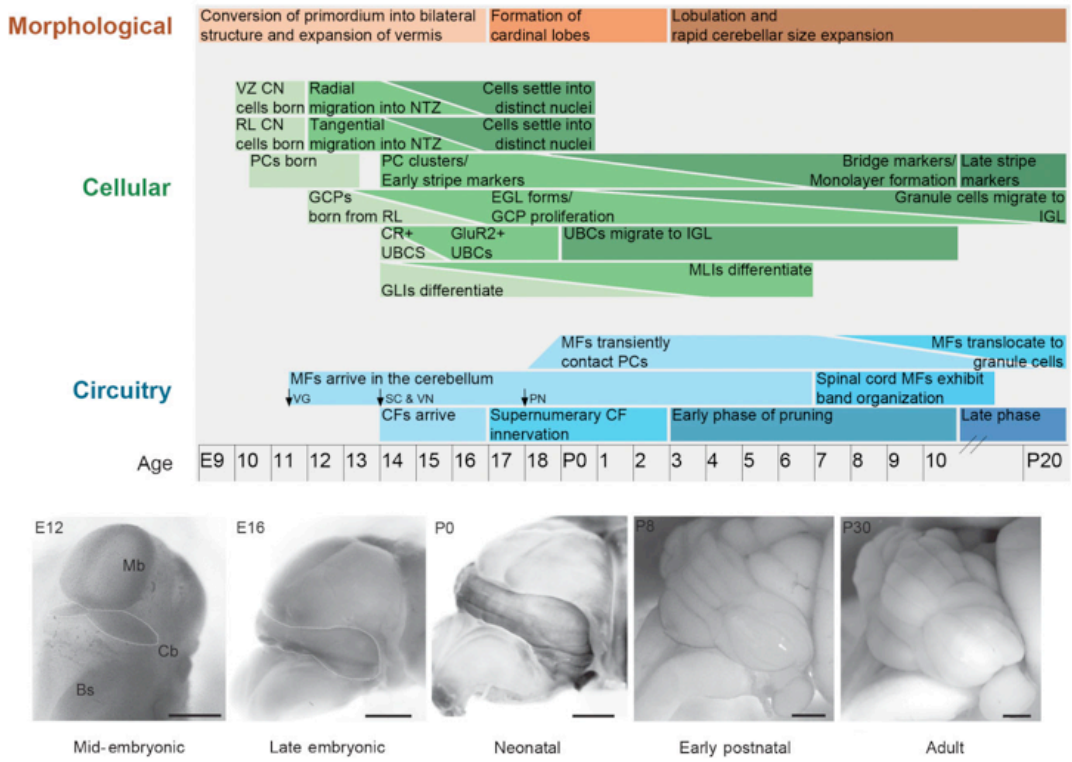

Fig. 1.8: Timeline of cerebellum development. The major steps of mouse cerebellar development and their respective time-points are indicated in the upper timetable. Below, a series of images that capture the morphological changes that occur during mouse cerebellar development are reported (scale bars = 1 mm).

Abbreviations: CFs, climbing fibers; CN, cerebellar nuclei; CR+, calretinin-positive; EGL, external granular layer; GCPs; granule cell precursors; GLIs, granular layer interneurons; GluR2+, GluR2-positive; IGL, internal granular layer; MFs, mossy fibers; MLIs, molecular layer interneurons; NTZ, nuclear transitory zone; PC, Purkinje cell; PN, pontine nuclei; RL, rhombic lip; SC, spinocerebellar; UBCs, unipolar brush cells; VG, vestibular ganglion; VN, vestibular nuclei; VZ, ventricular zone; Mb, Midbrain; Cb, Cerebellum; Bs, Brainstem (adapted from White and Sillitoe, 2013).

Different cell types are present in the cerebellum: the inhibitory GABAergic neurons, which include interneurons (INs) and Purkinje cells (PCs), that populate the cortex, and excitatory glutamatergic neurons, that are mainly represented by granule cells (GCs). The inner core of the cerebellum is composed of the deep cerebellar nuclei (DCN), which consist of both excitatory and inhibitory neurons.

As embryogenesis occurs, neural plate closes to form the neural tube, along which three primary brain vesicles can be clearly morphologically distinguished: forebrain, midbrain and hindbrain. The hindbrain is divided into 7 segments, called rhombomeres. The cerebellum anlage arises in the mid-gestation period, which in mice is between embryonic day 9.5 (E9.5) and E11.5, from dorsal rhombomere 1 in the anterior hindbrain. It is positioned along the antero-posterior axis of the neural tube, which is gradually converted in wing-like bilateral cerebellar primordia (Sgaier et al., 2005). As neurogenesis progresses, the bilateral wings fuse along the dorsal midline to form the central vermis flanked by two lateral hemispheres. Soon after the cerebellar primordium is formed at the midbrain/hindbrain boundary, two primary germinal zones are defined, the ventricular zone (VZ) and the rhombic lip (RL) (Goldowitz and Hamre, 1998; Sotelo, 2004).

The RL is directly adjacent to the roof of the fourth ventricle and it gives rise to excitatory glutamatergic neurons: the GCs, which are the most numerous neuronal cell type in the brain, some DCN neurons and unipolar brush cells (UBCs) (Machold and Fishell, 2005; Wang et al., 2005). The glutamatergic DCN are the first cells to become post-mitotic between E10 and E12 (Pierce, 1975; Hoshino et al., 2005) and thereafter migrate away from the RL tangentially over the cerebellar cortex, and once they reach the antero-dorsal aspect of the cerebellum they cluster in the nuclear transitory zone (NTZ) (Wang et al., 2005). GC precursors (GCPs) migrate from all medio-lateral point along the RL over the entire surface of the cerebellum forming the external granular layer (EGL) (Wingate and Hatten, 1999). The EGL forms by E15 and this region remains mitotically active until two postnatal weeks (Fujita et al., 1966). UBCs are generated from the RL between E13.5 and early neonatal period (Englund et al., 2006; Hevner et al., 2006). The migratory routes of UBCs have not been fully resolved, but it is known that after those cells are born, they migrate into the cerebellum through the developing white matter to eventually stop in the internal granular layer (IGL) (Hevner et al., 2006).

The VZ produces GABAergic inhibitory precursors of PCs and most INs in the

cerebellum. PCs become post-mitotic between E11 and E13 (Hoshino et al., 2005). All PCs have left the VZ by late E13 and apparently migrate radially along radial glial fibers and transiently form a multilayer below the EGL (Miyata et al., 2010). As the glutamatergic DCN, GABAergic DCN INs become post-mitotic between E10 and E12 (Wang et al., 2005). Apparently they migrate radially to their final location within the cerebellum (Altman and Bayer, 1997; Hoshino et al., 2005).

1.6.1 Cerebellar structure and neuronal circuitry

During embryogenesis, the cellular structure of the cerebellum consists of an EGL, colonised by glutamatergic GCs, and GABAergic Purkinje cells layer (PCL), located just underneath the EGL. PCs send inhibitory projections to the DCN, which represent the main output centers of the cerebellum. The DCN contain two types of neurons, glutamatergic neurons and GABAergic interneurons, which are produced from progenitor cells in the NTZ and in the cerebellar VZ, respectively. At birth, GCs migrate through the PCL to form the internal granular layer (IGL) of the mature cerebellum. Most outwardly there is the molecular layer (ML), which contains the projection fibers of GCs and PCs. Between these two layers is a monolayer of PC somata that make up the mature PCL (reviewed in Sillitoe and Joyner, 2007; Leto et al, 2016) (Fig. 1.9).

Approximately at E16.5, the cerebellum starts the foliation, a remodeling process that confers the final specific lobular architecture. Foliation begins with the sequential formation of anchoring centers: the inward thickening of the EGL that are followed by formation of the indentation of the outer surface, delineating the base of fissures (Sudarov and Joyner, 2007). Four initial anchoring centers define five cardinal lobes, which are further divided into final eleven lobules. Through the formation of the lobules, the surface area of the cerebellum extensively increases, thus permitting to house a large number of neurons in a layered cytoarchitecture in a small area (Cheng et al., 2010; Orvis et al., 2012).

The cerebellum is the primary center for motor coordination and is essential for cognitive processing. The precise formation of neuronal circuitry is the final step of cerebellar development and it is necessary for the cerebellum to function as a coordination center (Cajal, 1911). Cerebellum presents two main classes of afferent project: climbing fibers and mossy fibers. PCs receive excitatory input from climbing fibers, which are the axonal projections of cells that reside outside the cerebellum in the

inferior olivary complex, located within the medulla oblongata of the brainstem (Fu et al., 2011). PCs are initially innervated by multiple climbing fibers, but elimination of supernumerary fibers occurs until each mature PC is monoinnervated by a single climbing fiber. In addition, PCs indirectly receive excitatory input also from within the cerebellum from mossy fibers (Salinas et al., 1994). Mossy fibers originate from several nuclei in the brainstem and spinal cord and terminate within large synaptic glomeruli onto the dendrites of GCs (Fu et al., 2011). Ascending axons from GCs bifurcate in the molecular layer into parallel fibers. Along their trajectory, each parallel fiber contacts dendrites of about 300 PCs. By integrating excitatory and inhibitory signals, PCs can appropriately respond to incoming sensory information by controlling the output of DCN, which ultimately communicate with the rest of the brain (White and Sillitoe, 2013; Leto et al., 2016).

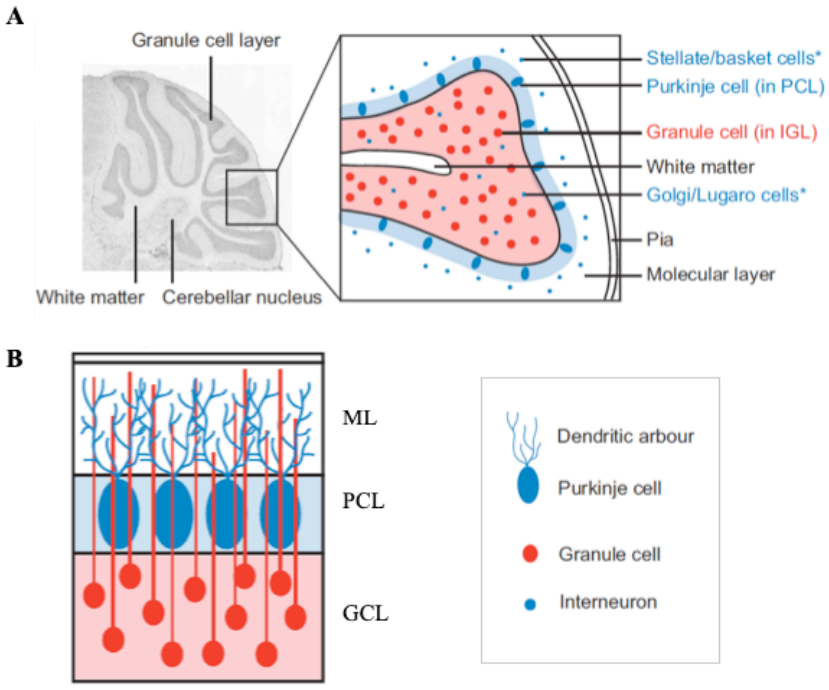

Fig. 1.9: Cellular structure of the cerebellum. A) Sagittal section of mature cerebellum shows different lobules. Each lobule presents a precise distribution of different cell types: Purkinje cell layer (PCL) in blue, internal granule cell layer (IGL) in red and molecular layer (ML) not colored, in which Purkinje cell dendrites and granule cell axons interact. Each layer also contains characteristic GABAergic interneuron subtypes (asterisks). B) Schematic magnified sagittal view of the molecular layer of the cerebellum (adapted from Butts et al., 2014).

1.7 Mouse model of OS: *Mid1* knock-out mouse line

As introduce above, the X-linked form of Opitz syndrome is associated with midline developmental birth defects, caused by mutations in *MID1* gene. To study in detail the pathological processes occurring during embryonic development that lead to the clinical manifestations observed in OS patients, *Mid1* knock-out ($Mid1^{-/Y}$) mouse line has been generated in the lab (Lancioni et al., 2010). $Mid1^{-/Y}$ mouse line carries a nonfunctional ortholog of the human *MID1* gene, obtained by disruption of the first ATG-containing exon. $Mid1^{-/Y}$ mice are viable and fertile and do not show evident midline defects, but present anatomical brain abnormalities in the dorsal midbrain and cerebellar regions (i.e. hypoplasia of the cerebellar vermis), thus recapitulating the neurological signs of the disease in humans. The first direct neuro-anatomical characterisation of whole-mount $Mid1^{-/Y}$ adult brains revealed a malformation in the midbrain/cerebellum junction region. Furthermore, histological analyses confirmed the presence of a defect in the cerebellar anterior part. In particular, vermis hypoplasia and abnormalities of the two most anterior lobes of cerebellar vermis are observed. It has emerged from deeper analyses that cerebellar lobe I was totally missing, while lobe II was not completely formed (Fig 1.10), although neuronal cells distribution maintains the proper organisation (Lancioni et al., 2010).

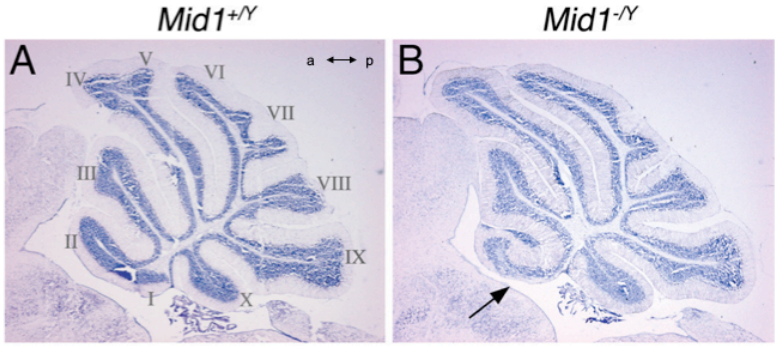

Fig. 1.10: Abnormal cerebellum in $Mid1^{-/Y}$ mice. Nissl staining of sagittal section of cerebellar vermis of wild type (A) and knock-out (B) adult mice, shows the antero-basal defect of the most anterior lobes in $Mid1^{-/Y}$ mice. Roman numerals indicate lobules; a, anterior; p, posterior (adapted from Lancioni et al., 2010).

Consistently with the observed cerebellar defects, *Mid1*$^{-/Y}$ mice present impairments in motor coordination and in non-associative and procedural learning. Analyses of different postnatal and embryonic stages have been useful to follow the gradual development of the defect and to assess the time of the first appearance of the cerebellar abnormalities. At P0, when the foliation process starts, an alteration in the position of the fissure that separates lobe III from lobe IV was detected, while at E14.5 the rostralization of the dorsal midbrain/hindbrain boundary (MHB) was clearly observed in *Mid1*$^{-/Y}$ mice, associated with ectopic positioning of PCs within the isthmic region, resulting in a shorter lower portion on the inferior colliculus (Fig 1.11) (Lancioni et al., 2010). These observations suggested that postnatal abnormal foliation of the cerebellar vermis was due to defects occurring during embryonic development.

Interestingly, another mid-gestation feature of the *Mid1*$^{-/Y}$ embryos is the decreased expression of *Fgf17*, a member of *Fgf8* subfamily, specifically expressed at the MHB from E13.5 to E14.5 (Lancioni et al., 2010). The strong reduction of *Fgf17* signal noticed in the E14.5 mutant embryos is interesting as fibroblast growth factors (*Fgfs*) are key molecules in the establishment and development of the dorsal midbrain-cerebellum border (Liu et al. 1999; Xu et al., 2000).

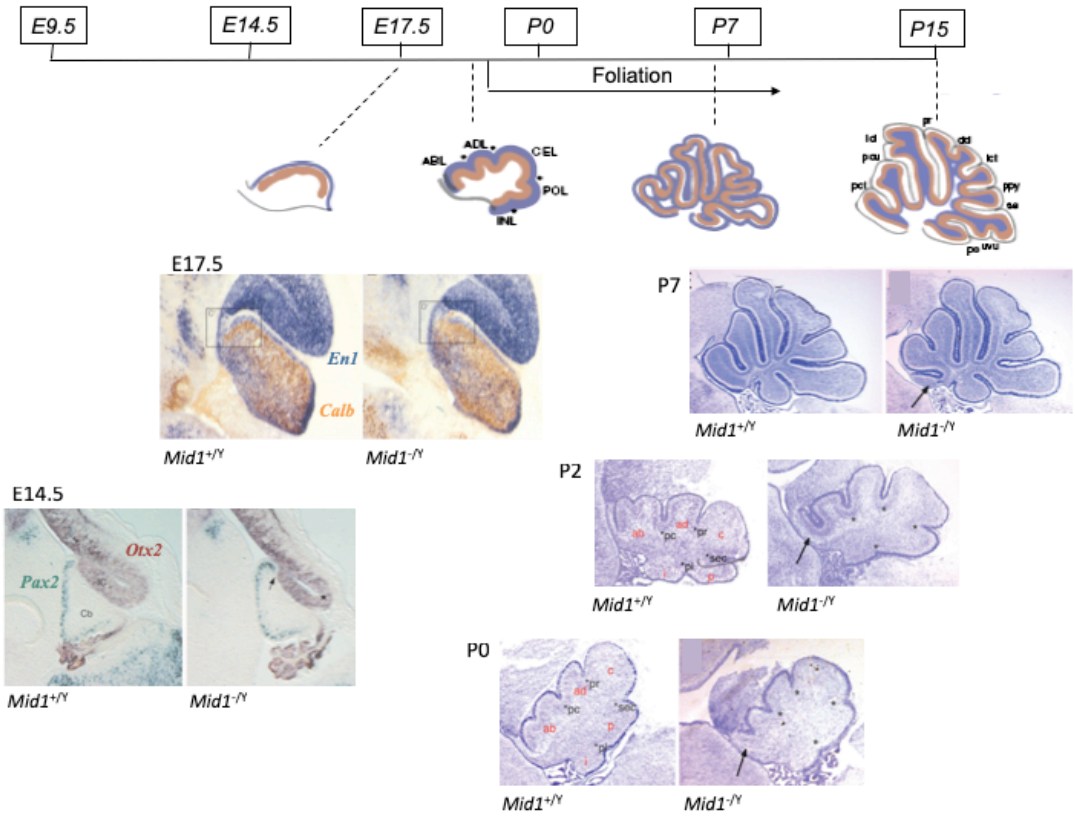

Fig. 1.11: Cerebellar defect in *Mid1*$^{-/Y}$ mice originates prenatally. Analysis of different post-natal (P) and embryonic (E) stages indicated the appearance of the cerebellar abnormalities. Sagittal sections through the vermis at birth (P0), P2 and P7 show the presence of the antero-basal lobe defect in *Mid1*$^{-/Y}$ mice. The four principal fissures (pc, pre-culminate; pr, primary; sec, secondary; pl, postero-lateral) are normally formed in P0 and P2 *Mid1*$^{-/Y}$ mice. The cardinal lobes generated by the principal fissures are correctly formed with the exception of the antero-basal lobe, rostral to the pre-culminate fissure, that shows the defect (ab, antero-basal; ad, antero-dorsal; c, central; p, posterior; i, inferior). At E17.5 immunohistochemistry analysis with anti-calbindin (Calb) and anti-engrailed1 (En1) revealed the inaccurate definition of the dorsal midbrain/cerebellum boundary in *Mid1*$^{-/Y}$ mice (grey box). The reduced inferior colliculus length and rostralization of midbrain/cerebellar boundary in *Mid1*$^{-/Y}$ mice is detected in 14.5 sagittal sections hybridised with Pax2 and Otx2 markers. The asterisks indicate the principal fissures. The arrows indicate the defects (adapted from Lancioni et al., 2010).

1.8 Vesicular trafficking in neurodevelopment and neurotransmission

Multiple biological processes throughout development require vesicular trafficking. In particular, neurogenesis requires proper synaptic vesicles trafficking and intercellular communication through the release of several signals, often conveyed by specialised extracellular vesicles. All stages of neurodevelopment, including cell migration, axonal development and synapse formation, are associated with intra- ad extra-cellular trafficking where the SNARE (soluble N-ethylmaleimide-sensitive factor (NSF) attachment protein (SNAP) receptors) complex plays a major role (Hepp and Langley, 2001). The core proteins forming the SNARE complex are SNAP (synaptosomal-associated protein), VAMP (vesicle-associated membrane protein) and Syntaxins (Cupertino et al., 2016). Other regulatory proteins interact with the SNARE complex, thus mediating the proper assembly and function, such as Synaptotagmin, Synaptophysin, Munc-18, alpha-Synuclein, Rab3, Complexin and cysteine string protein alpha (CSP-alpha) (Sudhof, 2013; Shin, 2014). Two classes of SNARE proteins have been defined: v-SNAREs (SNARE proteins associated with the vesicles) and t-SNARE (SNARE proteins associated with the target plasma membrane).

Accordingly to cell tissue and developmental stage, distinct family members of SNARE complex present different expression profile. In the brain, SNAP-25 is the best characterised isoform of this family of proteins. It is mainly expressed in neurons and directly involved in neurotransmitter release (Yamamori et al., 2011). Through the two SNARE domains, SNAP-25 binds VAMP and Syntaxin, in order to form the core SNARE complex. Moreover, SNAP-25 is anchored to the presynaptic membrane through palmytoylation of cysteine residues. The VAMP family includes seven proteins, but only VAMP-1 and VAMP-2 isoforms are expressed in neuronal cells (Trimble, 1993). Furthermore, within the Syntaxins family, the major isoforms observed in the brain are Syntaxin-1A and Syntaxin-1B (Ullrich et al., 1994). These SNARE proteins interact creating a four-helix bundle, formed by two helices of SNAP25, one vesicle-transmembrane VAMP and one presynaptic plasma membrane Syntaxin that approximates the vesicle and plasmatic membranes (Fig. 1.12).

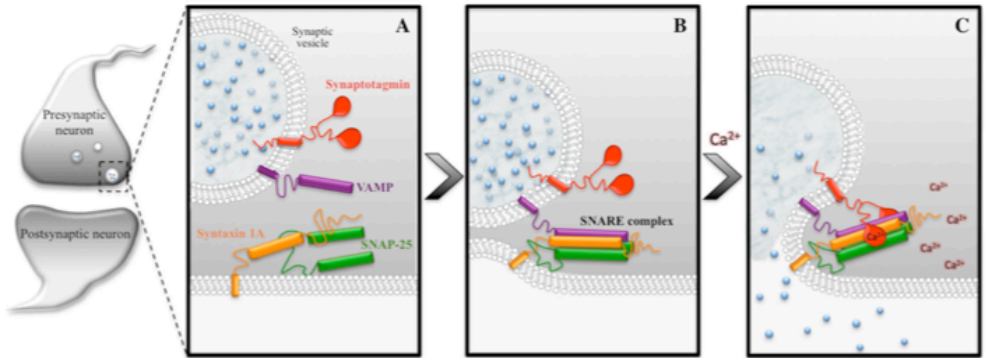

Fig. 1.12: SNARE complex assembly at the presynaptic zone allowing neurotransmitter release. A) Components of the SNARE complex (SNAP-25, VAMP and Syntaxin-1A) and regulatory protein Synaptotagmin are shown in the unbound conformation. B) Assembly of the core SNARE complex, approximating plasma and vesicle membranes. SNAP-25 and Syntaxin-1A form an heterodimer through the binding of their SNARE motifs. Then VAMP interacts with the second SNARE domain of SNAP-25, forming a four-helix bundle. C) The SNARE complex is stably and completely assembled upon calcium (Ca^{2+}) influx. Synaptic vesicle fuses with the plasma membrane, releasing neurotransmitters (blue dots) (from Cupertino et al., 2016).

SNARE complexes are described to regulate the exocytosis of different types of vesicles, including synaptic vesicles and extracellular vesicles, such as exosomes (Fig. 1.13).

The core SNARE complex proteins involved in neurotransmission are SNAP-25, VAMP (-1 or -2) and Syntaxin-1A and it plays a pivotal role in synaptic vesicle tethering, docking, priming and fusion (Ramakrishnan et al., 2012). Synaptic vesicles are lipid-bilayer structures, packaged with neurotransmitter molecules (De Robertis and Franchi, 1956). They originate from the endoplasmic reticulum or presynaptic plasma membrane and are transported by cellular trafficking to the presynaptic active zone, which is the region specialised in vesicles release. At the presynaptic membrane of neurons, Syntaxin-1A is attached to Munc-18, thus leaving the t-SNARE in a close conformation (Smyth et al., 2010). Different signals in the cells allow initiating the vesicle exocytosis for releasing neurotransmitters. The first step in vesicle fusion is the tethering process: Syntaxin-1A/Munc-18 complex is detached, freeing the t-SNARE in an open status (Dulubova et al., 1999). Thus, Syntaxin-1A and SNAP-25 form a heterodimer at the presynaptic membrane. This initial step is followed by docking of vesicles, where SNARE proteins interact via the SNARE motifs. In particular, when

synaptic vesicle reaches the site of exocytosis, the vesicle transmembrane protein VAMP binds to the SNAP-25/Syntaxin-1A heterodimer. Then SNARE proteins form a stable complex, in a step called vesicle priming, rendering the vesicles competent for fusion and allowing neurotransmitter release (Ramakrishnan et al., 2012; Sudhof, 2013). Therefore, the role of SNARE proteins and SNARE complexes in synaptic vesicle exocytosis is well documented. Conversely, the implication of SNAREs in exosome release has been more recently investigated (Ruiz-Martinez et al., 2016; Wei et al., 2017).

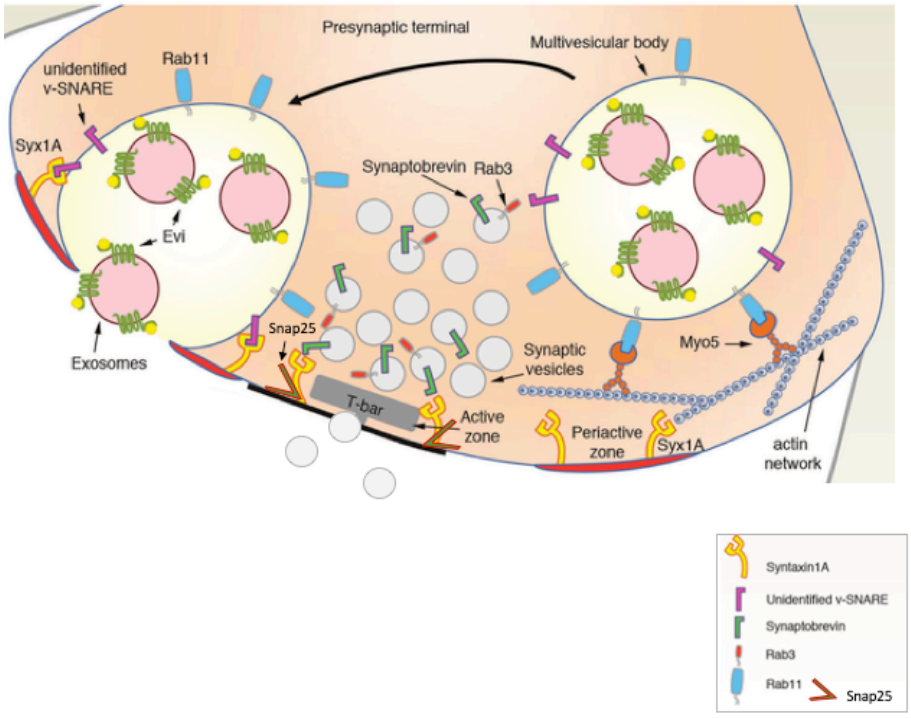

Fig. 1.13: SNARE proteins regulate exocytosis of exosomes and synaptic vesicles. Schematic representation of SNARE-mediated release of exosomes and synaptic vesicles in pre-synaptic neurons. Multivesicular bodies fuse with the presynaptic membrane releasing their exosomal content, by using v-SNARE and t-SNARE (i.e. Syntaxin-1A). In parallel, synaptic vesicles are secreted form the active zone of presynaptic terminal using Syntaxin-1A, Snap25 and v-SNARE Vamp (Synaptobrevin). Also Rab proteins are needed for mediating the vesicular exocytosis. Rab3 is associated with synaptic vesicles, wherease Rab11 is described in the exosomal pathway (adapted from Koles and Budnik, 2012).

Exosomes are small membranous vesicles, ranging from 30 to 100 nm, that are generated within multi-vesicular bodies (MVBs) in the endosomal system (Raposo et al. 1996). In particular, early endosomes mature into late endosomes (Stoorvogel et al. 1991), accumulating intraluminal vesicles (ILVs) in their lumen, thus forming the MVBs. ILVs can serve as storage compartment for proteins and signaling complexes and can re-enter the cytosol by backfusion with the MVB membrane (Abrami et al., 2004). MVBs can either fuse with lysosomes leading to the degradation of ILVs or with the plasma membrane, releasing the ILVs as exosomes into the extracellular space (Hessvik and Llorente, 2018).

Recently, several works underline the important role of exosomes in intercellular communication by serving as vehicles for transferring proteins, lipids and nucleic acid and they have been implicated in a wide range of physiological and pathogenic processes (reviewed in Raposo and Stoorvogel, 2013; Colombo et al, 2014; Schneider and Simons, 2016). Particularly, it has been found that exosomes are also implicated in controlling developmental signaling, by carrying signaling proteins, such as ligands of the Notch receptor and secreted proteins of the Hedgehog and WNT families (McGough and Vincent, 2016). Interestingly, exosomes are implicated in pathways that regulate nervous system development and homeostasis, mediating communication between oligodendrocytes and neurons by providing a mechanism for the transfer of protective proteins, mRNA and miRNA (Fruhbeis et al., 2013).

Therefore, the fusion of exosomes with the plasma membrane and the neurotransmission through the synaptic vesicle release are two essential SNARE-associated processes that regulate neurogenesis, leading to a proper development and intercellular communication.

1.9 RNA exosome complex

RNA exosome was first described in 1997 as a stable complex of RNase-like and RNA binding proteins implicated in ribosomal RNA (rRNA) biogenesis (Mitchell et al., 1997). Subsequent studies revealed that the RNA exosome is a ubiquitous ribonuclease complex which presents high evolutionarily conservation and participates in the processing, degradation, quality control and regulation of virtually all classes of RNA. Among the others, the functions of the RNA exosome complex are maturation of 3′ ends of rRNA and small nucleolar RNAs (snoRNAs), degradation of unstable RNAs, removal of excised introns, quality control of RNA in the nucleus as well as in the cytoplasm, and complete RNA decay (Schilders et al., 2006; Belostotsky 2009; Chlebowski et al., 2013; Kilchert et al., 2016; Łabno et al., 2016).

1.9.1 Composition and structure of the RNA exosome

The eukaryotic RNA exosome is composed of ten to eleven subunits with structural or functional contribution in the complex. In humans the exosome subunits are termed EXOsome Component (EXOSC) proteins, while in *S. cerevisiae* and *Drosophila* most exosome subunits are termed Rrp (Ribosomal RNA Processing) proteins. Both catalytic and structural subunits have been well described, owing to the crystal structure obtained for the human RNA exosome complex (Liu et al., 2006). The global architecture of the RNA exosome comprises a nine-subunit core exosome and two ribonucleases which associate with the core in different combination (Schneider and Tollervey, 2013; Januszyk and Lima, 2014; Morton et al., 2018). The structure of the exosome core comprises nine subunits, arranged in a two-layered ring (Fig 1.14). Six catalytically inert proteins presenting a single domain homologous to RNAse PH, an enzyme found in Escherichia coli, build the bottom layer, which forms the central channel. The PH ring subunits, termed “hexamer”, are EXOSC4-9 (also known as Rrp41/42/43/45/46/Mtr3). The top layer is called the “cap” and consists of three RNA binding subunits: EXOSC1-3 (Csl4/Rrp4/Rrp40). Within the cap the proteins do not interact, but each cap subunit strongly associates to two hexamer subunits (Liu et al., 2006; Makino et al., 2013; Zinder et al., 2016).

The catalytic activity of the exosome complex is due to two ribonucleases which bind the core: Dis3 (or Rrp44) associating with the base of the hexamer, and EXOSC10 (or Rrp6) interacting with the cap. Dis3 is a processive 3’ to 5’ exo- and endoribonuclease, composed by two cold-shock domains (CSDs), a central ribonuclease binding domain

(RNB) and an S1 domain at the C-terminal, responsible for the non-specific binding to RNA and for the processive exoribonuclease activity; while the Cysteine-Rich motif (CR3) and a Pilus-forming N-terminus (PIN) domain are located at the N-terminal and bear the exo- or endoribonuclease activity (Clissold and Ponting, 2000; Zuo and Deutscher, 2001). EXOSC10 exhibits a distributive 3' to 5' exonuclease activity, harbored by the catalytic exoribonuclease domain (EXO or DEDD), flanked by Homology to RNase D domain C-terminal (HRDC) and PMC2NT domains, that are crucial for full activity of the protein and mediate the binding with the core (Zuo and Deutscher, 2001; Chlebowski et al., 2013; Januszyk and Lima, 2014). Therefore, the core subunits present only weaker RNA binding properties, thus the RNA interaction in the exosome complex is largely due to the presence of Dis3 and EXOSC10 (Schneider et al., 2009; Januszyk et al., 2011; Wasmuth and Lima, 2017). Association between the exosome core and the catalytic subunits leads to the formation of the exosome holocomplex able to perform processing and degradation of a wide variety of RNAs that generally enter the central channel, which is wide enough to accommodate single-stranded RNA (ssRNA). RNA substrates can be threaded in the 3' to 5' orientation from the cap to the hexameric ring to Dis3, whose endonuclease activity facilitates the degradation process (Wasmuth and Lima, 2012).

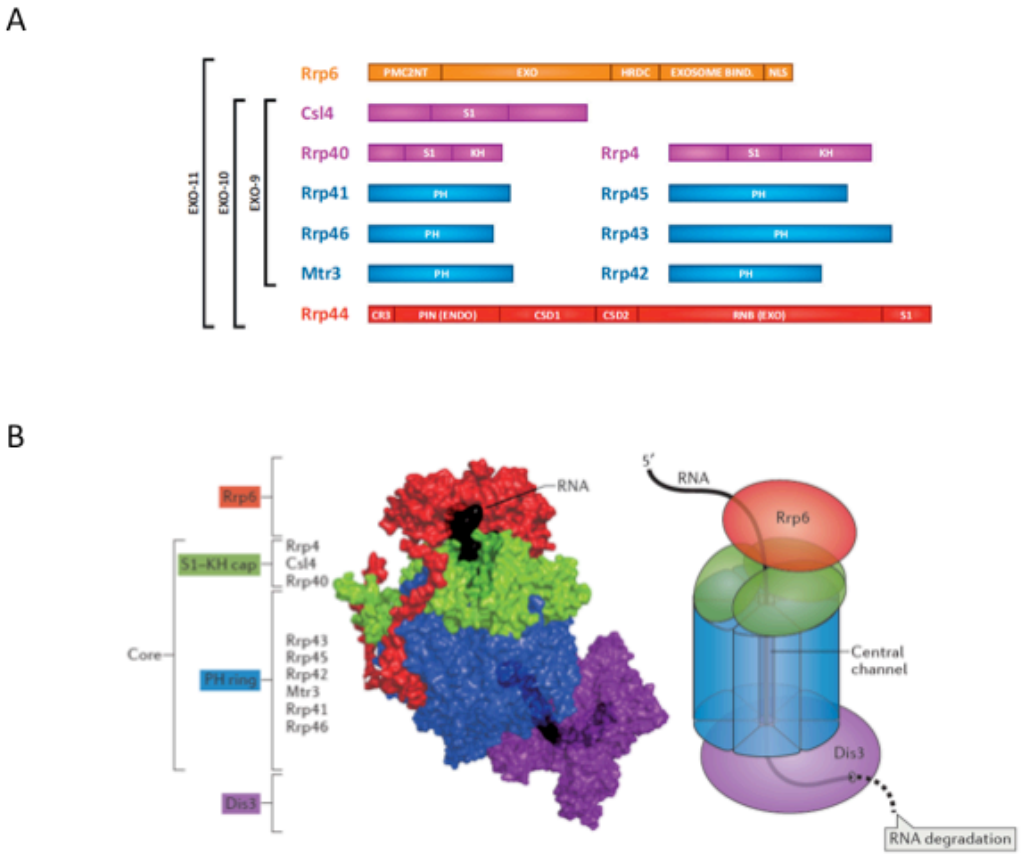

Fig. 1.14: Structure of RNA exosome complex. A) Domain structure of exosome components and composition of exosome complexes EXO-9 (core), EXO-10 and EXO-11. The domains are indicated as follow: EXO, exonuclease activity domain (also termed DEDD in Rrp6 and RNB in Rrp44); ENDO, endonuclease activity domain; PMC2NT, N-terminal domain of the 3' to 5' exonuclease Rrp6/EXOSC10; HRDC, Homology to RNase D domain C-terminal; EXOSOME BIND., region in Rrp6 that interacts with the exosome core; NLS, Nuclear Localisation Signal; S1 and KH, RNA-binding domains; PH, domain with homology to bacterial RNAse PH; CR3, motif containing 3 Cys residues; PIN (ENDO), endonuclease activity domain; CSD1 and CSD2, cold-shock RNA-binding domains (adapted from Schneider and Tollervey, 2013). B) Model of the RNA exosome holocomplex, comprising the exosome core (composed by 3 S1-KH cap subunits and 6 PH ring subunits) and the two ribonucleases, Rrp6 (EXOSC10) and Dis3 (adapted from Kilchert et al., 2016).

1.9.2 Subcellular localisation of the RNA exosome complex

The RNA exosome complex targets RNAs of virtually all classes at various stages of their lives, from maturation through quality control to final turnover. The wide variety

of the RNA substrates (including mRNAs, snoRNAs, rRNAs) suggests that the exosome might be localised in different subcellular compartment, such as the cytoplasm, the nucleoplasm as well as the nucleolus. Indeed, exosome localisation in nucleus and nucleolus and also in the cytoplasm, even if to a lesser extent, is reported in yeast (Mitchell et al., 1997; Allmang et al., 1999). Nevertheless, through immunofluorescence experiments the human RNA exosome was almost exclusively found in the nucleus with enrichment in the nucleoli (Tomecki et al., 2010). Further experiments elucidated this data, demonstrating that the relatively low concentration of substrate RNAs in the cytoplasm may explain why this cellular compartment is only poorly visible in immunofluorescent staining of exosome component in comparison to the nucleus and, even more, the nucleolus. Effectively, several biochemical fractionation experiments have shown that there is a significant cytoplasmic pool of exosome complexes (Chlebowski et al., 2013). Now it is clear that the eukaryotic RNA exosome exerts its activity both in the nucleus and in the cytoplasm, with various specialised functions in different cellular compartments. The cytoplasmic form of the RNA exosome mainly consists of the nine-subunits core and Dis3, whereas the nuclear RNA exosome includes also EXOSC10. In addition, the nucleolar exosome is composed by the core subunits and EXOSC10 as the only nuclease (Januszyk and Lima, 2014). In general, the cytoplasmic exosome is implicated in mRNA turnover, but also degrades the incorrectly processed RNAs in translation-dependent cytoplasmic quality control pathways, such as non-stop decay and nonsense-mediated decay (Łabno et al., 2016). In the nucleus, the exosome processes numerous non-coding RNAs (ncRNAs) but is also responsible for the nuclear surveillance pathways by degrading the defective RNAs (Ogami et al., 2018).

1.9.3 Role of RNA exosome in cellular processes

The RNA exosomes contribute to important and diverse biological processes in eukaryotes (Zinder and Lima, 2017). In particular, growing evidence underline the role of different components of RNA exosome in cellular proliferation and differentiation (van Dijk et al., 2007). Abnormal chromosome segregation and mitotic progression have been described in *Schizosaccharomyces pombe* as well as *Drosophila melanogaster*, when Exosc10 and Dis3 are mutated or knocked down (Graham et al., 2009; Harigaya et al., 2006; Murakami et al., 2007). In humans, Dis3 activity is generally associated with promoting cell division and alterations of Dis3 function are

frequently linked to mitotic defects, in particular mutation within the exoribonuclease domain, disrupting Dis3 RNA degradation activity, are often found in multiple myeloma (Chapman et al., 2011). Furthermore, a marked role of the RNA exosome in cell differentiation has been recently attested. Starting from experiment on murine embryonic stem cells, in which RNA exosome complex was demonstrated to be crucial for the formation of the embryoid bodies (Lloret-Llinares et al., 2018), the maturation of different cell types appears to be regulated via selective RNAs decay exerted by exosome complex. In mice, the onset of spermatogenesis is controlled by Exosc10, which is in turn regulated at the level of protein localisation and stability during male germ cell differentiation. Specifically, *Exosc10*-deleted mice present a severe decrease of spermatogenesis and hypofertility (Jamin et al., 2017). Whereas Exosc8 and other exosome core subunits are implicated in controlling the maturation process of the hematopoietic stem cells toward the erythrocytes, presumably owing to the degradation of specific transcripts that are regulated by master transcriptions factors such as GATA-1 and Foxo-3 in response to differentiation factors, such as erythropoietin (McIver et al., 2014). Thus, exosome core maintains the delicate balance between proliferation and differentiation in murine red blood cells. Similarly, in humans EXOSC9 prevents premature differentiation preserving a proliferative state of skin stem cells via selective degrading *GRHL3* transcript, necessary for epidermal differentiation (Mistry et al., 2012).

Furthermore, by regulating RNA metabolism, exosome functions are essential during organism development (Harigaya et al., 2006; Hou et al., 2012; Yap et al., 2012). In particular, it has been assessed that Dis3 is required for early *Drosophila melanogaster* embryogenesis, acting in reducing early expressed RNAs in a stage-specific manner during development (Hou et al., 2012).

1.9.4 Mutations in RNA exosome components cause distinct human diseases

Given the importance of the RNA exosome complex in many biological processes, it is not surprising that mutations in gene encoding different exosome components have been linked to distinct diseases. Specifically, mutations in the exosome subunit gene *EXOSC3*, *EXOSC8* and *EXOSC9* have been reported in cases of pontocerebellar hypoplasia (PCH) and spinal motor neuronopathy (Burns et al., 2018: Morton et al., 2018), while mutations in *EXOSC2* have been linked to a novel syndrome that impact widely several tissues (Di Donato et al., 2016).

Mutations in *EXOSC3* are associated with pontocerebellar hypoplasia type 1b (PCH1b), which is a distinctive subtype of PCH, characterised by significant atrophy of the pons and the cerebellum, Purkinje cells abnormalities and diffuse muscle wasting secondary to spinal motor neurons degeneration, starting at birth. A reported case of PCH1b linked to homozygous c.395A > C mutation in *EXOSC3* presents also with mitochondrial dysfunction (Schottmann et al., 2017). Exosome sequencing of several patients from unrelated families has indicated that different mutations in *EXOSC3* gene can cause disease phenotypes that can vary in severity and can impact different regions of the brain (Rudnik-Schöneborn et al., 2013; Eggens et al., 2014). Reducing *exosc3* level in zebrafish through morpholino knockdown experiments resulted in a shrunken and collapsed hindbrain, associated with reduced quantity of differentiated Purkinje cells, thus affecting neuronal systems similar to those in affected individuals. Notably, the expression of the human wild type *EXOSC3* rescued the hindbrain development aberration in zebrafish embryos, but the *EXOSC3* gene carrying the mutations found in patients fail to correct the defect (Wan et al., 2012). The functional consequences of the amino acid substitution identified in EXOSC3 in PCH1 patients have been also studied in other model organisms, such as *Saccharomyces cerevisiae* and mouse, by mutating the ortholog genes (Fasken et al., 2017). Mostly, the mutations lead to defective folding of the protein and subsequently disturb interactions with other exosome subunits, leading to compromised RNA exosome complex function.

Another subtype of PCH1, the pontocerebellar hypoplasia type 1c (PCH1c), has been linked to mutations in *EXOSC8* gene (Boczonadi et al., 2014). PCH1c is a neurodegenerative disorder characterised by psychomotor deficit, cerebellar and corpus callosum hypoplasia, hypomyelination and spinal muscular atrophy starting at birth. Commonly to PCH1b, patients affected by PCH1c present degeneration of spinal motor neurons and defects in Purkinje cells. Analysis of 10 affected individuals with severe PCH1c revealed the same mutation in *EXOSC8* (c.815G4C, p.Ser272Thr). Presumably this amino acid substitution prevents the interaction with EXOSC9 and/or limited the opening of the exosome central channel, affecting in both cases the functionality of exosome complex. As for *EXOSC3*, morpholino knockdown of *exosc8* in zebrafish embryos causes brain abnormalities, in particular in the hindbrain with defects in Purkinje cell layer of the cerebellum, neuromuscular junction alterations and impairment in motor neuron axons growth (Boczonadi et al., 2014), thus supporting the role of EXOSC8 in neurodevelopment.

Recently, a disorder closely related to PCH1 connected to *EXOSC9* variants has been described (Burns et al., 2018). Individuals affected by EXOSC9-related PCH, also termed PCH1d, displayed severe PCH1-like features, encompassing early-onset progressive axonal motor neuronopathy in combination with cerebellar atrophy. All the patients presented the same mutation on *EXOSC9* gene: c.41T>C (p.Leu14Pro), which is predicted to cause a disruption in the structure of EXOSC9 protein, whereas one affected individual was compound heterozygous for c.41T>C (p.Leu14Pro) and c.481C>T (p.Arg161*) (Burns et al., 2018; Bizzari et al., 2019). As result, the fibroblasts from patients showed lower level of EXOSC9 than in control cells. Intriguingly, EXOSC9 reduction was even more pronounced in fibroblasts from individuals harboring mutations in EXOSC3 and EXOSC8, suggesting that reduction in one component of the exosome complex leads to the destabilisation of all the exosome subunits, as well as the whole complex (Fig 1.15) (Burns et al., 2018).

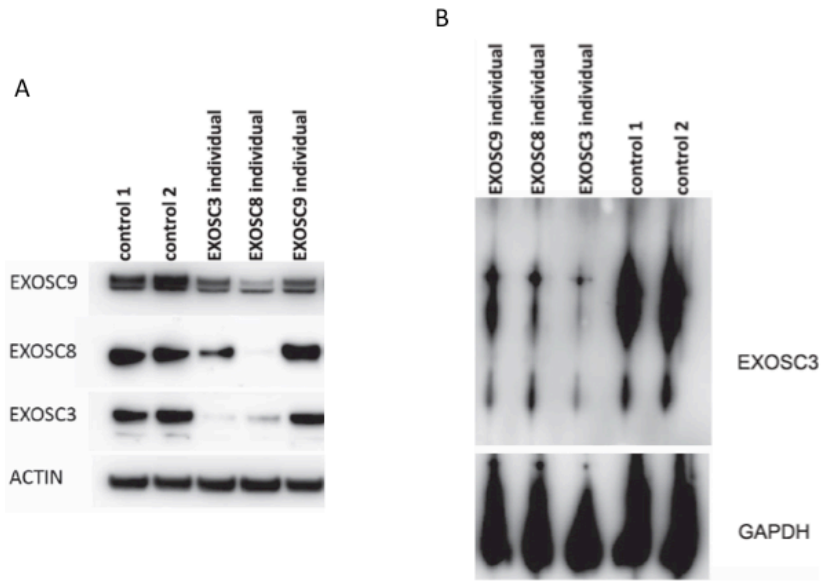

Fig. 1.15: Reduction of distinct exosome subunits destabilizes various components and the whole complex. A) Fibroblast from patients carrying variants in different components of the complex (EXOSC3, EXOSC8 and EXOSC9 individuals) show reduction in the amount of several exosome subunits. B) Native polyacrylamide gel electrophoresis shows the decrease in the assembly of the entire exosome complex (detected through anti-EXOSC3 antibody) in fibroblasts from all the affected individuals (adapted from Burns et al., 2018).

Additionally, the knockdown of *exosc9* in zebrafish recapitulated aspects of the human phenotype, as in the case of *exosc3* and *exosc8* studies. Specifically, portions of the cerebellum and hindbrain were absent, and motor neurons failed to develop and migrate properly, supporting the involvement of exosc9 in proper brain and neuromuscular development (Burns et al., 2018).

Differently, mutations in *EXOSC2* cause an intellectual disability syndrome with short stature, premature ageing, early onset retinitis pigmentosa, hypothyroidism and progressive hearing loss, combined with mild cognitive impairment and mild cerebellar atrophy (Di Donato et al., 2016). Exome sequencing of three patients from two unrelated families revealed a recurrent mutation in the N-terminal domain of *EXOSC2*, likely responsible for lack of interaction between cap and core exosome subunits.

The structural and functional characterisation of the exosome has led to new insights into the RNA processing pathways in eukaryotes. In recent years, the implication of exosome complex in several cellular mechanisms has been depicted and mutations in different exosome subunits have appeared evidently connected with distinct neurological disease in humans, making the study of the biology of the RNA exosomes an important aspect in the scientific knowledge progression.

2. AIM OF THE STUDY

The X-linked form of Opitz syndrome (OS), a genetic disorder characterised by midline developmental defects, is caused by mutations in the *MID1* gene, which encodes an E3 ubiquitin ligase that belongs to the tripartite motif (TRIM) subfamily of RING proteins (Quaderi et al., 1997). Although it is ubiquitously expressed in embryonic tissues, the highest levels of *MID1* transcript are observed in the progenitor cells of the central nervous system (Dal Zotto et al., 1998), exerting a role in proper neuronal development. Consistently, the mouse line carrying a nonfunctional ortholog of the human *MID1* gene, *Mid1*, (*Mid1*$^{-/Y}$) recapitulates the brain morphological abnormalities observed in patients, i.e. hypoplasia of the anterior cerebellar vermis (Lancioni et al., 2010). Nevertheless, the role of *Mid1* in cerebellar development is still unknown.

Therefore, the aim of the present thesis work has been to provide new insights in understanding the pathogenetic mechanisms underlying OS, exploiting the *Mid1*$^{-/Y}$ mouse line that reflects the neurological signs of the patients. In particular, starting from an unbiased proteomics study using differential mass spectrometry approach, we explored altered pathways in *Mid1*$^{-/Y}$ developing cerebella, disclosing potential molecular mechanisms involved in the establishment of the neurological defects observed in mouse embryos and in OS patients.

3. MATERIALS AND METHODS

3.1 Composition of the buffers and solutions employed

• 0.5M Tris-HCl pH 6.8: 6g Tris, H_2O up to 100 mL, adjust pH to 6.8 with HCl.

• 1.5M Tris-HCl, pH 8.8: 54.45g Tris, H_2O up to 300 mL, adjust pH to 8.8 with HCl.

• CE buffer: 10mM HEPES, 60mM KCl, 1mM EDTA, 1mM DTT, 1mM PMSF, 0,075% NP-40, 5µL/mL protease inhibitors cocktail (P8340 Sigma), adjust to pH 7.6.

• Complete growth medium: Dulbecco's Modified Eagle Medium (DMEM), 10% FBS, 4mM L-glutamine, 100U/ml penicillin, 100µg/ml streptomycin.

• Homogenising buffer: 0.32M sucrose, 1mM EDTA pH 8.0, 1mg/ml BSA, 5mM HEPES pH 7.4, 1mM PMSF, 2mM Na_3VO_4, 10mM NaF, 5µL/mL protease inhibitors cocktail (P8340 Sigma).

• IP wash buffer: 50mM Tris-HCl pH 7.4, 300mM NaCl, 5mM EDTA pH 8.0, 0,1% Triton X-100.

• Krebs-Ringer buffer: 140mM NaCl, 5mM KCl, 5mM glucose, 150mM EDTA pH 8.0, 10mM HEPES pH 7.4, 1mM PMSF, 2mM Na_3VO_4, 10mM NaF, 5µL/mL protease inhibitors cocktail (P8340 Sigma).

• Loading Buffer 1X: 62.5mM Tris-HCl pH 6.8, 10% Glycerol, 2% SDS, 2% β-Mercaptoethanol, 0.02% w/v bromophenol blue.

• NE buffer: 20mM Tris-HCl pH 8, 420mM NaCl, 1.5mM $MgCl_2$, 0.2mM EDTA, 1mM PMSF, 25% glycerol, 5µL/mL protease inhibitors cocktail (P8340 Sigma).

• Non-denaturing lysis buffer: 50mM Tris-HCl pH 7.4, 300mM NaCl, 5mM EDTA pH 8.0, 1% Triton X-100, 5µL/mL protease inhibitors cocktail (P8340 Sigma).

• PBS buffer 10X pH 7.4: 80g NaCl, 2 g KCl, 14.4 g $Na_2HPO_4 \cdot 2\ H_2O$, 2 g KH_2PO_4, H_2O up to 1L. Adjust pH 7.4 with NaOH 10M.

• PBST: 0.1% Triton X-100, 1X PBS.

• RIPA buffer: 50mM Tris-HCl pH 8, 0.1% SDS, 150mM NaCl, 0.5% NaDOC, 1% NP-40, 5µL/mL protease inhibitors cocktail (P8340 Sigma), phosphatase inhibitors (50mM NaF; 10mM $Na_4P_2O_7$; 20mM β-glycerophosphate; 1mM Na_3VO_4).

• TAE buffer 50X: 242g Tris base, 57.1mL glacial acetic acid, 100mL EDTA 0.5 M pH 8.0, H_2O up to 1 L.

• TKM lysis buffer: 20mM Tris-HCl pH 7.4, 100mM KCl, 5mM $MgCl_2$, 0,5% NP-40, 1mM DTT, 5µL/mL protease inhibitors cocktail (P8340 Sigma).

• TBS (Tris-buffered saline) buffer 10X: 12.11g Tris base, 87.66g NaCl. Dissolve in 900 mL distilled H_2O and adjust pH to 7.5 with HCl. Add H_2O to a final volume of 1 L.
• TBST: 0.1% Tween 20, 1X TBS.
• Transfer buffer 1X: 25mM Tris, 192mM Glycine, 20% v/v methanol.
• Tris-Glycine Running Buffer 1X: 25mM Tris, 192mM Glycine, 0.1% SDS.
• Urea buffer: 20mM Tris-HCl pH 7.4, 150mM NaCl, 1% NP-40, 5mM EDTA pH 8.0, 10% Glycerol, 1mM DTT, 8M Urea, 3% SDS.

3.2 Mice

All mice were housed and handled according to the institutional guidelines in compliance with the European Council Directive 86/609 and Italian law (Dl. 26/2014). *Mid1* knock-out (*Mid1*$^{-/Y}$) mouse line was previously generated in the lab by targeted recombination. The wild type *Mid1* locus was replaced with a non-functional *Mid1* allele by disruption of the first ATG containing exon (Lancioni et al., 2010).
The *Mid1*$^{-/Y}$ and their *Mid1* wild type (*Mid1*$^{+/Y}$) control embryos/mice used in this thesis work were obtained within the same litter by mating heterozygous female with wild type males.

3.2.1 Embryos harvesting and dissection

Embryos were collected at different stages from timed-pregnant mice, in which the day of the vaginal plug was designated embryonic day 0.5 (E0.5). E13 or E13.5 pregnant mice were euthanised by cervical dislocation, embryos were isolated and extracted from the placenta and washed in PBS 1X. E13 embryonic brains were dissected to isolate the cerebellar anlage (dorsal hindbrain region) together with the portion of midbrain, which includes the developing inferior and superior colliculus. Fine dissection was carried out for some experiments on E13 embryos, as follow: the brain was dissected separately collecting the developing cerebellum, the dorsal midbrain and the telencephalon (see Fig. 3.1). Tails were used for genotyping the embryos. All the collected tissues were immediately frozen in dry ice/ethanol bath and stored at -80°C.

3.2.2 Post-natal mouse brains harvesting and dissection

Pups at post-natal day 7 (P7) were sacrificed through decapitation, the brain was removed from the skull and fully stripped of meninges. Cerebellum was separated and used for primary cerebellar granule cells preparation.

Adult male mice were euthanised at 12 weeks old by cervical dislocation, the brain was removed from the skull and fully stripped of meninges. Cerebellum, hippocampus and cortex were separated and washed in PBS 1X (Fig. 3.1). All the collected tissues were immediately frozen in dry ice/ethanol bath and stored at -80°C.

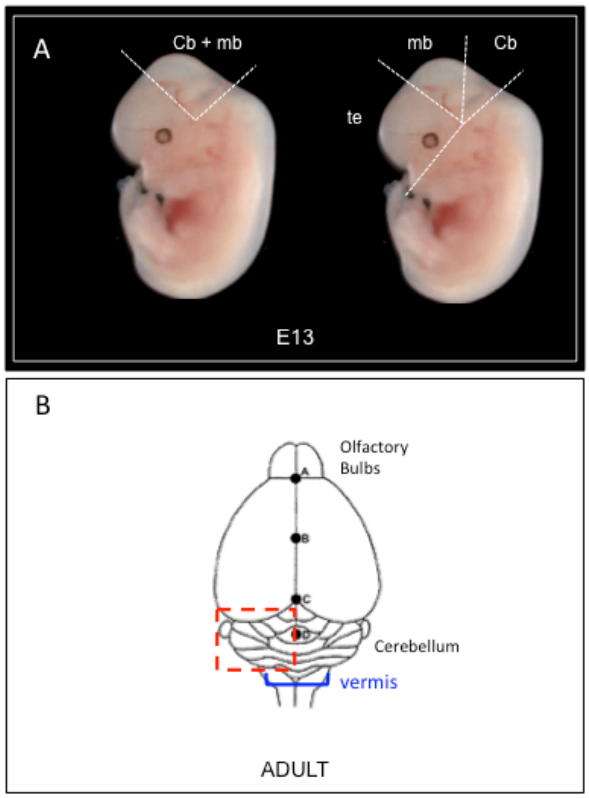

Fig. 3.1: Scheme of dissection of E13 embryos and adult brain. A) E13 embryonic brain is dissected by isolating the cerebellum (Cb) and portion of midbrain (mb) (left) or through a fine dissection (right) in which cerebellum, midbrain and telencephalon (te) are separated. B) Adult brain is dissected to isolate the cerebellum. For the analysis, half part of the cerebellum has been used (red dotted circumscribed portion).

3.3 Genotyping

The genotypes of the animals were assessed by extracting genomic DNA from tail. We used KAPA Mouse Genotyping Kit (KAPA Biosystems) for DNA extraction and amplification, as follow:

- *DNA extraction protocol*

Component	For 60 µl reaction	Final concentration
PCR-grade water	52.8 µl	–
10X KAPA Express Extract Buffer	6 µl	1X
1 U/µl KAPA Express Extract Enzyme	1.2 µl	1.2 U/reaction
Mouse tissue	as required	–

DNA extraction was performed in 60 µl volume. The reactions were incubated in a thermocycler for 10 minutes at 75°C to lyse cells and release DNA. The following incubation for 5 minutes at 95°C ensures the heat-inactivation of the thermostable KAPA Express Extract protease.

- *DNA amplification protocol*

DNA extracted from tissues was used as template for *Mid1* and *Sry* (on Y chromosome for sex determination) amplification. The reactions were assembled as indicated below:

Component	*Mid1* reaction	*Sry* reaction
PCR-grade water	Up to 15 µl	Up to 15 µl
2X KAPA2G Fast Genotyping Mix with dye	7.5 µl	7.5 µl
200 ng/µl Fw primer	0.25 µl	0.25 µl
200 ng/µl Rev primer	0.25 µl	0.25 µl
200 ng/µl Rev primer (Neo1)	0.25 µl	-
Template DNA	1 µl	1 µl

The PCR were performed with the following cycling protocol:

Step	Temperature	Time	Cycles
Initial denaturation	95 ºC	3 min	1
Denaturation	95 °C	15 sec	30
Annealing	58 °C (for *Mid1*) 54°C (for *Sry*)	15 sec	
Extension	72 °C	15 sec	
Final extension	72 °C	3 min	1

Mid1 PCR reactions were performed with the following primers:

- MID1 Null F and Neo1 to identify the presence of the knock-out allele (320 bp)
- MID1 Null F and MID1 Null R to identify the presence of the wild type allele (400 bp)

The PCR products were separated through electrophoresis on 1.5% agarose gel with intercalating dye (Gel Red Nucleic Acid Stain, Biotium) in 1X TAE buffer and visualised under UV light.

Example of the genotyping of E13 embryos is shown in Fig. 3.2.

Primer sequence:

MID1 Null F (Forward) 5'-GCTCCCAGTAAAGACAGAG-3'

MID1 Null R (Reverse) 5'-GAGCCCGTCTAGACCTCGC-3'

Neo1 (Reverse) 5'-CCAGAGGCCACTTGTGTAG-3'

mSRYf (Forward) 5'-GAGAGCATGGAGGGCCAT-3'

mSRYr (Reverse) 5'-CCACTCCTCTGTGACACT-3'

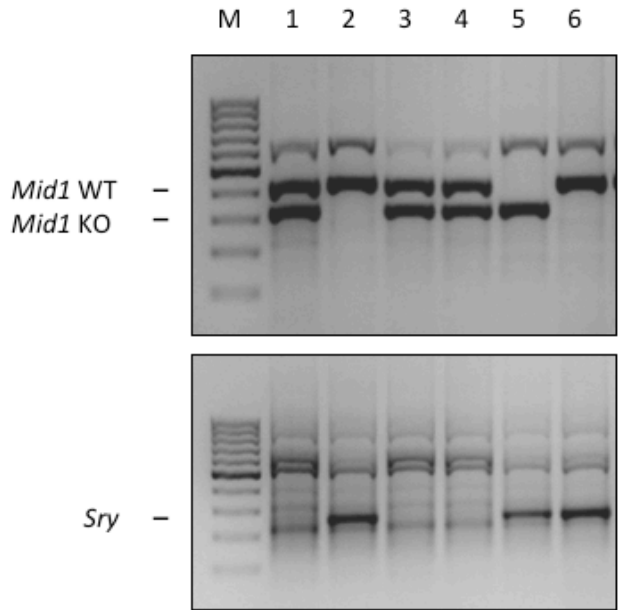

Fig. 3.2: E13 embryos genotyping. M: 100 bp molecular weight marker; Lane 1, 3, 4: heterozygote females; Lane 2, 6: *Mid1*$^{+/Y}$ male; Lane 5: *Mid1*$^{-/Y}$ male.

3.4 Constructs

MycGFP-MID1, expressing a MycGFP-tagged form of human MID1, and MycGFP-empty vector constructs are pcDNA3 cloning vector-based (Cainarca et al., 1999). Plasmids were prepared with the QIAGEN-tip 100 plasmid kit following the manufacturer's instructions.

3.5 Mass Spectrometry

The tissues from three pairs of *Mid1* wild type and knock-out embryos were collected from E13 embryonic brains as previously described (see *3.2.1 Embryos harvesting and dissection*). The samples were sent frozen to the FingerPrints Proteomics Facility - Centre for Translation and Interdisciplinary Research (CTIR) - (College of Life Sciences, University of Dundee), for mass spectrometry analysis. Briefly, the samples were processed with the Filter Aided Sample Preparation (FASP) method, followed by a quality control checking through the Linear Trap Quadropole (LTQ) Velos MS system. The label-free quantitative mass spectrometry (LFQ-MS) was carried out by nano LC-MS/MS using LTQ Orbitrap Velos Pro MS systems. The data were processed through MaxQuant software and analysed with ProStar software (Wieczorek et al., 2017).

3.6 Cell line culture

HEK293T (human embryonic kidney), hTERT-RPE (human retinal pigment epithelium) and NIH/3T3 (mouse embryonic fibroblast) were maintained in Dulbecco's Modified Eagle Medium (DMEM) supplemented with 10% FBS, 4mM L-glutamine, 100U/ml penicillin, 100μg/ml streptomycin, at 37°C with 5% CO_2.

3.7 Mouse embryonic fibroblasts

Mouse Embryonic Fibroblasts (MEFs) were prepared from *Mid1*$^{+/Y}$ and *Mid1*$^{-/Y}$ embryos as follow. Embryos from E13.5 pregnant mice were harvested and the head of the embryos was removed and saved for genotyping (see above). The embryos were placed in 10-cm cell culture dish and minced with a sterile razor blade. After 10 minutes of trypsin digestion at 37°C, complete growth medium was added and the suspension was pipetted 10-20 times to further break up tissues. The cellular suspension was then transferred to 10-cm plate and regularly cultured.

3.8 Primary cerebellar granule cells

Primary erebellar Granule Cells (GCs) were obtained from P7 *Mid1* wild type and knock-out mice. Every neuronal preparation started from mice belonging to the same litter. The day before pups were collected, coverslips and plates were coated with 20μg/ml poly-L-ornithine o/n at 37°C. The pups were sacrificed by decapitation and immediately brain was removed from the skull and kept in cold 1X PBS. The cerebellum was carefully separated and the dorsal cerebellar meninges were removed piecewise. When the cerebellum was fully stripped of meninges and choroid plexus, the dissected tissue was transferred in Hank's Balanced Salt Solution (HBSS), cut in 3-4 pieces with a sterile blade and digested with 2.5% trypsin (Euroclone) for 10 minutes at 37°C. The enzyme was inactivated through 0.5mg/ml trypsin inhibitor (Sigma) in HBSS and 0.1 mg/ml DNAse I (Sigma) in HBSS was added. Tissue was mechanically dissociated in 1ml dissociation medium (0,03mg/ml DNAse I, 0.3mg/ml trypsin inhibitor, HBSS) with 1ml serological pipette by repeatedly passing the cell suspension throughout the tip of the pipette pressed against the bottom of the tube, since the suspension resulted as homogenous as possible. The single cell suspension was then centrifuged and the pellet was resuspended in the desired volume of GCs complete medium (10% FBS, 25mM KCl, 2mM L-glutamine, 10mM HEPES pH 7.3, 100U/ml penicillin, 100μg/ml streptomycin, Basal Medium Eagle). Neurons were plated at about

250,000 cells/cm^2 and after 24 hours were supplemented with 10μM cytosine β-D-arabinofuranoside (AraC) to block the synthesis of DNA, thus decreasing the amount of glial cells in the culture. Neurons on coverslips were fixed at different days in vitro (DIV) with 4% PFA/PBS and coverslips were stored in PBS 1X at 4°C before immunofluorescence experiments.

3.9 Transient transfection

HEK293T cells were transiently transfected with standard calcium phosphate method of plasmid transfection (Graham and van der Eb, 1973):

- Solution A was prepared with 2X HBS (Hepes 10g/L, NaCl 16g/L) pH 7.1 and 100X 1:1 mix of 70mM Na_2HPO_4 and 70mM NaH_2PO_4.
- Solution B was prepared with 2M $CaCl_2$ (final concentration = 125mM), DNA and ddH_2O.
- Solution B was slowly (drop-wise) added to solution A while aerating the mix.
- This final mix was left for 20 minutes at RT and then added to cell culture.
- After 16 hours the cell medium was replaced with fresh complete growth medium.

For NIH/3T3 and hTERT-RPE cells transient transfection, MycGFP-MID1 and MycGFP-empty vector were transfected with Lipofectamine 3000 (Invitrogen) according to the manufacturer's instructions.

3.10 Co-immunoprecipitation

HEK293T cells were lysed in non-denaturing lysis buffer (or the less stringent TKM lysis buffer, as indicated) 60 hours after transfection. Cell lysates were incubated with 0,5μg of the antibody overnight at 4°C. The immunocomplexes were incubated with protein A sepharose beads for 3 hours at 4°C and then collected by centrifugation (at 4000 rcf for 5 minutes). The unbound proteins were kept in the supernatant. The beads were washed once with the lysis buffer and three times with IP wash buffer (or with PBST when the cells are lysed with TKM buffer). Immunoprecipitated (IP) proteins were resuspended with 2X loading buffer and analysed by immunoblot, after 5 minutes of boiling.

3.11 Immunofluorescence

For immunofluorescence analysis 25,000 cells/cm^2 were seeded on glass coverslips. When they reached the confluency needed for each experiment, cells were washed in

PBS 1X and fixed with 4% PFA in PBS for 10 minutes at RT. Cells were then washed 3 times in PBS 1X.

Fixed cells were permeabilised with 0.1% Triton X-100 in PBS for 30 minutes at RT, washed 3 times in PBS 1X and blocked with 5% BSA/PBST for 1 hour at RT. Cells were then incubated with primary antibodies in 1% BSA/PBST for 3 hours at RT and washed 3 times in PBS 1X before the incubation with Cy3-conjugated secondary antibodies (1 hour at RT). Coverslips were washed 3 times in PBS 1X and once with distilled water and then mounted with Vectashield mounting medium with DAPI (Vector Laboratories) for nuclei staining and cells were analysed with epifluorescent microscopy.

3.11.1 Immunofluorescence signal analysis

All the immunofluorescence experiments are performed as biological triplicate. Three random fields for each experiment are selected and the analysis has been performed as follow. For each experiment cells have been classified into two categories: transfected (MycGFP-empty vector or MycGFP-MID1) or non-transfected cells. Within each category cells have been grouped in two additional categories (strong- or weak-signal) depending on the intensity of the detected nuclear signal. Percentage of the cells falling onto single category has been assessed for each experiment and then the mean of the three percentages has been calculated. The results are expressed as the delta between the transfected cells and the mean of the non-transfected cells, both for strong-signal and weak-signal groups.

3.12 Subcellular fractionation

hTERT-RPE cells were transfected as described above. After 48 hours cells were collected and washed in PBS 1X. The cell pellet was lysed in CE buffer and 1/5 of the total volume was saved as whole cell lysate. After 4 minutes centrifugation at 210 rcf at 4°C, the cytoplasmic proteins were kept in the supernatant. The pellet that contained the nuclear fraction was washed once with CE buffer without NP-40. The nuclear pellet was resuspended with NE buffer supplemented with 1.2M NaCl and mixed by repeatedly vortexing the fraction. 20% of glycerol was added to the cytoplasmic fraction before freezing. The whole cell lysate and all the fractions were diluted with loading buffer and analysed through western blot.

3.13 SDS-PAGE and immunoblotting

Collected tissues and cell pellet were lysed in RIPA buffer and, after 17,000 rcf centrifugation for 15 minutes, soluble fraction was collected, whereas the insoluble part was protein extracted using Urea buffer. The extracted proteins were quantified through Bradford assay and prepared for immunoblot analysis by adding loading buffer to 1X final concentration. Protein samples were separated on 7.5%, 10% or 12% SDS-PAGE and blotted onto PVDF membranes (Millipore), previously rinsed in isopropanol. The transfer conditions were 30V 90mA for 16 hours at 4°C (for >80kDa proteins) or 100V 350mA for 90 minutes at room temperature (RT) (for <80kDa proteins). The membranes were incubated with Ponceau red solution, then washed in TBST and blocked in 5% dry milk/TBST for 1 hour. Incubation with primary antibodies was performed for 1-3 hours at RT or over-night (o/n) at 4°C. Membranes were washed 3 times in TBST and incubated at RT for 1h with HRP-conjugated secondary antibodies. After 3 washing in TBST, signal was detected with ECL substrate (Millipore). Relative quantification of blots was performed with ImageJ software (http://rsb.info.nih.gov/ij/index.html), which provides densitometry plot corresponding to the intensity of each band. Ponceau red staining was used as loading control.

3.14 SNARE complexes analysis

Brain tissues were collected as described above. Samples were homogenised in RIPA buffer and clarified by a centrifugation at 17,000 rcf for 15 minutes. Protein concentration from each sample was measure through the Bradford method. Equal amount of proteins was either boiled (5 minutes at 95°C) to disrupt SDS complexes or kept at 4°C (non-boiled samples, SDS resistant complexes) before being subjected to SDS-PAGE. Proteins were separated on 10% acrylamide gel in order to detect both the higher molecular weight complexes and the lower molecular weight monomers. The blotting on PVDF membrane was performed at 4°C (30V 90mA for 16 hours) and SNARE complexes and SNARE proteins were visualised by immunoblotting using anti-Snap25, anti-Syntaxin1A and anti-Vamp2 antibodies.

3.15 Antibodies

The following antibodies were used in this work:

Antibody	Code	WB	IF	IP
anti-Arl13B	17711-1-AP ProteinTech	1:6000		
anti-β tubulin TUB2.1	T4026 Sigma	1:8000		
anti-Exosc10	A303-987A Bethyl	1:5000	1:200	0.5µg
anti-Exosc8	EPP12871-60 Elabscience	1:5000	1:100	
anti-MID1	A302-227A Bethyl	1:4000		
anti-Snap25	111 011 SYSY	1:5000		
anti-Syntaxin1A	110 001 SYSY	1:5000		
anti-Vamp2	104 211 SYSY	1:5000		
Anti-c-Myc 9E10	M4439 Sigma	1:5000		0.5µg

3.16 Synaptosome fractionation

Embryonic cerebellum was dissected from E13 mouse embryo as previously described and kept on ice. Tissue was homogenised in 500µl of ice-cold homogenising buffer and then centrifuged 10 minutes, at 3000 rcf at 4°C. The pellet, containing membranous and lipid fraction, was stored at -80°C. The supernatant, containing cytoplasm, synaptosomes, myelin and mytochondria was recovered and centrifuged for 12 minutes at 14,000 rcf at 4°C. Cytosolic fraction in the supernatant was stored at -80°C, while the pellet was resuspended in 110µl of ice-cold Krebs-Ringer buffer. 90µl of ice-cold Percoll (final ~45% v/v) was added and mixed well by gently inverting the tube. Centrifugation at 17,000 rcf for 2 minutes at 4°C separated the synaptosome-enriched fraction on the surface of the flotation gradient. The underlying solution was discarded, the synaptosome fraction was resuspended in 1ml of ice-cold Krebs-Ringer buffer and centrifuged for 30 seconds at 17,000 rcf at 4°C. The pelleted synaptosomes were resuspended in 50µl of ice-cold RIPA buffer and stored at -80°C. All the collected fractions were prepared in loading buffer and boiled at 95°C for 5 minutes before been subjected to SDS-PAGE analysis. For immunoblot detection, examined protein amounts for each fraction are the following: homogenate 8µl/500µl; synaptosomes 8µl/50µl; membranes 10µl/100µl; cytosol 15µl/2ml.

4. RESULTS AND DISCUSSION

4.1 *Mid1*$^{+/Y}$ and *Mid1*$^{-/Y}$ differential proteomics analysis in the developing cerebellum.

Mutations in the *MID1* gene are responsible for the Opitz G/BBB syndrome in human, which is characterised by midline developmental defects. The mouse line carrying a nonfunctional ortholog of the human *MID1* gene, *Mid1*, (*Mid1* knock-out, *Mid1*$^{-/Y}$) recapitulates the brain morphological abnormalities observed in patients, i.e. hypoplasia of the anterior cerebellar vermis. However, the role of *Mid1* in cerebellar development is still unknown. The *Mid1*$^{-/Y}$ cerebellar defect is first morphologically observed at Embryonic day (E) 13.5, a stage when we detect rostralization of the midbrain-hindbrain boundary as well as *Fgf17* down-regulation (Lancioni et al., 2010) (see Introduction).

In order to further dissect the molecular pathways affected by the lack of *Mid1*, we focused on stage E13 when *Mid1* is highly expressed in the developing cerebellar and dorsal midbrain regions but no morphological signs are observed yet. With an unbiased approach of differential proteomic profiling we compared *Mid1* wild type (*Mid1*$^{+/Y}$) and *Mid1*$^{-/Y}$ developing cerebella. To minimize staging-associated variability as much as possible, we employed 3 pairs of *Mid1*$^{-/Y}$ and *Mid1*$^{+/Y}$ male littermates. E13 embryos have been harvested and dissected to isolate the cerebellar anlage (the site of the future defect) and the inferior and superior colliculus (the region of elevated *Mid1* expression at this stage). The 6 *Mid1*$^{-/Y}$ and *Mid1*$^{+/Y}$ collected samples have been protein extracted and subjected to label-free quantitative mass spectrometry (LFQ-MS) with LTQ Orbitrap Velos Pro MS systems, followed by processing by MaxQuant software at the FingerPrints Proteomics Facility of the School of Life Sciences at the University of Dundee, UK. Analysis of the 2,401 proteins detected by the MS system revealed peptides accounting for only 5 proteins presenting quantitative unbalance: Thsd7a, Gprin1, Osbpl9, Rab3a and Llph (FDR = 6.65%). Clustering of the wild-type and knock-out genotypes was assessed through heatmap visualisation of protein values (data not shown).

Due to the features of the analysis performed, the dataset included missing values. Indeed, this is quite common in this kind of studies as the data can be missing either when proteins are quantified in some replicates but not in others or when proteins are not quantified in specific conditions (i.e. depending on genotype), indicating that

proteins are below the detection limit in specific sample, which biologically could be highly meaningful. Thus, as commonly performed, an additional analysis was carried out to integrate the results through imputation of the missing values. We first filtered out proteins that contain too many missing values along the 6 samples and the non randomic missing data were imputed by a left-censored imputation method (quantile regression-based left-censored function "QRILC"). By a deterministic approach, QRILC replaces the missing entries with a minimal value observed in that sample, which is estimated as being the q-th quantile (e.g. q = 0.01) of the observed values in that sample. The new data set obtained after imputation, accounts for 2,614 proteins and was analysed through the ProStar software and the clustering of the genotypes was visualised on heatmap (Fig. 4.1A). These bioinformatics analyses have been performed in collaboration with Danilo Licastro, Cluster in Biomedicine, Trieste.

Statistical analysis revealed 26 proteins presenting quantitative unbalance: 16 proteins more abundant and 10 proteins showing reduced level in *Mid1*$^{-/Y}$ compared to the *Mid1*$^{+/Y}$ (logFC 0.5; p-value 0.05) (Fig. 4.1B, Table 4.1).

A

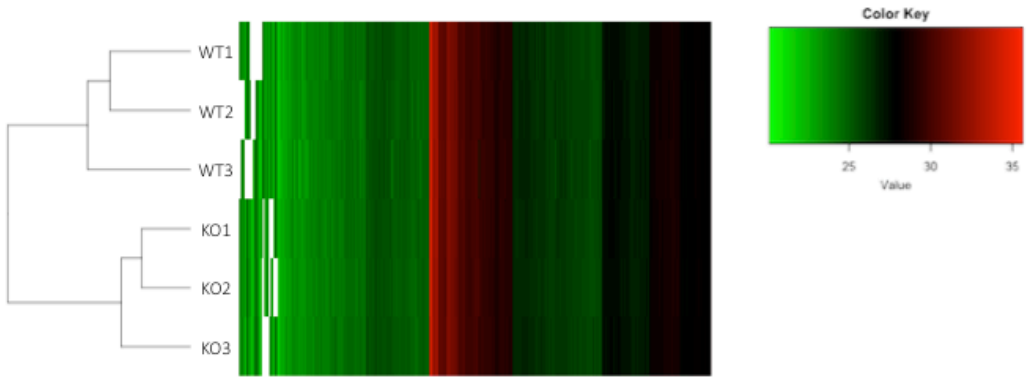

B

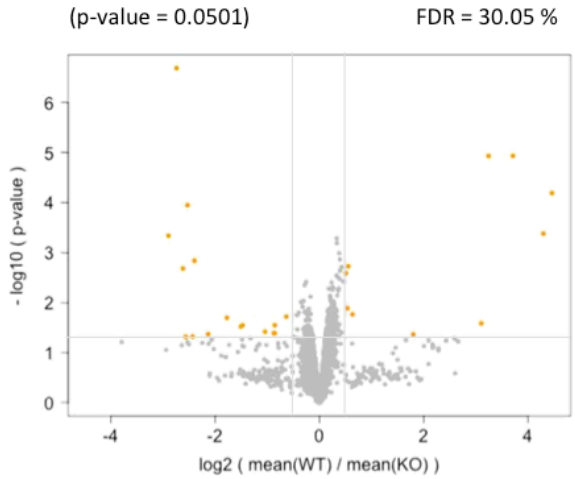

Fig. 4.1: Mass spectrometry data analysis after imputation. A) Heatmap reflecting protein expression value in *Mid1*$^{+/Y}$ (WT) and *Mid1*$^{-/Y}$ (KO) samples. Note the separate clustering of the genotypes. B) Volcano plot showing proteomic results (–log10(p-value) threshold: 1.3; logFC 0.5; p-value 0.05).

Protein symbol	Full name	p value	Log FC (WT/KO)
Igsf8	immunoglobulin superfamily member 8	0,0004592	-2,8945
Polr2j	RNA polymerase II subunit j	0,0000002	-2,7403
Pwp1	PWP1 homolog, endonuclein	0,0020747	-2,6173
Exosc10	exosome component 10	0,0481957	-2,5616
Rfc5	replication factor C subunit 5	0,0001124	-2,5294
Myl9	myosin light chain 9	0,0475105	-2,4308
Q5EBG8	uncharacterized protein C1orf50 homolog	0,0014461	-2,3979
Exosc8	exosome complex component RRP43	0,0423510	-2,1331
Cops9	COP9 signalosome complex subunit 9	0,0199773	-1,7727
Erbin	Erbb2 interactin protein	0,0298222	-1,5061
Gins4	DNA replication complex GINS protein SLD5	0,0283804	-1,4709
Lrwd1	leucine rich repeats and WD repeat domain containing 1	0,0379177	-1,0432
Iars2	isoleucine--tRNA ligase, mitochondrial	0,0406060	-0,8728
Ptgis	prostacyclin synthase	0,0407752	-0,8582
Arsa	arylsulfatase A	0,0281152	-0,8557
Llph	protein LLP homolog	0,0189780	-0,6328
Gprin1	G protein-regulated inducer of neurite outgrowth 1	0,0025832	0,5085
Osbpl9	Oxysterol-binding protein-related protein 9	0,0129280	0,5396
Rab3a	Ras-related protein Rab-3A	0,0018626	0,5584
Thsd7a	thrombospondin type-1 domain-containing protein 7A	0,0171536	0,6351
Dst	dystonin	0,0428048	1,8012
Snap25	Synaptosomal-associated protein 25	0,0259495	3,1079
Ube2r2	Ubiquitin-conjugating enzyme E2 R2	0,0000117	3,2471
Tarbp2	RISC-loading complex subunit TARBP2	0,0000117	3,7147
a-syn	alpha-synuclein	0,0004160	4,2985
Tmx3	Protein disulfide-isomerase TMX3	0,0000643	4,4625

Up-regulated Down-regulated

Table 4.1: List of 26 unbalanced proteins in *Mid1*$^{+/Y}$ (WT) and *Mid1*$^{-/Y}$ (KO) E13 developing embryos (green: up-regulated proteins; red: down-regulated proteins). The five proteins identified through the first analysis before imputation are indicated with the black bar on the left.

4.2 Altered pathway in *Mid1*$^{-/Y}$ developing cerebella.

The differentially expressed (DE) proteins were subjected to Ingenuity Pathway Analysis (IPA) in order to identify the main networks and biological functions possibly affected in *Mid1*$^{-/Y}$ embryos. Not surprisingly neurological diseases were predicted to be the main term in the mutant embryos, as nervous system resulted the top score physiological system associated with the DE proteins. Moreover, IPA analysis suggested that *Mid1*$^{-/Y}$ embryos could present defects in cell morphology, cellular assembly and organisation as well as in cell-to-cell signaling and interaction (Table 4.2).

Top diseases and biological functions	*p value*	*#Molecules*
Neurological disease	4.91E-02 - 1.86E-04	8
Cancer	4.49E-02 - 1.12E-03	20
Cardiovascular disease	3.84E-02 - 1.12E-03	3
Connective tissue disorders	1.12E-03 - 1.12E-03	1
Top biological functions	*p value*	*#Molecules*
Cellular assembly and organization	4.81E-02 - 1.20E-05	10
Cell morphology	4.27E-02 - 2.63E-05	7
Cell-to-cell signaling and interaction	4.59E-02 - 6.56E-05	6
Cellular movement	3.63E-02 - 7.59E-05	4
Cell death and survival	4.88E-02 - 1.86E-04	5
Physiological system development and function	*p value*	*#Molecules*
Nervous system development and function	4.88E-02 - 2.63E-05	7
Tissue morphology	4.90E-02 - 2.63E-05	7
Behavior	4.81E-02 - 1.12E-03	4
Connective tissue development and function	3.35E-03 - 1.12E-03	2
Embryonic development	4.27E-02 - 1.12E-03	7
Top associated networks		
Cell morphology		
Cell-to-cell signaling and interaction		
Cellular assembly and organization		

Table 4.2: IPA analysis. Top networks and functions associated with the *Mid1*$^{+/Y}$ (WT)/ *Mid1*$^{-/Y}$ (KO) differentially expressed proteins.

4.3 Exosc8 is altered following lack of Mid1 in mutant embryos.

Our differential proteomic analysis showed that, among others, developing *Mid1*$^{-/Y}$ cerebella present increased protein level of two RNA exosome complex components: Exosc8 and Exosc10. Exosomes are multi-protein complexes essential for proper RNA processing (Chlebowski et al., 2013; Kilchert et al., 2016) and several mutations in various components are known to cause widespread developmental defects (Di Donato et al., 2016; Burns et al., 2018; Morton et al., 2018). Therefore, the central nervous system appears the most affected compartment. In particular, different EXOSC2, EXOSC3, EXOSC8 and EXOSC9 variants in humans are associated with progressive neurological disease, characterised by intellectual disability, abnormal myelination of central nervous system, spinal muscular atrophy and also cerebellar and corpus callosum hypoplasia (Boczonadi et al., 2014; Di Donato et al., 2016; Fasken et al., 2017; Schottmann et al., 2017; Burns et al., 2018). Specifically, EXOSC8 is an essential protein of the exosome core and mutations in *EXOSC8* gene have been linked to pontocerebellar hypoplasia type 1c (Boczonadi et al., 2014). In addition, experiments in zebrafish embryos defined that deregulation of *exosc8* lead to morphological brain abnormalities, suggesting that exosc8 is essential for proper brain development in zebrafish (Boczonadi et al., 2014). This evidence prompted us to investigate the role of Exosc8 in developing mouse cerebella, assessing the possible involvement of Mid1 in its regulation. In order to confirm the MS results, independent E13 *Mid1*$^{+/Y}$ (n=10) and *Mid1*$^{-/Y}$ (n=10) embryos have been collected and dissected as previously described. The developing cerebellum and dorsal midbrain samples were protein extracted and the soluble fractions subjected to electrophoretic separation through SDS-PAGE system before being analysed with anti-Exosc8 antibody (Fig. 4.2A, left panel). Strikingly however, opposed to MS differential proteomic data, the results show a decrease of Exosc8 protein level in *Mid1*$^{-/Y}$ samples compared to the *Mid1*$^{+/Y}$ (Fig 4.2B, left). Nonetheless, since exosome proteins are associated in a stable ribonuclease complex within either the nuclear or cytoplasmic compartment of the cell (Chlebowski et al., 2013), we reasoned that exosome complex components might not be completely soluble in canonical RIPA buffer. Therefore, we examined protein extracted from the insoluble fraction for Exosc8 protein level (Fig. 4.2A, right panel) and we found a slight increase of protein amount in developing mutant cerebella compared to the *Mid1*$^{+/Y}$ (Fig. 4.2B, right), in accordance with MS results. Notably, in the *Mid1*$^{-/Y}$ compared to the *Mid1*$^{+/Y}$ samples we observed an opposite trend regarding the Exosc8 protein level in the two

fractions, suggesting that the variation of the exosome core protein amount could depend on its subcellular localisation or activity. However, taken together, the difference of Exosc8 protein level in the soluble and insoluble fraction was not sufficient to support the MS data. A possible reason for that could concern the relatively high variability of the samples, due to inevitable biological diversity between embryos at that stage. Considered that, we decided to study not only the protein amount, but also the localisation of Exosc8 in a simplified biological system.

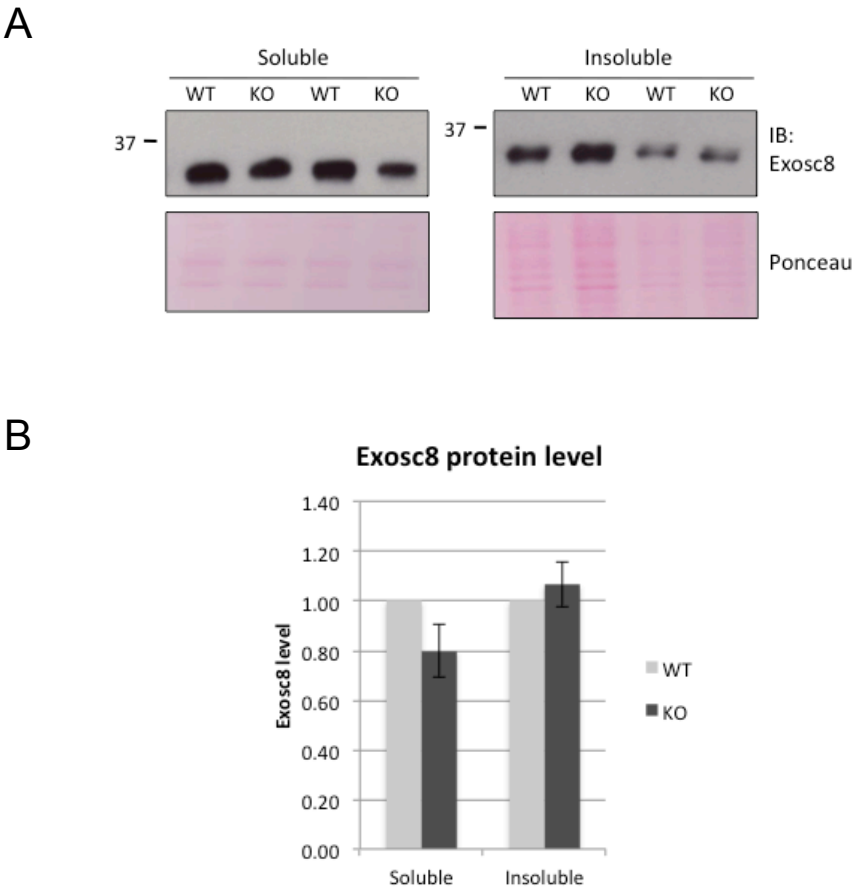

Fig. 4.2: Exosc8 protein level in E13 *Mid1*$^{+/Y}$ (WT) and *Mid1*$^{-/Y}$ (KO) developing cerebella and dorsal midbrain. A) Representative immunoblot of Exosc8 level in soluble (left) and insoluble (right) fractions. Signal intensity was normalised to ponceau red staining as loading control. B) Quantification of the immunoblots in A as the mean of 5 *Mid1*$^{+/Y}$ and 4 *Mid1*$^{-/Y}$ embryos for the soluble fraction, and 9 *Mid1*$^{+/Y}$ and 9 *Mid1*$^{-/Y}$ embryos for the insoluble fraction. Exosc8 protein level in the *Mid1*$^{+/Y}$ samples is considered as 1 (bars = sem).

In literature, different patterns of exosome core subunits localisation have been reported, owing to the cell type and the organism that have been considered (Brouwer et al., 2001; Graham et al., 2006; Graham et al., 2009; Tomecki et al., 2010; Silla et al., 2018). Consequently we first defined the normal distribution of Exosc8 in *Mid1*$^{+/Y}$ primary cells. Since, granule neurons represent the most abundant neuronal population in cerebellum and it is commonly assumed that growing them in culture for several days recapitulates many of the processes that occur during cerebellar development, primary cerebellar granule cells (GCs) were isolated from seven-days old wild-type pups (P7) and maintained in culture for 8 days. Exosc8 localisation was assessed through immunofluorescence in *Mid1*$^{+/Y}$ GCs after 3 days in vitro (DIV3), DIV6 and DIV8 (Fig 4.3). The results showed a clear nuclear localisation for Exosc8 at DIV3, while starting from DIV6, until DIV8, the exosome core protein migrated from the nucleus to a perinuclear structure, which could likely be the Golgi apparatus or the endoplasmic reticulum.

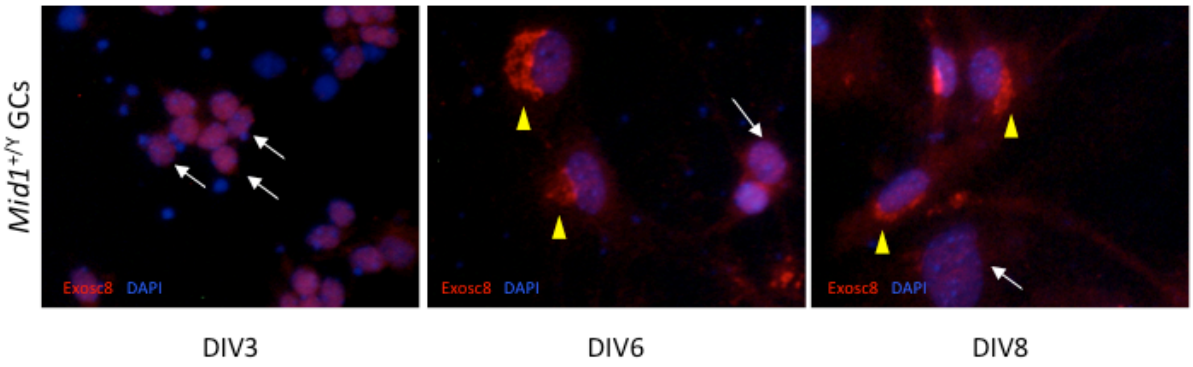

Fig. 4.3: Subcellular localisation of Exosc8 in P7 *Mid1*$^{+/Y}$ primary GCs. Immunofluorescence shows the distribution of Exosc8 (in red) in *Mid1*$^{+/Y}$ primary granule neurons at days in vitro (DIV) 3, DIV6 and DIV8. White arrows indicate the nuclear localisation of the protein; yellow arrowheads indicate the cytoplasmic distribution of Exosc8 in the Golgi-like structure. DAPI blue is used as nuclear staining.

We then assessed Exosc8 subcellular localisation in primary mouse embryonic fibroblasts (MEFs) prepared from E13.5 *Mid1*$^{+/Y}$ and *Mid1*$^{-/Y}$ embryos. Immunofluorescence using anti-Exosc8 of *Mid1*$^{+/Y}$ MEFs corroborated the specific localisation of the exosome core component observed from DIV6 GCs (Fig 4.4, upper panels). Interestingly, in *Mid1*$^{-/Y}$ MEFs Exosc8 appeared markedly mislocalised as compared with the *Mid1*$^{+/Y}$ cells (Fig 4.4, lower panels). In fact, *Mid1*$^{-/Y}$ MEFs presented a predominant nuclear distribution of exosome core component, with a punctate pattern within the nucleus, whereas the Golgi-like localisation was virtually completely absent. These results indicate that the depletion of Mid1 is associated with defective distribution of Exosc8 between nucleus and cytoplasm, rather than with alteration of the total amount of the exosome core protein.

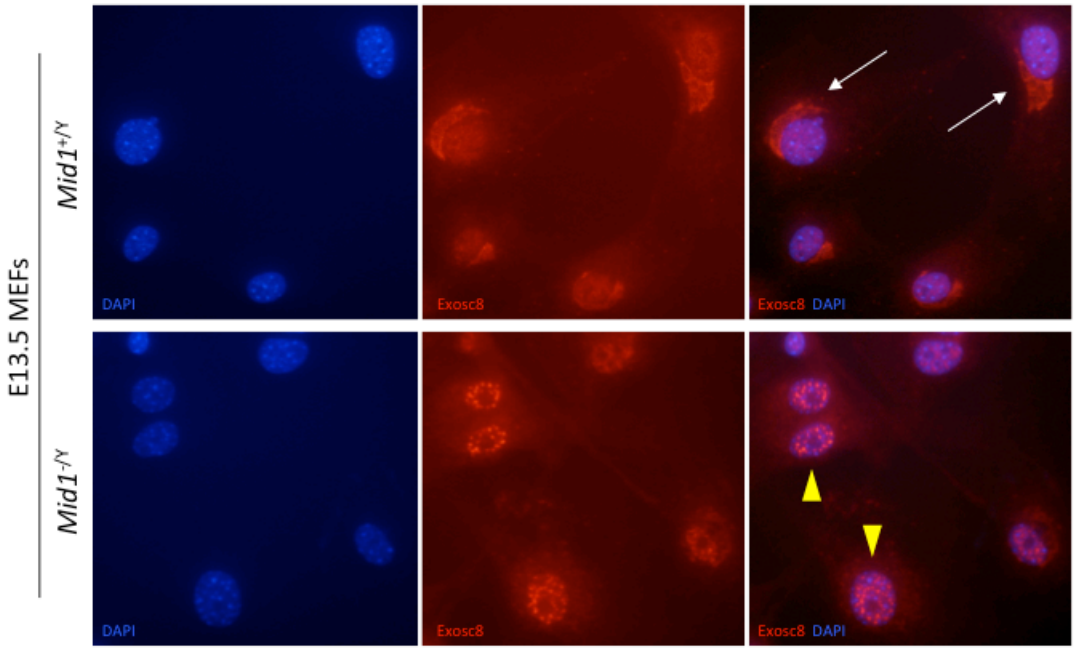

Fig. 4.4: Exosc8 presents a mislocalisation in *Mid1*$^{-/Y}$ MEFs. Immunofluorescence experiment showing Exosc8 localisation in E13.5 *Mid1*$^{+/Y}$ (upper panels) and *Mid1*$^{-/Y}$ MEFs (lower panels). White arrows indicate the proper perinuclear distribution of Exosc8 in wild type fibroblasts; yellow arrowheads indicate the predominant nuclear localisation of the protein in the *Mid1*$^{-/Y}$ MEFs. DAPI blue is used as nuclear staining.

4.4 EXOSC8 level and nuclear distribution are affected by overexpression of MID1.

The above data confirm that localisation of Exosc8 is affected in *Mid1*$^{-/Y}$ embryos, at least in embryonic fibroblasts. As Mid1 is an E3 ubiquitin ligase, we reasoned that physiologically it could regulate the stability of this protein in specific subcellular compartment through proteasome-mediated ubiquitin degradation, or control the transport between nucleus and cytoplasm, as it is reported that ubiquitination can mediate the nucleocytoplasmic shuttling of the proteins (Komander and Rape, 2012). In order to understand the mechanism that mediates the deregulation of Exosc8 in the *Mid1*$^{-/Y}$ embryos, we started investigating the connection between Mid1 and the RNA exosome core component. First, HEK293T cells were transfected with MycGFP-MID1 or MycGFP-empty vector as negative control and protein extracted. The soluble and the insoluble fractions were analysed through immunoblot with anti-EXOSC8 antibody (Fig. 4.5A). In line with the MS differential proteomic data, the quantification of both soluble and insoluble extracts revealed that MID1-overexpressing cells present reduced levels of the exosome core component compared to the control (Fig 4.5B).

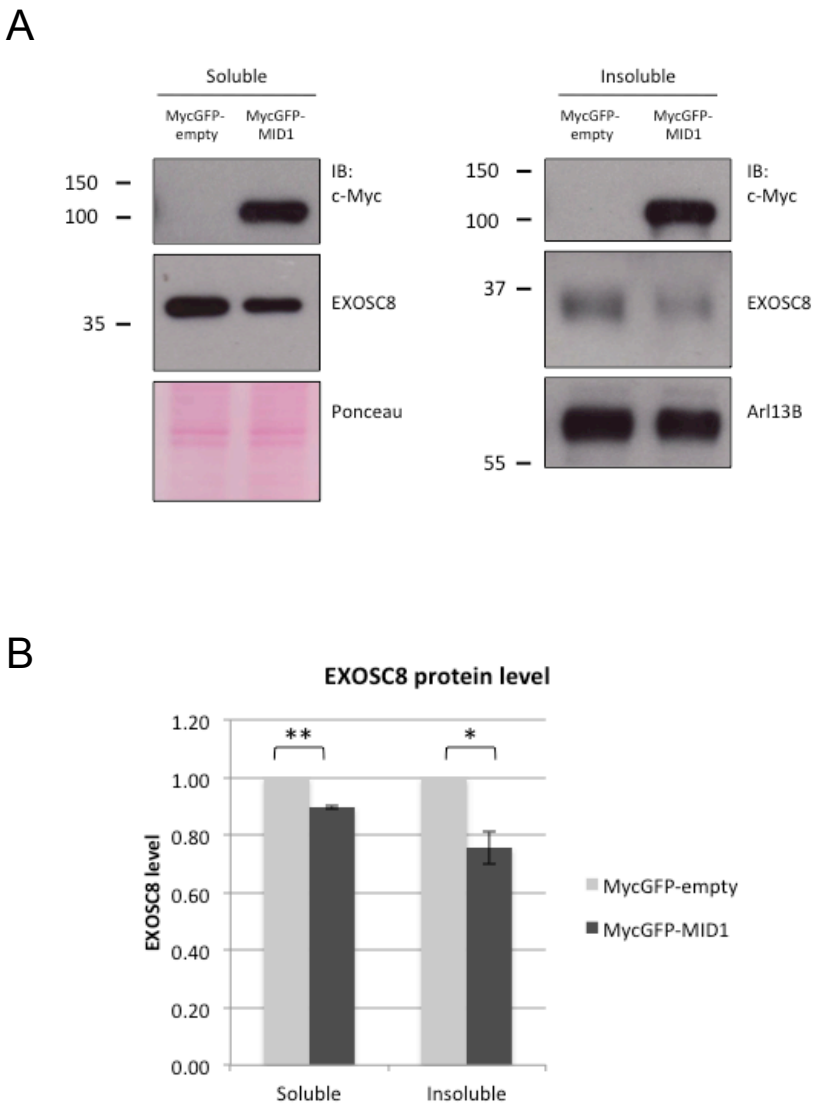

Fig. 4.5: EXOSC8 protein amount is affected by overexpression of MID1 in HEK293T cells. A) Representative immunoblots showing the reduction of the EXOSC8 endogenous level in both soluble and insoluble fraction of MID1-transfected HEK293T cells. MycGFP-empty vector is used as negative control. Overexpression of MycGFP-MID1 vector was confirmed by immunodetection of MycGFP-MID1 fusion protein using anti-c-Myc antibody. Ponceau red staining and immunoblot anti-Arl13B are used as loading control in soluble and insoluble experiments, respectively. B) EXOSC8 levels relative to loading control were quantified and reported in the graph as the mean of three independent experiments, considering EXOSC8 levels of MycGFP-transfected cells as 1 (bars = sem; t-test: *$p<0.05$ and **$p<0.01$).

In addition, in order to explore whether overexpression of MID1 is associated with altered distribution of EXOSC8 protein, as previously observed in *Mid1*$^{-/Y}$ MEFs, the epithelial cell line hTERT-RPE was transfected with MycGFP-MID1 construct or MycGFP-empty vector and EXOSC8 was detected through immunofluorescence with specific antibody (Fig. 4.6A). As reported in the literature, the exosome core protein clearly showed a preponderant nuclear localisation in non-transfected cells. The MID1-overexpressing cells display a significantly reduced EXOSC8 signal in the nucleus (Fig 4.6B). MycGFP-empty vector was used as negative control for the assay, confirming that reduction of nuclear level of EXOSC8 was effectively due to the presence of MID1 and not to unspecific GFP overexpression. Although GFP overexpression has indeed an effect on the detection of EXOSC8 signal, overexpression of MID1 has a significantly stronger effect on EXOSC8 change of localisation despite the fact that its expression level is much more physiological than that of GFP alone. Collectively, the results obtained in HEK293T and hTERT-RPE cells indicate that overexpression of MID1 not only causes downregulation of EXOSC8 protein level but also alters the nuclear localisation of this RNA exosome core component.

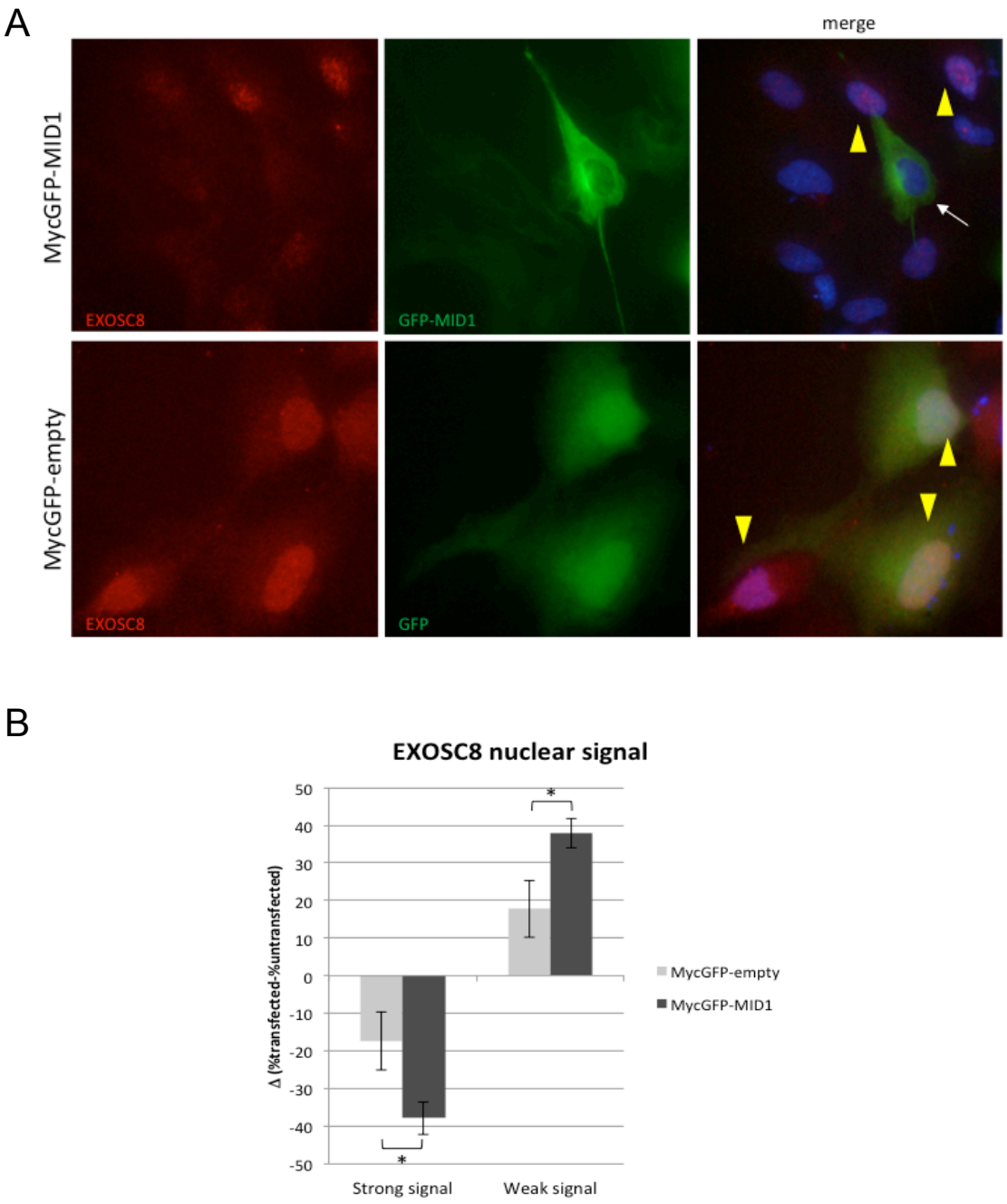

Fig. 4.6: MID1 overexpression is associated with reduction of EXOSC8 nuclear staining. A) Immunofluorescence experiments showing the localisation of EXOSC8 (red signal) in hTERT-RPE cells transfected with MycGFP-MID1 (upper panels) or MycGFP-empty vector (lower panels). Yellow arrowheads indicate the usual nuclear distribution of EXOSC8 in non-transfected and MycGFP-transfected cells; white arrows indicate change in EXOSC8 nuclear staining in MycGFP-MID1 transfected cells. B) Percentage of cells presenting strong or weak nuclear signal corresponding to EXOSC8 protein were calculated and plotted in the graph as Δ(%transfected-%untransfected). Despite the effect of MycGFP overexpression on EXOSC8 distribution, overexpression of MID1 determines a significantly stronger reduction of nuclear signal (bars = sem; t-test: *$p<0.05$).

4.5 Exosc10 protein level is specifically modulated by Mid1.

Another component of the RNA exosome complex that emerged from our MS differential proteomic data is Exosc10. EXOSC10 associates with the RNA exosome core and cleaves several types of RNAs through its 3′ to 5′ exoribonuclease activity (Chlebowski et al., 2013; Januszyk and Lima, 2014). Even though EXOSC10 is known to be important in the regulation of a variety of cellular processes (e.g. cellular differentiation, cell cycle progression, quality control of mRNA) (van Dijk et al., 2007; Graham et al., 2009; Januszyk et al., 2011; Fox and Mosley, 2016), the role of EXOSC10 in neuronal cells and in the development of the nervous system is still unknown. In order to validate the MS results, additional developing cerebellum and dorsal midbrain samples have been collected from independent E13 *Mid1*$^{+/Y}$ (n=10) and *Mid1*$^{-/Y}$ (n=10) embryos. The soluble and the insoluble protein fractions of the extracted samples were examined by immunoblot with specific anti-Exosc10 antibody, after electrophoretic separation through SDS-PAGE system (Fig 4.7A). Consistent with the MS data, the results showed higher amount of Exosc10 protein in *Mid1*$^{-/Y}$ sample compared to the *Mid1*$^{+/Y}$ both in soluble and insoluble extracts with the latter being less variable and reaching statistical significance (Fig 4.7B).

The increased Exosc10 protein level was specifically due to the loss of Mid1, as the overexpression of the MycGFP-MID1 construct in HEK293T cells was able to revert this trend, leading to about 30% of decrease of the ribonuclease amount compared to the MycGFP-empty vector transfected cells (Fig 4.8A and B). The amount of EXOSC10 protein in the insoluble fractions was quite different amongst samples, making it difficult to unveil altered level of protein in this fraction, if any. On the contrary, the low variability of the soluble proteins enabled us to assess the strong reduction of EXOSC10 amount as a consequence of MID1 overexpression.

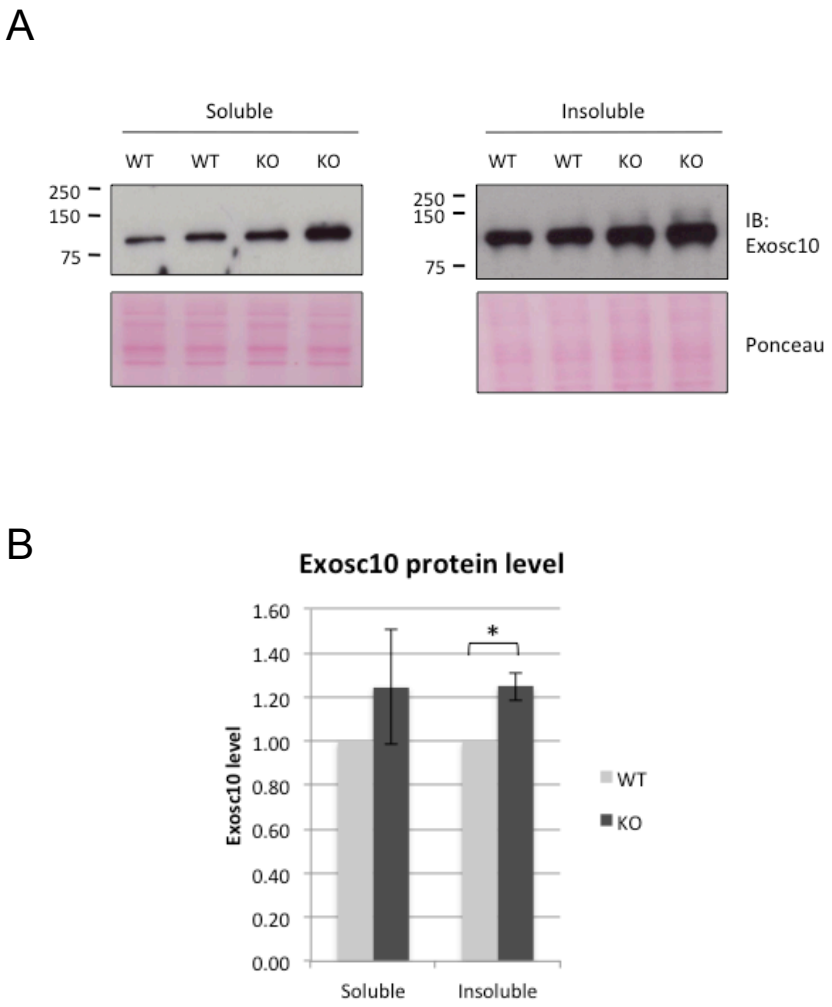

Fig. 4.7: Mid1 depletion increases the protein amount of Exosc10 in E13 developing cerebella. A) Representative immunoblot of Exosc10 level in soluble (left) and insoluble (right) protein fractions obtained from E13 *Mid1*$^{+/Y}$ (WT) and *Mid1*$^{-/Y}$ (KO) developing cerebella and midbrain. Ponceau red staining is used as loading control. B) Exosc10 levels were quantified and plotted in the graph. Results are indicated as the mean of 9 pairs of *Mid1*$^{+/Y}$ and *Mid1*$^{-/Y}$ embryos, considering Exosc10 protein level in the *Mid1*$^{+/Y}$ samples as 1 (bars = sem; t-test: *$p<0.05$).

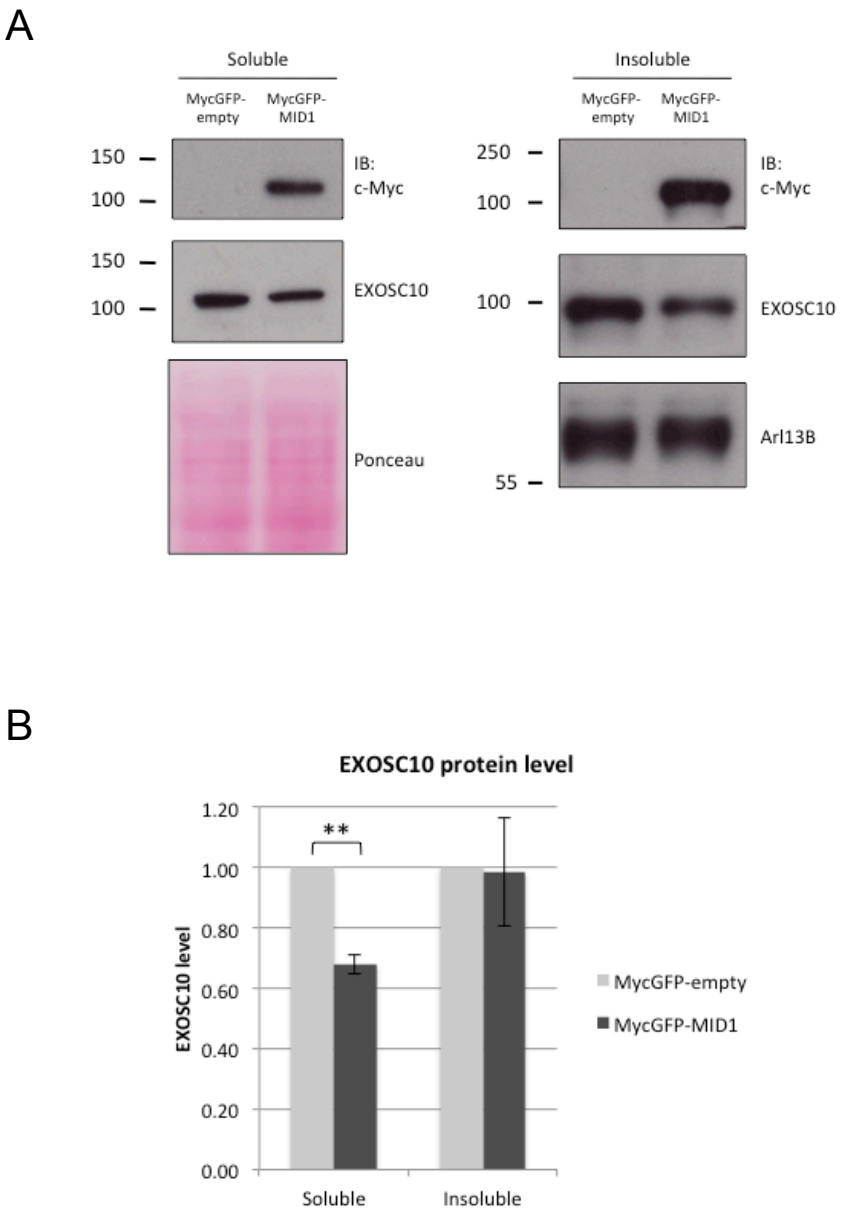

Fig. 4.8: MycGFP-MID1 transfected HEK293T cells exhibit decreased level of EXOSC10 protein. A) Representative immunoblots showing the endogenous amount of EXOSC10 in both soluble and insoluble fraction of MID1-transfected HEK293T cells. MycGFP-empty vector is used as negative control. Overexpression of MycGFP-MID1 vector was confirmed by immunodetection of MycGFP-MID1 fusion protein using anti-c-Myc antibody. Ponceau red staining and immunoblot anti-Arl13B are used as loading control in soluble and insoluble experiments, respectively. B) Normalised EXOSC10 levels are reported in the graph as the mean of three independent experiments, considering EXOSC10 levels of MycGFP-transfected cells as 1 (bars = sem; t-test: **$p<0.01$).

4.6 MID1 overexpression and Mid1 depletion do not affect the nuclear localisation of Exosc10.

The involvement of MID1 on EXOSC10 protein regulation was further examined through immunofluorescence analysis. hTERT-RPE cells were transfected with MycGFP-MID1 or MycGFP-empty vector as negative control and EXOSC10 was detected with specific antibody (Fig. 4.9A). Unlike EXOSC8, exhibiting a significant mislocalisation upon MID1 overexpression, the signal corresponding to EXOSC10, which is almost completely nuclear, did not undergo any variation in MID1-ovexpressing cells compared to either the non-transfected or negative control cells (Fig 4.9B). In accordance with this result, not even the loss of Mid1 resulted in the alteration of the nuclear localisation of Exosc10 protein in *Mid1*$^{-/Y}$ MEFs if compared to the *Mid1*$^{+/Y}$ MEFs (Fig 4.10).

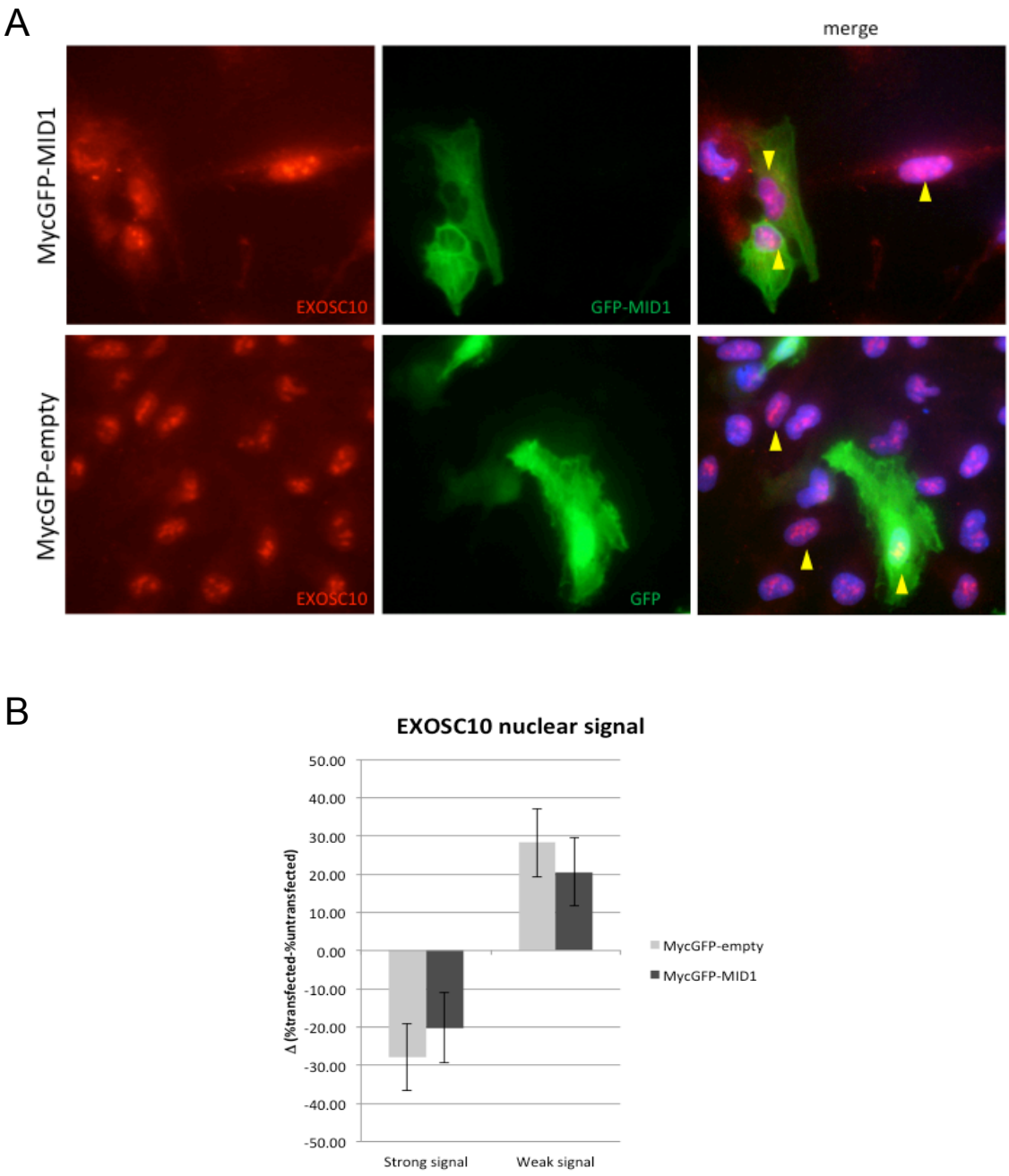

Fig. 4.9: MID1 overexpression does not affect the nuclear localisation of EXOSC10. A) Immunofluorescence experiments showing the localisation of EXOSC10 (red signal) in hTERT-RPE cells transfected with MycGFP-MID1 (upper panels) or MycGFP-empty vector (lower panels). Yellow arrowheads indicate the unchanged distribution of EXOSC10 within the nucleus of non-transfected, MycGFP-empty vector transfected and MycGFP-MID1 transfected cells. B) The graph represents the percentage of cells with strong or weak EXOSC10 nuclear staining expressed as Δ(%transfected-%untransfected). No significant variation in nuclear signal is observed between MycGFP and MycGFP-MID1 overexpressing cells (bars = sem).

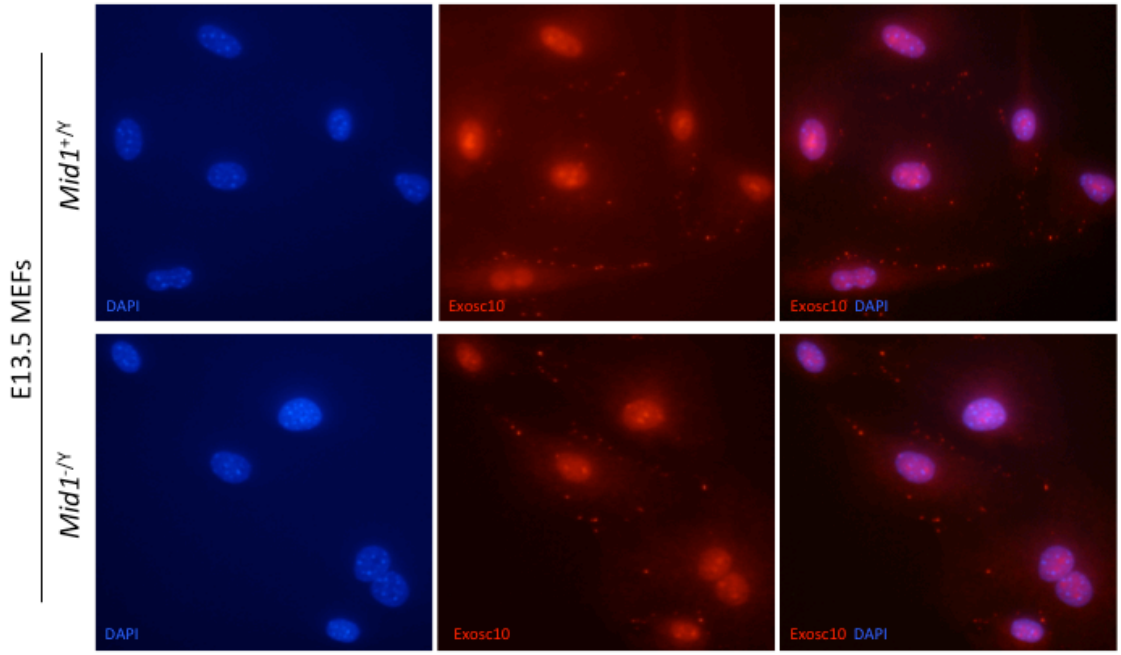

Fig. 4.10: Subcellular distribution of Exosc10 is not altered in *Mid1*$^{-/Y}$ fibroblasts. Exosc10 (red signal) shows an almost exclusively nuclear localisation in E13.5 *Mid1*$^{+/Y}$ (upper panels), which does not change upon Mid1 depletion (*Mid1*$^{-/Y}$ MEFs, lower panels). DAPI blue is used as nuclear staining.

Interestingly, by examining the subcellular distribution of EXOSC10 protein upon fractionation of transfected hTERT-RPE cells, we observed a slight reduction of cytoplasmic EXOSC10 level in the MID1-overexpressing cells with respect to the GFP-control cells (Fig 4.11). Whereas the nuclear fraction, which contains the majority of the protein, appeared similar in terms of EXOSC10 amount, as expected from above immunofluorescence results.

According to these results, a possibility is that Mid1 is involved in regulating the protein level of Exosc10 and this modulation might occur in the cytoplasm rather than in the nucleus.

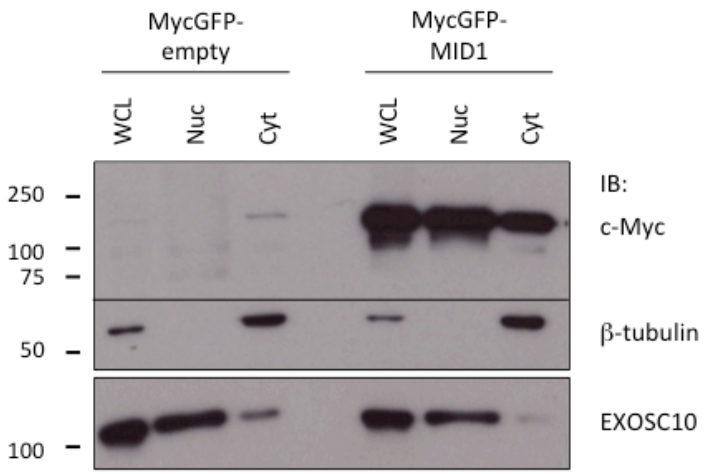

Fig. 4.11: EXOSC10 distribution in subcellular compartments. MycGFP-MID1 or MycGFP-empty transfected hTERT-RPE cells were fractionated in subcellular compartments. Whole cell lysates (WCL), nuclear (Nuc) and cytosolic (Cyt) fractions were subjected to SDS-PAGE protein separation and EXOSC10 protein was visualised through immunoblotting. MycGFP-MID1 overexpression was confirmed by immunodetection of MycGFP-MID1 fusion protein using anti-c-Myc antibody. b-tubulin was used as cytoplasmic marker to attest the correct fractionation of the samples.

4.7 EXOSC8 and EXOSC10 do not directly interact with MID1.

Our results demonstrated that Exosc8 and Exosc10 are both regulated by Mid1, presumably to different extent. However this modulation could be due to either a direct or indirect connection between Mid1 and the two RNA exosome components. To clarify this aspect, HEK293T cells were transfected with MycGFP-MID1 or MycGFP-empty vector for 60 hours before lysis in non-denaturing conditions to preserve protein interactions and co-immunoprecipitation was performed. MycGFP-MID1 protein was immunoprecipitated with anti-c-Myc, then endogenous EXOSC8 and EXOSC10 presence in complex with MID1 was investigated through immunoblot analysis with specific antibodies (Fig. 4.12A). The results showed that neither EXOSC8 nor EXOSC10 is retrieved with the immunoprecipitation of overexpressed MID1, at least in the conditions employed, indicating that MID1 regulates the RNA exosome complex proteins through an indirect mechanism. The same result was obtained also when the cells are lysed in the less stringent TKM buffer (data not shown). To further confirm the

lack of direct association between MID1 and two exosome components, EXOSC10 endogenous protein was immunoprecipitated and immunoblot analysis revealed the absence of binding with the endogenous MID1, while the association with EXOSC8 was distinctly detected, as expected (Fig 4.12B).

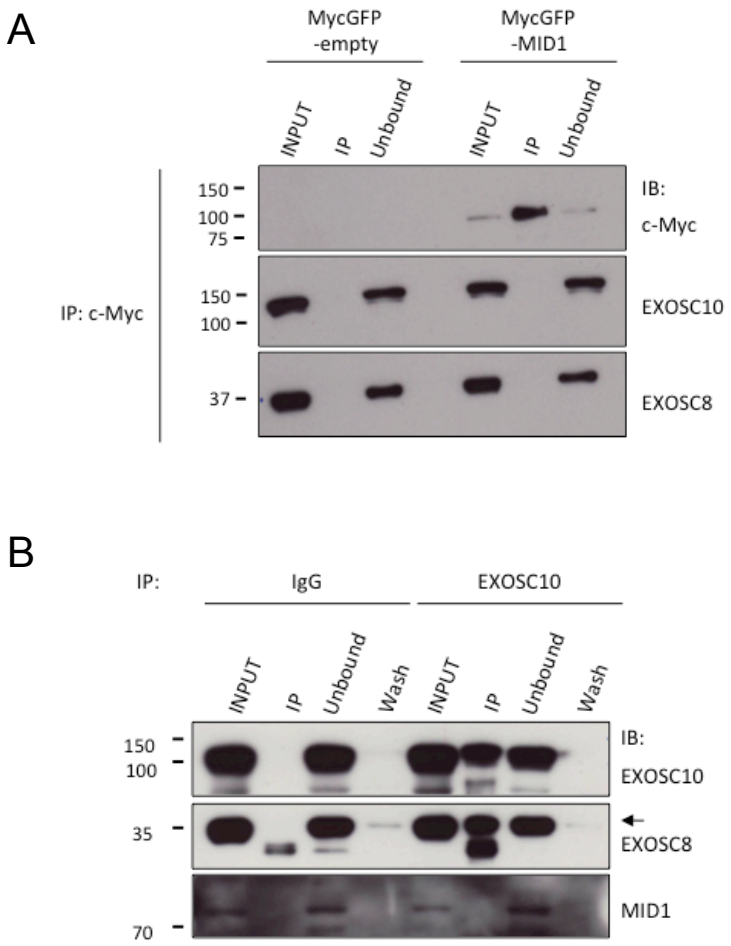

Fig. 4.12: EXOSC8 and EXOSC10 do not directly interact with MID1. A) Immunoprecipitation experiment in MycGFP-MID1 overexpressing HEK293T cells. MID1 is immunoprecipitated using anti-c-Myc antibody. Neither EXOSC8 nor EXOSC10 coimmunoprecipitate with MID1 (IP lane) and consistently the proteins are completely found in the unbound fraction. MycGFP-empty vector is used as negative control. B) HEK293T cell pellet was used for immunoprecipitation experiment using anti-EXOSC10 antibody. Total cell lysate (INPUT), immunoprecipitated proteins (IP), unbound proteins (Unbound) and the first wash of the beads (Wash) were separated by SDS-PAGE system. EXOSC8 is immunodetected in the IP fraction, while endogenous MID1 does not bind EXOSC10. Immunoprecipitation using normal rabbit IgG was performed as negative control.

4.8 SNARE complexes are reduced in *Mid1* knock-out developing brains.

The differential proteomic data illustrated in section 4.1 has revealed the enrichment of differentially expressed proteins belonging to the vesicular subcellular compartment (i.e. Snap25, Rab3a, Osbpl9, alpha-synuclein). Since IPA analysis identified cell organisation, morphology and cell-to-cell signaling as the main networks potentially affected in embryonic *Mid1*$^{-/Y}$ cerebella, we decided to explore the mechanisms of vesicular trafficking in our *Mid1*$^{-/Y}$ OS mouse model. In fact vesicular trafficking is one of the most important mechanism in cell-to-cell interaction, particularly during development, a stage in which cells communicate through different processes that are responsible for supplying specific signals for proper cellular movement, function and maturation (Hepp and Langley, 2001). In neuronal cells, Snap25, a well-known member of Soluble N-ethylmaleimide-sensitive factor Attachment protein REceptors (SNARE) proteins, exerts a pivotal role in mediating intra- and extra-cellular vesicular trafficking and exocytosis through the formation of a complex consisting of Snap25, Syntaxin-1A and Vamp2. During neurogenesis, SNARE proteins are essential to mediate directed cell migration and neurite outgrowth thus allowing the achievement of proper neuronal connectivity. Neuronal migration requires a precise control of plasmalemma turnover through specialised trafficking that delivers new plasma membrane material in selected regions of the cell (Winkle and Gupton, 2016). SNARE proteins regulate axon guidance and growth cone formation through the assembly of the SNARE complex to connect synaptic vesicles to the membrane (Cotrufo et al., 2012; Shin, 2014; Barrecheguren et al., 2017). Moreover, SNARE complexes are involved in the fusion of extracellular vesicles, such as exosomes, with the plasma membrane, thus regulating their release and promoting the exosome-related intercellular communication (Colombo et al., 2014). In the brain, the SNARE complex assembly is physiologically chaperoned by alpha-synuclein (Burrè et al., 2010), which was found downregulated in *Mid1*$^{-/Y}$ developing cerebella through mass spectrometry analysis, suggesting that E13 embryos lacking of *Mid1* might present impairment in SNARE complex formation mechanism.

In order to start examining this aspect, we investigated SNARE proteins and SNARE complexes in the *Mid1*$^{+/Y}$ and *Mid1*$^{-/Y}$ mouse embryos.

Therefore, we analysed the level of the SNARE proteins specifically involved in formation of the SNARE complexes in the brain: Snap25, Vamp2 and Syntaxin-1A.

A new set of E13 developing brains (10 *Mid1*$^{+/Y}$ and 14 *Mid1*$^{-/Y}$) were collected and dissected as previously described. SNARE proteins were separated on SDS-PAGE

system and immunoblot was performed using anti-Snap25, anti-Vamp2 and anti-Syntaxin-1A specific antibodies (Fig. 4.13A). Consistent with MS data, we observed decreased Snap25 protein level in the *Mid1*$^{-/Y}$ samples with respect to the *Mid1*$^{+/Y}$ although with high variability among the samples. Interestingly, also Vamp2 levels are reduced in *Mid1*$^{-/Y}$ cerebella despite not being fished out from the differential analysis, while Syntaxin-1A presented a very slight increase of protein level in Mid1-depleted embryos (Fig. 4.13B).

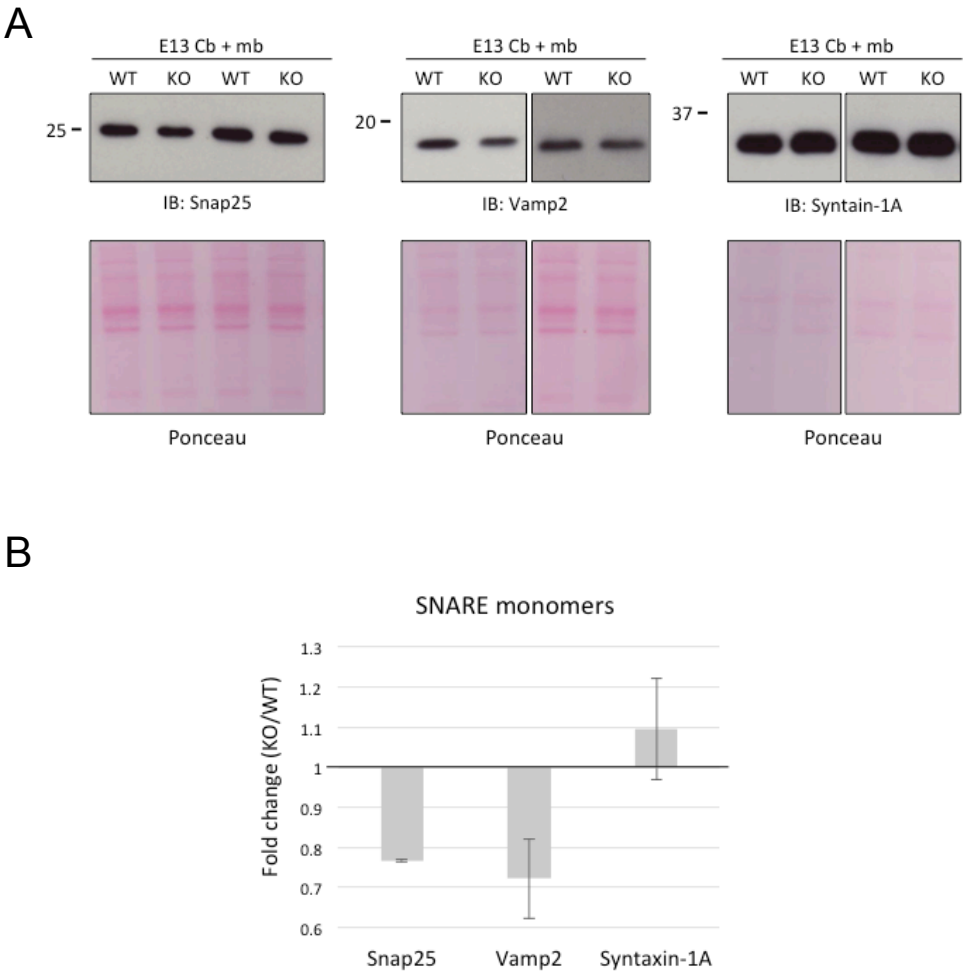

Fig. 4.13: SNARE proteins level in E13 *Mid1*$^{-/Y}$ (KO) and *Mid1*$^{+/Y}$ (WT) developing cerebella and dorsal midbrain. A) Representative immunoblot showing SNARE protein monomers in *Mid1*$^{-/Y}$ and *Mid1*$^{+/Y}$ samples detected with anti-Snap25, anti-Vamp2 and anti-Syntaxin1A antibodies. Quantification of the proteins is normalised to ponceau red staining, showed below. B) Fold change KO/WT referred to Snap25, Vamp2 and Syntaxin-1A (bars = sem) indicating that Snap25 and Vamp2 monomers are reduced in *Mid1*-depleted developing cerebella and midbrain (E13 Cb + mb), where Syntaxin-1A monomer levels are barely increased.

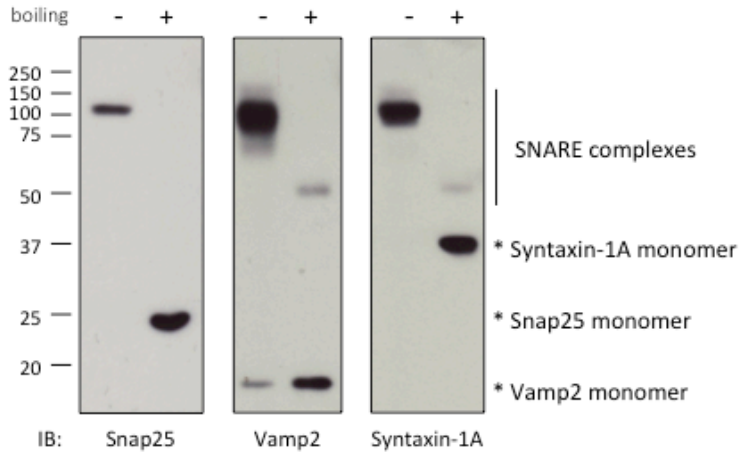

Fig. 4.14: SNARE monomers and complexes visualisation. The immunoblot shows the visualisation of both SNARE monomers (boiled lanes, asterisks) and SDS-resistant SNARE complexes (unboiled lanes, right bar) in a *Mid1*$^{+/Y}$ (WT) sample, detected using anti-Snap25, anti-Vamp2 and anti-Syntaxin1A antibodies. The complex is detected at the identical molecular weight, indicating the participation of all the three SNARE proteins to the formation of the same complex.

It is possible to detect the formed SNARE complexes in a classical PAGE as these are SDS-resistant if the sample is not boiled before loading. In order to visualize SDS-resistant SNARE complexes, equal amount of proteins was either boiled for SNARE monomer analysis or non-boiled to preserve the SDS-resistant complexes, before being subjected to SDS-PAGE. First we tested the actual detection of the SNARE complexes employing a *Mid1*$^{+/Y}$ sample. By using the three different antibodies, complexes were found at the identical molecular weight in the non-boiled samples indicating that Snap25, Vamp2 and Syntaxin-1A collectively participate to the same complex formation (Fig. 4.14).

The subsequent comparison between *Mid1*$^{-/Y}$ and *Mid1*$^{+/Y}$ samples showed that Mid1-depleted cerebella exhibited reduced SNARE complex levels as expected also from the decrease amount of some of the monomer components (Fig. 4.15A-B).

These results corroborate the hypothesis that the assembly of SNARE complexes is affected in the absence of Mid1.

A

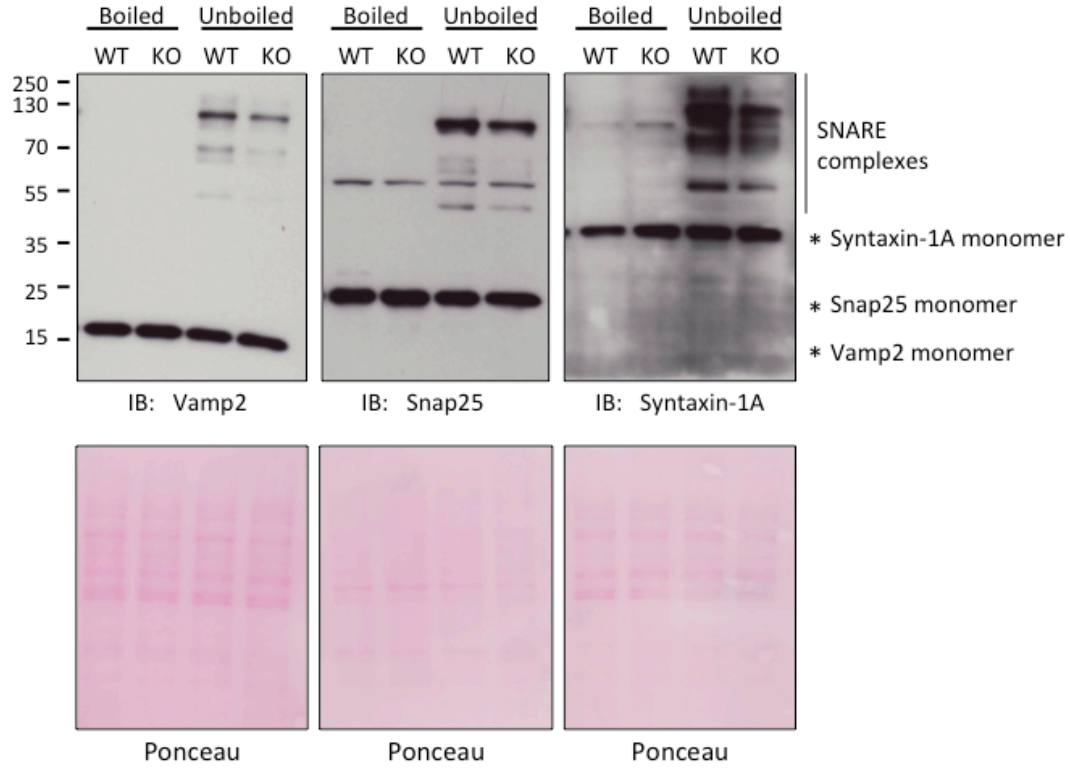

B

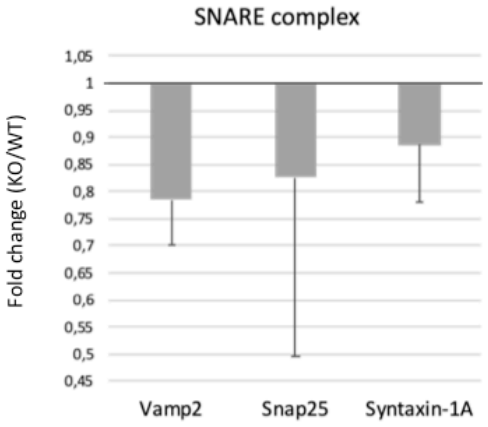

Fig. 4.15: SNARE complexes reduction in *Mid1*$^{-/Y}$ (KO) developing cerebella. A) Representative immunoblot of boiled and unboiled *Mid1*$^{+/Y}$ (WT) and *Mid1*$^{-/Y}$ samples showing SNARE complexes detected with anti-Vamp2, anti-Snap25 and anti-Syntaxin1A antibodies. The monomers are observed in both the boiled and unboiled samples (asterisks). Quantification of the complexes is normalised to ponceau red staining B) Fold change KO/WT referred to Vamp2, Snap25 and Syntaxin-1A (WT n=10;KO n=14) indicating that SNARE complexes are reduced in *Mid1*-depleted developing cerebella (bars = sem).

As the defect observed in the *Mid1*$^{-/Y}$ mouse line is specifically observed in the cerebellum (see Introduction), SNARE complex formation was further analysed in closer correlation with the developing region where the defect is then observed. Additional E13 mouse embryos were collected and the brains were more accurately dissected in order to separate the developing cerebellum, the dorsal midbrain region and the telencephalon. Immunoblot analysis of the unboiled samples using anti-Vamp2 antibody revealed a decrease in SNARE complex in all the regions examined, clearly stronger specifically in the cerebellar extracts (Fig. 4.16).

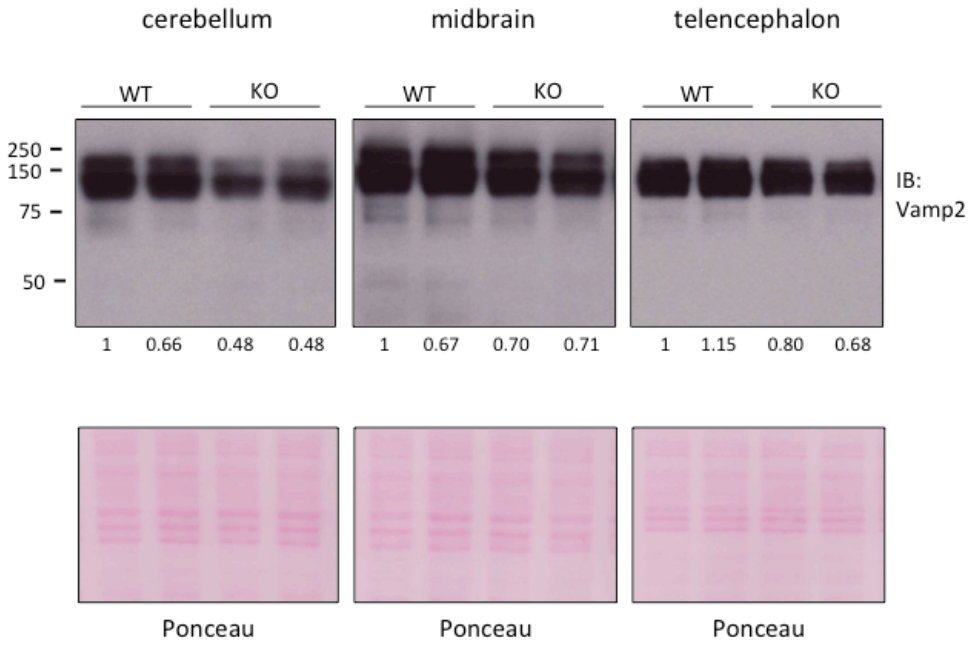

Fig. 4.16: SNARE complexes are particularly reduced in cerebellum. Fine dissection of cerebellum, midbrain and telencephalon revealed that the strongest SNARE complex reduction is present in E13 *Mid1*$^{-/Y}$ (KO) cerebella. SNARE complexes are detected using anti-Vamp2 antibody. Signals are quantified and normalised to ponceau red staining, for loading control. SDS-resistant SNARE complex intensity is indicated below each lane as referred to the first *Mid1*$^{+/Y}$ sample of each immunoblot experiment.

Furthermore, we decided to assess if the SNARE complex assembly decrease in OS embryos is observed even in adulthood.

One pair of *Mid1*$^{+/Y}$ and *Mid1*$^{-/Y}$ mice from 3 unrelated litters have been euthanised at

12 weeks old. The brains were collected and the cerebellum was dissected. Unboiled extracts underwent SDS-PAGE separation and complexes were visualised with antibodies specific for the three SNARE proteins (Fig. 4.17). SNARE complex reduction was observed in all *Mid1*$^{-/Y}$ cerebella when compared to *Mid1*$^{+/Y}$ littermate, by using either anti-Snap25, anti-Vamp2 and anti-Syntaxin-1A antibody, indicating that *Mid1*-depletion is associated with the embryonic defect in SNARE complex formation and the impairment is maintained even after cerebellar complete maturation.

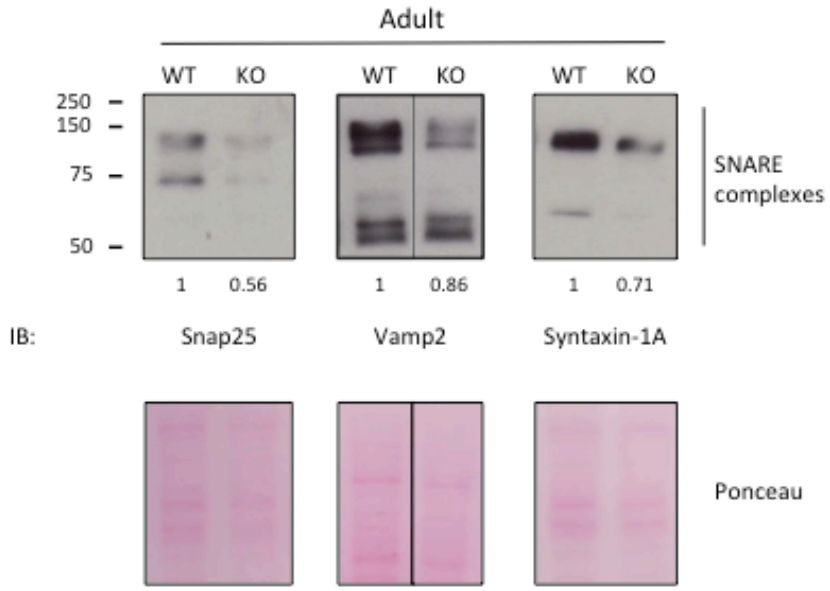

Fig. 4.17: Decrease of SNARE complexes is maintained up to adulthood in *Mid1*$^{-/Y}$ (KO) cerebellum. Representative immunoblot showing SNARE complexes detected using anti-Snap25, anti-Vamp2 and anti-Syntaxin-1A antibodies in adult *Mid1*$^{+/Y}$ (WT) and *Mid1*$^{-/Y}$ cerebella. Ponceau red-normalised amount of SNARE complexes is indicated below each lane, considering the level of SNARE complexes in the WT cerebella as 1.

4.9 Synaptosome-associated SNARE proteins are decreased at embryonic *Mid1*$^{-/Y}$ synapsis.

Synaptic transmission assures the proper neurotransmitter release and, during embryogenesis, provides signals that drive neuronal commitment, maturation and plasticity. Exocytosis of synaptic vesicles at the pre-synaptic active zone and their internalisation at the post-synaptic site are mediated by SNARE proteins through the assembly of SNARE complex (Ramakrishnan et al., 2012). In this respect, the appropriate distribution of SNARE proteins in the subcellular compartments has a crucial role in neurodevelopment.

Therefore Snap25, Syntaxin-1A and Vamp2 neuronal distribution in developing cerebella was investigated. E13 cerebella and dorsal midbrain from *Mid1*$^{+/Y}$ and *Mid1*$^{-/Y}$ embryos were dissected as previously described and subjected to subcellular fractionation. The synaptosomal fraction, representative of pre- and post-synaptic neuronal components, was isolated by sequential centrifugation and examined through immunoblot. Anti-Vamp2, anti-Snap25 and anti-Syntaxin-1A antibodies revealed vesicle-associated SNARE proteins in the synaptosomal fraction as well as in other membranous or cytosolic fractions (Fig. 4.18A). The absence of the β-tubulin along with the presence of all the SNARE proteins in the fraction corresponding to the synaptosomes confirm that the subcellular compartments have been properly fractionated, as different SNAREs are commonly used as synaptosomal markers. Despite the high variability that we often observe in this type of samples, probably as a consequence of the embryonic biological diversity, analysis of the results showed that the enrichment of vesicle-associated SNARE complex components in the synaptosomal fraction derived from *Mid1*-depleted cerebella is reduced compared to *Mid1*$^{+/Y}$ synaptosomes (Fig. 4.18B).

This suggests either a reduction in embryonic synaptic vesicles formation or a reduction in the amount of SNARE components associated to the vesicles. In any case this would lead to a decrease functionality of the synapsis trafficking (i. e. defect in synaptic vesicles exocytosis and neurotransmitter release) in the *Mid1*$^{-/Y}$ developmental processes.

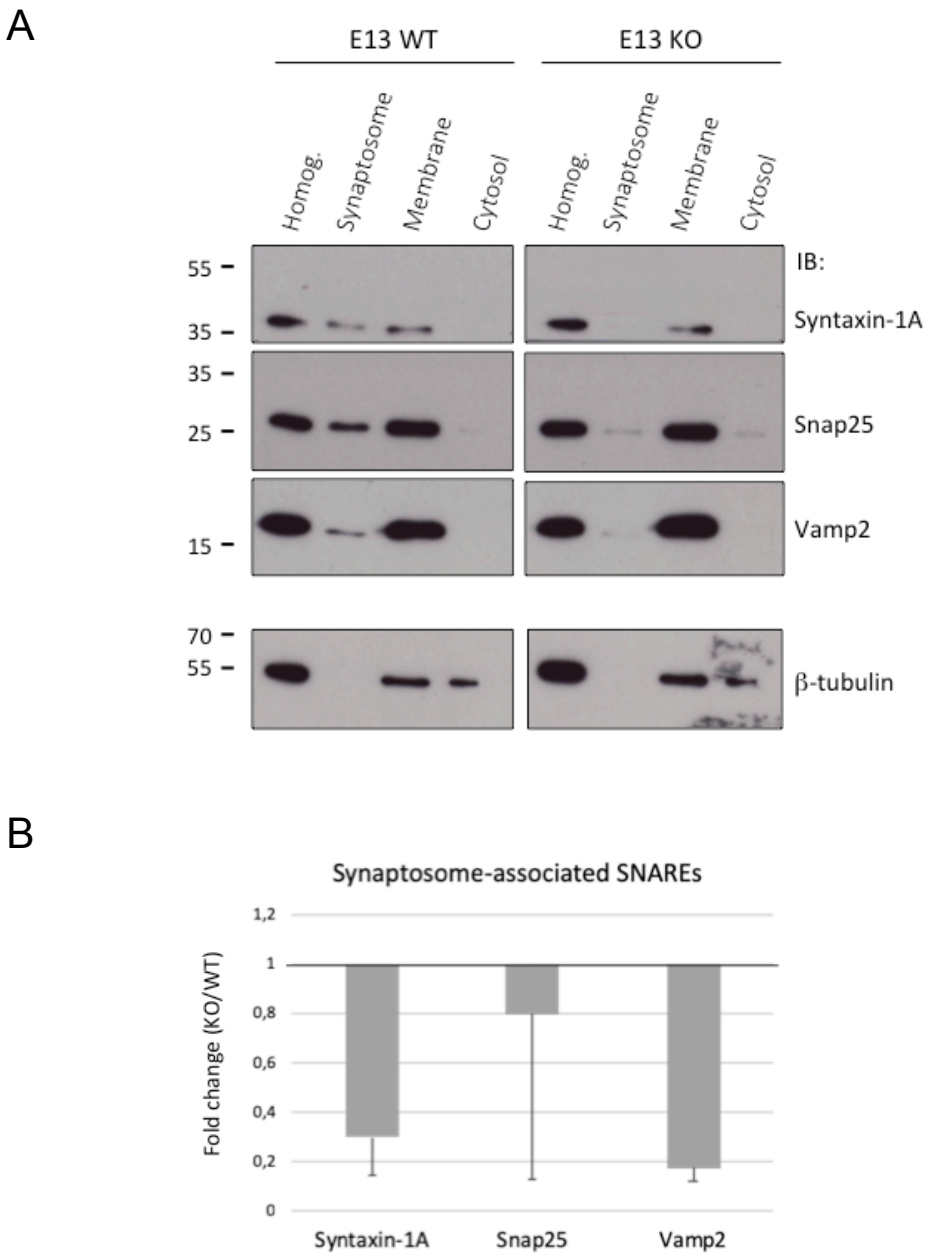

Fig. 4.18: Vesicle-associated SNARE proteins are decreased in *Mid1*$^{-/Y}$ (KO) synaptosomes. A) SNARE proteins distribution is examined upon subcellular fractionation. Different fractions derived from E13 *Mid1*$^{+/Y}$ (WT) and *Mid1*$^{-/Y}$ cerebella and dorsal midbrain are blotted using specific antibodies for SNARE proteins (Syntaxin-1A, Snap25, Vamp2). In the total homogenate (Homog.) all the SNAREs are abundantly detected, both in *Mid1*$^{+/Y}$ and *Mid1*$^{-/Y}$ samples. The *Mid1*$^{+/Y}$ synaptosome-enriched fraction shows higher level of SNARE proteins compared to *Mid1*$^{-/Y}$ synaptosome. b-tubulin immunodetection is used as control. B) Quantification of Syntaxin-1A, Snap25 and Vamp2 protein level in the synaptosome fraction relative to the total amount of proteins in the tissue homogenate. The results are expressed as fold change KO/WT, indicating that synaptosome-associated SNARE proteins are reduced in *Mid1*$^{-/Y}$ embryos (bars = sem).

5. CONCLUSIONS

In the present thesis work, we investigated MID1-associated molecular mechanisms in order to provide new insights in understanding the pathogenesis of the X-linked form of Opitz syndrome (OS).

This developmental disease is characterised by defects in the midline structures, including brain anatomical abnormalities that result in cognitive impairment and intellectual disabilities. In OS patients, several loss-of-function mutations in the *MID1* gene, encoding for an E3 ubiquitin ligase of the tripartite motif (TRIM) protein family, are described.

The mouse line carrying a nonfunctional ortholog of the human *MID1* gene, *Mid1*, (*Mid1*$^{-/Y}$) recapitulates the neuroanatomical defects observed in patients, i.e. hypoplasia of the anterior cerebellar vermis, although the role of *Mid1* in cerebellar development is still undefined. Previous evidence obtained in the lab demonstrated that the alteration of the cerebellum in *Mid1*$^{-/Y}$ mice originates prenatally, starting from the embryonic day (E) 13.5 (Lancioni et al., 2010). Therefore, we further explored the molecular pathways affected by the lack of *Mid1*, focusing on stage E13, just before the defect appears.

An unbiased proteomics study using differential mass spectrometry approach was carried out on selected E13 embryonic regions (i.e. cerebellum anlage and inferior/superior colliculus). The comparison of the *Mid1* wild-type *(Mid1*$^{+/Y}$) and the *Mid1*$^{-/Y}$ samples and the subsequent statistical analysis revealed 26 proteins presenting quantitative unbalance in *Mid1*$^{-/Y}$ embryonic brains.

Among the unbalanced proteins two components of RNA exosome complex are detected. These protein complexes are physiologically implicated in RNA processing and degradation of a variety of RNAs (Chlebowski et al., 2013; Kilchert et al., 2016), regulate diverse cellular processes (Zinder and Lima, 2017) and their alteration in structure or functionality is linked to distinct human diseases (Morton et al., 2018). EXOSC8 participates in the hexamer structure of the exosome core, described both in cytoplasm and within the nucleus of cells (Chlebowski et al., 2013). We observe a physiological migration of Exosc8 from the nucleus to a perinuclear compartment (presumably the Golgi or the endoplasmic reticulum) when mouse P7 pups-derived cerebellar granule cells are maintained in culture up to 8 days. Intriguingly, this specific localisation is completely lost in *Mid1*$^{-/Y}$ fibroblasts, suggesting a role for Mid1 in defining the proper distribution of Exosc8 and possibly of the exosome core. Indeed,

overexpression of MID1 significantly alters the nuclear localisation of the RNA exosome core component in hTERT-RPE cell line, where it is also responsible for the dowregulation of Exosc8 protein level. According to our results and considering that exosome core subunits variants have been associated with neurological diseases that present hypoplasia of the cerebellum as a common feature (Di Donato et al., 2016; Burns et al., 2018; Morton et al., 2018), we could speculate that the lack of *Mid1* in knock-out embryos might be associated with the deleterious retention of this exosome component in the nucleus, disrupting the physiological RNA processing and stability ensured by RNA exosome complexes, thus causing cerebellar defect.

EXOSC10 is a 3′ to 5′ exoribonuclease which associates with the RNA exosome core, conferring the catalytic activity to the complex (Zuo and Deutscher, 2001; Januszyk and Lima, 2014). In our embryonic tissues we observe an increase in Exosc10 protein level upon *Mid1* depletion; consistently overexpression of MID1 in HEK293T cells is accompanied by reduction in the amount of EXOSC10 protein. However, MID1 seems not to be implicated in this ribonuclease nuclear localisation since the protein distribution in the nucleus remains unchanged in case of both MID1 overexpression and Mid1 depletion. Considering that no EXOSC10 function has been so far described in neuronal cells or in the development of the nervous system, our data assume a particular relevance, showing a new role of the ribonuclease in neurodevelopmental processes and indicating that alteration in Exosc10 should be involved in promoting cerebellar abnormalities.

Although the pathway involved in the regulation of the Exosc8 and Exosc10 needs to be further investigated, we demonstrated that Mid1 influences the level of the two exosome complex components through an indirect mechanism, as neither Exosc10 nor Exosc8 directly interacts with Mid1. Interestingly, MID1 has been reported involved in mRNA binding and translational regulation. Further analysis will be necessary to possibly integrate our results and the available literature data.

Within the network analysis of affected pathways in *Mid1*$^{-/Y}$ embryos, as expected, neurological diseases appear the main disorders predictably associated with the unbalanced proteins and more interestingly, cell-to-cell signaling and interaction are highlighted by Ingenuity Pathway Analysis among the top score physiological systems possibly affected in *Mid1*-depleted embryos.

During development, cells communicate through different processes that are responsible for supplying specific signals for proper cellular movement, function and maturation.

Vesicular trafficking is one of the most important mechanisms in cell-to-cell interaction, providing proteins and developmental signals to different cell types (Hepp and Langley, 2001). Interestingly, several proteins belonging to the vesicular-related compartment of subcellular structure have been detected by our differential proteomic analysis (i.e. the SNARE protein Snap25, Rab3A, alpha-synuclein and Osbpl9). We thus hypothesised that intracellular and/or extracellular vesicular trafficking might be impaired in *Mid1*$^{-/Y}$ embryos, resulting in defects of intercellular communication.

Soluble N-ethylmaleimide-sensitive factor Attachment protein REceptors (SNARE) proteins exert a pivotal role in mediating directed cell migration and neurite outgrowth by tightly controlling plasmalemma turnover through specialised vesicular trafficking (Winkle and Gupton, 2016). In fact, in the nervous system, SNARE proteins regulate the connection of synaptic vesicles (Shin, 2014) and exosomes (Colombo et al., 2014) to the plasma membrane, thus regulating their release and promoting distinct intercellular communication. Snap25 is a well-known member of SNARE proteins and exerts its role in vesicular exocytosis through the formation of a complex consisting of Snap25, Syntaxin-1A and Vamp2 (Ramakrishnan et al., 2012). In the brain, the SNARE complex assembly is physiologically chaperoned by alpha-synuclein (Burrè et al., 2010).

According to the differential proteomic data, developing *Mid1*$^{-/Y}$ cerebella present a reduction in both Snap25 and alpha-synuclein protein level. Interestingly, further analysis revealed that also Vamp2 levels are decreased in *Mid1*$^{-/Y}$ samples with respect to the *Mid1*$^{+/Y}$ counterpart. These data prompted us to explore the SNARE complex status in our OS mouse model. Indeed, a decrease in SNARE complexes is observed in E13 *Mid1*$^{-/Y}$ embryonic brains, corroborating the hypothesis that SNARE complexes are affected in the absence of Mid1. In addition, at E13 the reduction is found particularly high in the cerebellar territory of embryonic brain, compared to developing midbrain and telencephalon and it is markedly maintained also in adult mice, when the maturation process of the cerebellum is completed. These results suggest that the neuroanatomical alterations in *Mid1*$^{-/Y}$ embryos might be associated with the assembly and the amount of SNARE complexes.

Moreover, during embryogenesis synaptic transmission provides signals that drive neuronal commitment, maturation and plasticity. SNARE complexes are known to control the exocytosis of synaptic vesicles at the presynaptic active zone as well as their internalisation at the postsynaptic site (Ramakrishnan et al., 2012). In this respect, the

appropriate distribution of SNARE proteins in the subcellular compartments has a crucial role in neurodevelopment. In our OS mouse model, we found either a reduction in embryonic synaptic vesicles formation or a reduction in the amount of SNARE components associated to these vesicles. Therefore, a decrease functionality of the synapsis trafficking (i. e. defect in synaptic vesicles exocytosis and neurotransmitter release) presumably occurs in the *Mid1*$^{-/Y}$ developmental processes and the defects are maintained even after cerebellar complete maturation.

Taken together the results suggest that depletion of *Mid1* in mouse embryos leads to two main deleterious effects. On one hand we observed the increase of the level of RNA exosome components that could affect RNA stability in developing neurons. On the other hand, the reduction of SNARE complex assembly, associated with abnormalities in the functionality of synaptic vesicles, in the *Mid1*$^{-/Y}$ developing cerebellum might affect the proper cells distribution, neuronal maturation and signal transmission. The impairment of RNA processing and intra- and extra-cellular vesicular trafficking during embryogenesis probably leads to the morphological brain abnormalities that are described in OS patients.

Further investigations are required to provide new evidence confirming our data and the results may be helpful to unravel the OS pathogenesis not only in the cerebellar compartments but also in the other midline-affected structures.

6. REFERENCES

Abrami L, Lindsay M, Parton RG, Leppla SH, van der Goot FG (2004) Membrane insertion of anthrax protective antigen and cytoplasmic delivery of lethal factor occur at different stages of the endocytic pathway. *J Cell Biol* 166(5):645-51.

Alexander M, Selman G, Seetharaman A, Chan KK, D'Souza SA, Byme AB, Roy PJ (2010) MADD-2, a homolog of the Opitz syndrome protein MID1, regulates guidance to the midline through UNC-40 in Caenorhabditis elegans. *Dev Cell* 18(6):961–972.

Allmang C, Petfalski E, Podtelejnikov A, Mann M, Tollervey D, Mitchell P (1999) The yeast exosome and human PM-Scl are related complexes of 3' → 5' exonucleases. *Genes Dev* 13(16):2148-58.

Altman J and Bayer SA (1997) Development of the cerebellar system in relation to its evolution, structure, and functions. New York: *CRC Press*. 783 pp.

Alzheimer A, Stelzmann RA, Schnitzlein HN, Murtagh FR (1995) An english translation of Alzheimer's 1907 paper, "Uber eine eigenartige Erkankung der Hirnrinde". *Clin Anat* 8(6), 429-31.

Apps R and Garwicz M (2005) Anatomical and physiological foundations of cerebellar information processing. *Nat Rev Neurosci* 6(4):297-311.

Aranda-Orgillés B, Aigner J, Kunath M, Lurz R, Schneider R, Schweiger S (2008a) Active transport of the ubiquitin ligase MID1 along the microtubules is regulated by protein phosphatase 2A. *PLoS One*, 3(10):e3507.

Aranda-Orgillés B, Trockenbacher A, Winter J, Aigner J, Köhler A, Jastrzebska E, Stahl J, Müller EC, Otto A, Wanker EE, Schneider R, Schweiger S (2008b) The Opitz syndrome gene product MID1 assembles a microtubule-associated ribonucleoprotein complex. *Hum Genet* 123(2):163-76.

Barrecheguren PJ, Ros O, Cotrufo T, Kunz B, Soriano E, Ulloa F, Stoeckli ET, Araújo

SJ (2017) SNARE proteins play a role in motor axon guidance in vertebrates and invertebrates. *Dev Neurobiol* 77(8):963-974.

Bell JL, Malyukova A, Holien JK, Koach J, Parker MW, Kavallaris M, Marshall GM, Cheung BB (2012). TRIM16 acts as an E3 ubiquitin ligase and can heterodimerize with other TRIM family members. *PLoS One* 7(5):e37470.

Belostotsky D (2009) Exosome complex and pervasive transcription in eukaryotic genomes. *Curr Opin Cell Biol* 21(3):352-8.

Berndsen CE and Wolberger C (2014) New insights into ubiquitin E3 ligase mechanism. *Nat Struct Mol Biol* 21(4):301-7.

Bizzari S, Hamzeh AR, Mohamed M, Al-Ali MT, Bastaki F (2019) Expanded PCH1D phenotype linked to EXOSC9 mutation. *Eur J Med Genet* pii: S1769-7212(18)30706-7.

Boczonadi V, Müller JS, Pyle A, Munkley J, Dor T, Quartararo J, Ferrero I, Karcagi V, Giunta M, Polvikoski T, Birchall D, Princzinger A, Cinnamon Y, Lützkendorf S, Piko H, Reza M, Florez L, Santibanez-Koref M, Griffin H, Schuelke M, Elpeleg O, Kalaydjieva L, Lochmüller H, Elliott DJ, Chinnery PF, Edvardson S, Horvath R (2014) EXOSC8 mutations alter mRNA metabolism and cause hypomyelination with spinal muscular atrophy and cerebellar hypoplasia. *Nat Commun* 5:4287.

Boding L, Hansen AK, Meroni G, Johansen BB, Braunstein TH, Bonefeld CM, Kongsbak M, Jensen BA, Woetmann A, Thomsen AR, Odum N, von Essen MR, Geisler C (2014a) Midline 1 directs lytic granule exocytosis and cytotoxicity of mouse killer T cells. *Eur J Immunol* 44(10):3109-18.

Boding L, Hansen AK, Nielsen MM, Meroni G, Braunstein TH, Woetmann A, Ødum N, Bonefeld CM, Geisler C (2014b). Midline 1 controls polarization and migration of murine cytotoxic T cells. *Immun Inflamm Dis* 2(4):262-71.

Brouwer R, Allmang C, Raijmakers R, van Aarssen Y, Egberts WV, Petfalski E, van Venrooij WJ, Tollervey D, Pruijn GJ (2001) Three novel components of the human

exosome. *J Biol Chem* 276(9):6177-84.

Burns DT, Donkervoort S, Müller JS, Knierim E, Bharucha-Goebel D, Faqeih EA, Bell SK, AlFaifi AY, Monies D, Millan F, Retterer K, Dyack S, MacKay S, Morales-Gonzalez S, Giunta M, Munro B, Hudson G, Scavina M, Baker L, Massini TC, Lek M, Hu Y, Ezzo D, AlKuraya FS, Kang PB, Griffin H, Foley AR, Schuelke M, Horvath R, Bönnemann CG (2018) Variants in EXOSC9 disrupt the RNA exosome and result in cerebellar atrophy with spinal motor neuronopathy. *Am J Hum Genet* 102(5):858-873.

Burré J, Sharma M, Tsetsenis T, Buchman V, Etherton MR, Südhof TC (2010) Alpha-synuclein promotes SNARE-complex assembly in vivo and in vitro. *Science* 329(5999):1663-7.

Butts T, Green MJ, Wingate RJ (2014) Development of the cerebellum: simple steps to make a 'little brain'. *Development* 141(21):4031-41.

Cainarca S, Messali S, Ballabio A, Meroni G (1999). Functional characterization of the Opitz syndrome gene product (midin): evidence for homodimerization and association with microtubules throughout the cell cycle. *Hum Mol Genet* 8(8):1387-96.

Cajal SRY (1911) Histologie du Systeme Nerveux de l'Homme et des Vertebres, vol. 2. Madrid: Consejo Superior de Investigaciones Cientificas.

Chapman MA, Lawrence MS, Keats JJ, Cibulskis K, Sougnez C, Schinzel AC, Harview CL, Brunet JP, Ahmann GJ, Adli M, Anderson KC et al. (2011) Initial genome sequencing and analysis of multiple myeloma. *Nature* 471(7339):467-72.

Cheng Y, Sudarov A, Szulc KU, Sgaier SK, Stephen D, Turnbull DH, Joyner AL (2010) The Engrailed homeobox genes determine the different foliation patterns in the vermis and hemispheres of the mammalian cerebellum. *Development* 137(3):519–29.

Chizhikov V and Millen KJ (2003) Development and malformations of the cerebellum in mice. *Mol Genet Metab* 80(1-2):54-65.

Chlebowski A, Lubas M, Jensen TH, Dziembowski A (2013) RNA decay machines: the exosome. *Biochim Biophys Acta* 1829(6-7):552-60.

Clissold PM and Ponting CP (2000) PIN domains in nonsense-mediated mRNA decay and RNAi. *Curr Biol* 10(24):R888-90.

Collison A, Hatchwell L, Verrills N, Wark PA, de Siqueira AP, Tooze M, Carpenter H, Don AS, Morris JC, Zimmermann N, Bartlett NW, Rothenberg ME, Johnston SL, Foster PS, Mattes J (2013) The E3 ubiquitin ligase midline 1 promotes allergen and rhinovirus-induced asthma by inhibiting protein phosphatase 2A activity. *Nat Me*d 19(2):232-7.

Colombo M, Raposo G, Théry C (2014) Biogenesis, secretion, and intercellular interactions of exosomes and other extracellular vesicles. *Annu Rev Cell Dev Biol* 30:255-89.

Corrales JD, Blaess S, Mahoney EM, Joyner AL (2006) The level of sonic hedgehog signaling regulates the complexity of cerebellar foliation. *Development* 133(9):1811-21.

Cotrufo T, Andrés RM, Ros O, Pérez-Brangulí F, Muhaisen A, Fuschini G, Martínez R, Pascual M, Comella JX, Soriano E (2012) Syntaxin 1 is required for DCC/Netrin-1-dependent chemoattraction of migrating neurons from the lower rhombic lip. *Eur J Neurosci* 36(9):3152-64.

Cox TC, Allen RL, Cox LL, Hopwood B, Goodwin B, Haan E, Suthers GK (2000) New mutations in MID1 provide support for loss of function as the cause of X-linked Opitz syndrome. *Hum Mol Genet* 9(17):2553-62.

Cupertino RB, Kappel DB, Bandeira CE, Schuch JB, da Silva BS, Müller D, Bau CH, Mota NR (2016) SNARE complex in developmental psychiatry: neurotransmitter exocytosis and beyond. *J Neural Transm (Vienna)* 123(8):867-83.

Dal Zotto L, Quaderi NA, Elliot R, Lingerfelter PA, Carrel L, Valsecchi V, Montini E, Yen CH, Chapman V, Kalcheva I, Arrigo G, Zuffardi O, Thomas S, Willar H, Ballabio

A, Disteche CM, Rugarli EI (1998) The mouse Mid1 gene: implications for the pathogenesis of Opitz syndrome and the evolution of the mammalia pseudoautosomal region. *Hum Mol Genet* 7(3):489-99.

De Falco F, Cainarca S, Andolfi G, Ferrentino R, Berti C, Rodriguez Criado G, Rottinger O, Dennis N, Odent S, Rastaghi A, Liebelt J, Chitayat D, Winter R, Jawanda H, Ballabio A, Franco B, Meroni G (2003) X-linked Opitz syndrome: novel mutations in the MID1 gene and redefinition of the clinical spectrum. *Am J Med Genet* 120A(2):222-8.

De Robertis E and Franchi CM (1956) Electron microscope observations on synaptic vesicles in synapses of the retinal rods and cones. *J Biophys Biochem Cytol* 2(3):307-18.

Demir U, Koehler A, Schneider R, Schweiger S, Klocker H (2014) Metformin anti-tumor effect via disruption of the MID1 translational regulator complex and AR downregulation in prostate cancer cells. *BMC Cancer* 14:52.

Di Donato N, Neuhann T, Kahlert AK, Klink B, Hackmann K, Neuhann I, Novotna B, Schallner J, Krause C, Glass IA, Parnell SE, Benet-Pages A, Nissen AM, Berger W, Altmüller J, Thiele H, Weber BH, Schrock E, Dobyns WB, Bier A, Rump A (2016) Mutations in EXOSC2 are associated with a novel syndrome characterised by retinitis pigmentosa, progressive hearing loss, premature ageing, short stature, mild intellectual disability and distinctive gestalt. *J Med Genet* 53(6):419-25.

Dierssen M, Fedrizzi L, Gomez-Villafuertes R, de Lagran MM, Gutierrez-Adan A, Sahún I, Pintado B, Oliveros JC, Dopazo XM, Gonzalez P, Brini M, Mellström B, Carafoli E, Naranjo JR (2012) Reduced Mid1 expression and delayed neuromotor development in daDREAM transgenic mice. *Front Mol Neurosci* 5:58.

van Dijk EL, Schilders G, Pruijn GJ (2007) Human cell growth requires a functional cytoplasmic exosome, which is involved in various mRNA decay pathways. *RNA* 13(7):1027-35.

Du H, Huang Y, Zaghlula M, Walters E, Cox TC, Massiah MA (2013) The MID1 E3

ligase catalyzes the polyubiquitination of Alpha4 (α4), a regulatory subunit of protein phosphatase 2A (PP2A): novel insights into MID1-mediated regulation of PP2A. *J Biol Chem* 288(29):21341-50.

Dulubova I, Sugita S, Hill S, Hosaka M, Fernandez I, Südhof TC, Rizob J (1999) A conformational switch in syntaxin during exocytosis: role of munc18. *EMBO J* 18(16):4372-82.

Eggens VR, Barth PG, Niermeijer JM, Berg JN, Darin N, Dixit A, Fluss J, Foulds N, Fowler D, Hortobágyi T, Jacques T, King MD, Makrythanasis P, Máté A, Nicoll JA, O'Rourke D, Price S, Williams AN, Wilson L, Suri M, Sztriha L, Dijns-de Wissel MB, van Meegen MT, van Ruissen F, Aronica E, Troost D, Majoie CB, Marquering HA, Poll-Thé BT, Baas F (2014) EXOSC3 mutations in pontocerebellar hypoplasia type 1: novel mutations and genotype-phenotype correlations. *Orphanet J Rare Dis* 9:23.

Englund C, Kowalczyk T, Daza RA, Dagan A, Lau C, Rose MF, Hevner RF (2006) Unipolar brush cells of the cerebellum are produced in the rhombic lip and migrate through developing white matter. *J Neurosci* 26(36):9184-95.

Fasken MB, Losh JS, Leung SW, Brutus S, Avin B, Vaught JC, Potter-Birriel J, Craig T, Conn GL, Mills-Lujan K, Corbett AH, van Hoof A (2017) Insight into the RNA exosome complex through modeling pontocerebellar hypoplasia type 1b disease mutations in yeast. *Genetics* 205(1):221-237.

Fontanella B, Russolillo G, Meroni G (2008) MID1 mutations in patients with X-linked Opitz G/BBB syndrome. *Hum Mutat* 29(5):584-94.

Fox MJ and Mosley AL (2016) Rrp6: Integrated roles in nuclear RNA metabolism and transcription termination. *Wiley Interdiscip Rev RNA* 7(1):91-104.

Freemont PS (1993) The RING finger. A novel protein sequence motif related to the zinc finger. *Ann N Y Acad Sci* 684:174-92.

Frühbeis C, Fröhlich D, Kuo WP, Krämer-Albers EM (2013) Extracellular vesicles as

mediators of neuron-glia communication. *Front Cell Neurosci* 7:182.

Fu Y, Tvrdik P, Makki N, Paxinos G, Watson C (2011) Precerebellar cell groups in the hindbrain of the mouse defined by retrograde tracing and correlated with cumulative Wnt1-cre genetic labeling. *Cerebellum* 10(3):570-84.

Fujita S, Shimada M, Nakamura T (1966) H3-thymidine autoradiographic studies on the cell proliferation and differentiation in the external and the internal granular layers of the mouse cerebellum. *J Comp Neurol* 128(2):191-208.

Goldowitz D and Hamre K (1998) The cells and molecules that make a cerebellum. *Trends Neurosci* 21(9):375-82.

Govek EE, Newey SE, Van Aelst L (2005) The role of the Rho GTPases in neuronal development. *Genes Dev* 19(1):1-49.

Graham FL and van der Eb AJ (1973) A new technique for the assay of infectivity of human adenovirus 5 DNA. *Virology* 52(2):456-67.

Graham AC, Kiss DL, Andrulis ED (2006) Differential distribution of exosome subunits at the nuclear lamina and in cytoplasmic foci. *Mol Biol Cell* 17(3):1399-409.

Graham AC, Kiss DL, Andrulis ED (2009) Core exosome-independent roles for Rrp6 in cell cycle progression. *Mol Biol Cell* 20(8):2242-53.

Han X, Du H, Massiah MA (2011) Detection and characterization of the in vitro E3 ligase activity of the human MID1 protein. *J Mol Biol* 407(4):505-20.

Harigaya Y, Tanaka H, Yamanaka S, Tanaka K, Watanabe Y, Tsutsumi C, Chikashige Y, Hiraoka Y, Yamashita A, Yamamoto M (2006) Selective elimination of messenger RNA prevents an incidence of untimely meiosis. *Nature* 442(7098):45-50.

Hasenpusch-Theil K, Magnani D, Amaniti EM, Han L, Armstrong D, Theil T (2012) Transcriptional analysis of Gli3 mutants identifies Wnt target genes in the developing

hippocampus. *Cereb Cortex* 22(12):2878-93.

Hepp R and Langley K (2001) SNAREs during development. *Cell Tissue Res* 305(2):247-53.

Hessvik NP and Llorente A (2018) Current knowledge on exosome biogenesis and release. *Cell Mol Life Sci* 75(2):193-208.

Hettich MM, Matthes F, Ryan DP, Griesche N, Schröder S, Dorn S, Krauβ S, Ehninger D (2014) The anti-diabetic drug metformin reduces BACE1 protein level by interfering with the MID1 complex. *PLoS One* 9(7):e102420.

Hevner RF, Hodge RD, Daza RA, Englund C (2006) Transcription factors in glutamatergic neurogenesis: conserved programs in neocortex, cerebellum, and adult hippocampus. *Neurosci Res* 55(3):223-33.

Hoshino M, Nakamura S, Mori K, Kawauchi T, Terao M, Nishimura Y, Fukuda A, Fuse T, Matsuo N, Sone M, Watanabe M, Bito H, Terashima T, Wright CV, Kawaguchi Y, Nakao K, Nabeshima Y (2005) Ptf1a, a bHLH transcriptional gene, defines GABAergic neuronal fates in cerebellum. *Neuron* 47(2):201-13.

Hou D, Ruiz M, Andrulis ED (2012) The ribonuclease Dis3 is an essential regulator of the developmental transcriptome. *BMC Genomics* 13:359.

Jamin SP, Petit FG, Kervarrec C, Smagulova F, Illner D, Scherthan H, Primig M (2017) EXOSC10/Rrp6 is post-translationally regulated in male germ cells and controls the onset of spermatogenesis. *Sci Rep* 7(1):15065.

Januszyk K, Liu Q, Lima CD (2011) Activities of human RRP6 and structure of the human RRP6 catalytic domain. *RNA* 17(8):1566-77.

Januszyk K and Lima CD (2014) The eukaryotic RNA exosome. *Curr Opin Struct Biol* 24:132-40.

Kilchert C, Wittmann S, Vasiljeva L (2016) The regulation and functions of the nuclear RNA exosome complex. *Nat Rev Mol Cell Biol* 17(4):227-39.

Koles K and Budnik V (2012) Exosomes go with the Wnt. *Cell Logist* 2(3):169-173.

Komander D and Rape M (2012) The ubiquitin code. *Annu Rev Biochem* 81:203-29.

Krauss S, Foerster J, Schneider R, Schweiger S (2008) Protein phosphatase 2A and rapamycin regulate the nuclear localization and activity of the transcription factor GLI3. *Cancer Res* 68(12):4658-65.

Krauss S, Griesche N, Jastrzebska E, Chen C, Rutschow D, Achmüller C, Dorn S, Boesch SM, Lalowski M, Wanker E, Schneider R, Schweiger S (2013) Translation of HTT mRNA with expanded CAG repeats is regulated by the MID1-PP2A protein complex. *Nat Commun* 4:1511.

Kruszka P, Li D, Harr MH, Wilson NR, Swarr D, McCormick EM, Chiavacci RM, Li M, Martinez AF, Hart RA, McDonald-McGinn DM, Deardoff MA, Falk MJ, Allanson JE, Hudson C, Johnson JP, Saadi I, Hakonarson H, Muenke M, Zackai EH (2015) Mutations in SPECC1L, encoding sperm antigen with calponin homology and coiled-coil domains 1-like, are found in some cases of autosomal dominant Opitz G/BBB syndrome. *J Med Genet* 52(2):104-10.

Łabno A, Tomecki R, Dziembowski A (2016) Cytoplasmic RNA decay pathways – Enzymes and mechanisms. *Biochim Biophys Acta* 1863(12):3125-3147.

Lancioni A, Pizzo M, Fontanella B, Ferrentino R, Napolitano LM, De Leonibus E, Meroni G (2010) Lack of Mid1, the mouse ortholog of the Opitz syndrome gene, causes abnormal development of the anterior cerebellar vermis. *J Neurosci* 30(8):2880-7.

Larsell O (1971) The comparative anatomy and histology of the cerebellum from monotremes through apes. Minneapolis: University of Minnesota Press. *Yale J Biol Med* 43(6): 412.

Leto K, Arancillo M, Becker EB, Buffo A, Chiang C, Ding B , Dobyns WB, Dusart I, Haldipur P, Hatten ME, Hoshino M, Joyner AL, Kano M, Kilpatrick DL, Koibuchi N, Marino S, Martinez S, Millen KJ, Millner TO, Miyata T, Parmigiani E, Schilling K, Sekerková G, Sillitoe RV, Sotelo C, Uesaka N, Wefers A, Wingate RJ, Hawkes R (2016) Consensus paper: cerebellar development. *Cerebellum* 15(6):789-828.

Liu A, Losos K, Joyner AL (1999) FGF8 can activate Gbx2 and transform regions of the rostral mouse brain into a hindbrain fate. *Development* 126(21):4827-38.

Liu J, Prickett TD, Elliott E, Meroni G, Brautigan DL (2001) Phosphorylation and microtubule association of the Opitz syndrome protein mid-1 is regulated by protein phosphatase 2A via binding to the regulatory subunit alpha 4. *Proc Natl Acad Sci U S A* 98(12):6650-5.

Liu Q, Greimann JC, Lima CD (2006) Reconstitution, activities, and structure of the eukaryotic RNA exosome. *Cell* 127(6):1223-37.

Liu E, Knutzen CA, Krauss S, Schweiger S, Chiang GG (2011) Control of mTORC1 signaling by the Opitz syndrome protein MID1. *Proc Natl Acad Sci U S A* 108(21):8680-5.

Lloret-Llinares M, Karadoulama E, Chen Y, Wojenski LA, Villafano GJ, Bornholdt J, Andersson R, Core L, Sandelin A, Jensen TH (2018) The RNA exosome contributes to gene expression regulation during stem cell differentiation. *Nucleic Acids Res* 46(21):11502-11513.

Lu T, Chen R, Cox TC, Moldrich RX, Kurniawan N, Tan G, Perry JK, Ashworth A, Bartlett PF, Xu L, Zhang J, Lu B, Wu M, Shen Q, Liu Y, Richards LJ, Xiong Z (2013) X-linked microtubule-associated protein, Mid1, regulates axon development. *Proc Natl Acad Sci U S* A 110(47):19131-6.

Machold R and Fishell G (2005) Math1 is expressed in temporally discrete pools of cerebellar rhombic-lip neural progenitors. *Neuron* 48(1):17-24.

Makino DL, Baumgärtner M, Conti E (2013) Crystal structure of an RNA-bound 11-subunit eukaryotic exosome complex. *Nature* 495(7439):70-5.

Massiah MA, Simmons BN, Short KM, Cox TC (2006) Solution structure of the RBCC/TRIM B-box1 domain of human MID1: B-box with a RING. *J Mol Biol* 358(2):532-45.

Matthes F, Hettich MM, Schilling J, Flores-Dominguez D, Blank N, Wiglenda T, Buntru A, Wolf H, Weber S, Vorberg I, Dagane A, Dittmar G, Wanker E, Ehninger D, Krauss S (2018) Inhibition of the MID1 protein complex: a novel approach targeting APP protein synthesis. *Cell Death Discov* 4:4.

McGough IJ and Vincent JP (2016) Exosomes in developmental signalling. *Development* 143(14):2482-93.

McIver SC, Kang YA, DeVilbiss AW, O'Driscoll CA, Ouellette JN, Pope NJ, Camprecios G, Chang CJ, Yang D, Bouhassira EE, Ghaffari S, Bresnick EH (2014) The exosome complex establishes a barricade to erythroid maturation. *Blood* 124(14):2285-97.

Meroni G and Diez-Roux G (2005) TRIM/RBCC, a novel class of 'single protein RING finger' E3 ubiquitin ligases. *Bioessays* 27(11):1147-57.

Migliore C, Athanakis E, Dahoun S, Wonkman A, Lees M, Calabrese O, Connel F, Lynch SA, Izzi C, Pompilii E, Thakur S, van Maarle M, Wilson LC, Meroni G (2013) Complex rearrangement of the exon 6 genomic region among Opitz G/BBB syndrome MID1 alterations. *Eur J Med Genet* 56(8):404-10.

Mistry DS, Chen Y, Sen GL (2012) Progenitor function in self-renewing human epidermis is maintained by the exosome. *Cell Stem Cell* 11(1):127-35.

Mitchell P, Petfalski E, Shevchenko A, Mann M, Tollervey D (1997) The exosome: a conserved eukaryotic RNA processing complex containing multiple 3′→5′ exoribonucleases. *Cell* 91(4):457-66.

Miyata T, Ono Y, Okamoto M, Masaoka M, Sakakibara A, Kawaguchi A, Hashimoto M, Ogawa M (2010) Migration, early axonogenesis, and Reelin-dependent layer-forming behavior of early/posterior-born Purkinje cells in the developing mouse lateral cerebellum. *Neural Dev* 5:23.

Morton DJ, Kuiper EG, Jones SK, Leung SW, Corbett AH, Fasken MB (2018) The RNA exosome and RNA exosome-linked disease. *RNA* 24(2):127-142.

Murakami H, Goto DB, Toda T, Chen ES, Grewal SI, Martienssen RA, Yanagida M (2007) Ribonuclease activity of Dis3 is required for mitotic progression and provides a possible link between heterochromatin and kinetochore function. *PLoS One* 2(3):e317.

Nakamura T, Ueyama T, Ninoyu Y, Sakaguchi H, Choijookhuu N, Hishikawa Y, Kiyonari H, Kohta M, Sakahara M, de Curtis I, Kohmura E, Hisa Y, Aiba A, Saito N (2017) Novel role of Rac-Mid1 signaling in medial cerebellar development. *Development* 144(10):1863-1875.

Napolitano LM, Jaffray EG, Hay RT, Meroni G (2011) Functional interactions between ubiquitin E2 enzymes and TRIM proteins. *Biochem J* 434(2):309-19.

Ogami K, Chen Y, Manley JL (2018) RNA surveillance by the nuclear RNA exosome: mechanisms and significance. *Noncoding RNA* 4(1). pii: 8.

Opitz JM, Summitt RL, Smith DW (1969a) The BBB syndrome familial telecanthus with associated congenital anomalies. Birth Defects: Original Article Series V:86-94.

Opitz JM, Frías JL, Gutenberger JE, Pellet JR (1969b) The G syndrome of multiple congenital anomalies. Birth defects: Original Article Series V:95-102.

Opitz JM (1987) G syndrome (hypertelorism with esophageal abnormality and hypospadias, or hypospadias-dysphagia, or "Opitz-Frias" or "Opitz-G" syndrome)-perspective in 1987 and bibliography. *Am J Med Genet* 28(2):275-85.

Orvis GD, Hartzell AL, Smith JB, Barraza LH, Wilson SL, Szulc KU, Turnbull DH, Joyner AL (2012) The engrailed homeobox genes are required in multiple cell lineages to coordinate sequential formation of fissures and growth of the cerebellum. *Dev Biol* 367(1):25-39.

Pfirrmann T, Jandt E, Ranft S, Lokapally A, Neuhaus H, Perron M, Hollemann T (2016) Hedgehog-dependent E3-ligase Midline1 regulates ubiquitin-mediated proteasomal degradation of Pax6 during visual system development. *Proc Natl Acad Sci U S A* 113(36):10103-8.

Pickart CM, Eddins MJ (2004) Ubiquitin: structures, functions, mechanisms. *Biochim Biophys Acta* 1695(1-3):55-72.

Pierce ET (1975) Histogenesis of the deep cerebellar nuclei in the mouse: an autoradiographic study. *Brain Res* 95(2-3):503-18.

Pinson L, Augé J, Audollent S, Mattéi G, Etchevers H, Gigarel N, Razavi F, Lacombe D, Odent S, Le Merrer M, Amiel J, Munnich A, Meroni G, Lyonnet S, Vekemans M, Attié-Bitach T (2004) Embryonic expression of the human MID1 gene and its mutations in Opitz syndrome. *J Med Genet* 41(5):381-6.

Quaderi NA, Schweiger S, Gaudenz K, Franco B, Rugarli EI, Berger W, Feldman GJ, Volta M, Andolfi G, Gilgenkrantz S, Marion RW, Hennekam RC, Opitz JM, Muenke M, Ropers HH, Ballabio A (1997) Opitz G/BBB syndrome, a defect of midline development, is due to mutations in a new RING finger gene on Xp22. *Nat Genet* 17(3):285-91.

Ramakrishnan NA, Drescher MJ, Drescher DG (2012) The SNARE complex in neuronal and sensory cells. *Mol Cell Neurosci* 50(1):58-69.

Raposo G, Nijman HW, Stoorvogel W, Liejendekker R, Harding CV, Melief CJ, Geuze HJ (1996) B lymphocytes secrete antigen-presenting vesicles. *J Exp Med* 183(3):1161-72.

Raposo G and Stoorvogel W (2013) Extracellular vesicles: exosomes, microvesicles, and friends. *J Cell Biol* 200(4):373-83.

Reymond A, Meroni G, Fantozzi A, Merla G, Cairo S, Luzi L, Riganelli D, Zanaria E, Messali S, Cainarca S, Guffanti A, Minucci S, Pelicci PG, Ballabio A (2001) The tripartite motif family identifies cell compartments. *Embo J* 20(9):2140-51.

Richman JM, Fu KK, Cox LL, Sibbons JP, Cox TC (2002) Isolation and characterisation of the chick orthologue of the Opitz syndrome gene, Mid1, supports a conserved role in vertebrate development. *Int J Dev Biol* 46(4):441-8.

Robin NH, Feldman GJ, Aronson AL, Mitchell HF, Weksberg R, Leonard CO, Burton BK, Josephson KD, Laxovà R, Aleck KA, Allanson JE, Guion- Almeida ML, Martin RA, Leichtman LG, Price RA, Opitz JM, Muenke M (1995) Opitz syndrome is genetically heterogeneous, with one locus on Xp22, and a second locus on 22q11.2. *Nat Genet* 11(4):459-61.

Robin NH, Opitz JM, Muenke M (1996) Opitz G/BBB syndrome: clinical comparisons of families linked to Xp22 and 22q, and a review of the literature. *Am J Med Genet* 62(3):305-17.

Rudnik-Schöneborn S, Senderek J, Jen JC, Houge G, Seeman P, Puchmajerová A, Graul-Neumann L, Seidel U, Korinthenberg R, Kirschner J, Seeger J, Ryan MM, Muntoni F, Steinlin M, Sztriha L, Colomer J, Hübner C, Brockmann K, Van Maldergem L, Schiff M, Holzinger A, Barth P, Reardon W, Yourshaw M, Nelson SF, Eggermann T, Zerres K (2013) Pontocerebellar hypoplasia type 1: clinical spectrum and relevance of EXOSC3 mutations. *Neurology* 80(5):438-46.

Ruiz-Martinez M, Navarro A, Marrades RM, Vinolas N, Santasusagna S, Munoz C, Ramirez J, Molins L, Monzo M (2016) YKT6 expression, exosome release, and survival in non-small cell lung cancer. *Oncotarget* 7(32):51515-51524.

Salinas PC, Fletcher C, Copeland NG, Jenkins NA, Nusse R (1994) Maintenance of Wnt-3 expression in Purkinje cells of the mouse cerebellum depends on interaction with

granule cells. *Development* 120(5):1277-86.

Sardiello M, Cairo S, Fontanella B, Ballabio A, Meroni G (2008) Genomic analysis of the TRIM family reveals two groups of genes with distinct evolutionary properties. *BMC Evol Biol* 8:225.

Schilders G, van Dijk E, Raijmakers R, Pruijn GJ (2006) Cell and molecular biology of the exosome: how to make or break an RNA. *Int Rev Cytol* 251:159-208.

Schneider C, Leung E, Brown J, Tollervey D (2009) The N-terminal PIN domain of the exosome subunit Rrp44 harbors endonuclease activity and tethers Rrp44 to the yeast core exosome. *Nucleic Acids Res* 37(4):1127-40.

Schneider C and Tollervey D (2013) Threading the barrel of the RNA exosome. *Trends Biochem Sci* 38(10):485-93.

Schneider A and Simons M (2016) Exosomes: vesicular carriers for intercellular communication in neurodegenerative disorders. *Cell Tissue Res* 352(1):33-47.

Schottmann G, Picker-Minh S, Schwarz JM, Gill E, Rodenburg RJT, Stenzel W, Kaindl AM, Schuelke M (2017) Recessive mutation in EXOSC3 associates with mitochondrial dysfunction and pontocerebellar hypoplasia. *Mitochondrion* 37:46-54.

Schweiger S, Foerster J, Lehmann T, Suckow V, Muller YA, Walter G, Davies T, Porter H, van Bokhoven H, Lunt PW, Traub P, Ropers HH (1999) The Opitz syndrome gene product, MID1, associates with microtubules. *Proc Natl Acad Sci U S A* 96(6):2794-9.

Schweiger S, Dorn S, Fuchs M, Köhler A, Matthes F, Müller EC, Wanker E, Schneider R, Krauß S (2014) The E3 ubiquitin ligase MID1 catalyzes ubiquitination and cleavage of Fu. *J Biol Chem* 289(46):31805-17.

Schweiger S, Matthes F, Posey K, Kickstein E, Weber S, Hettich MM, Pfurtscheller S, Ehninger D, Schneider R, Krauß S (2017) Resveratrol induces dephosphorylation of

Tau by interfering with the MID1-PP2A complex. *Sci Rep* 7(1):13753.

Sgaier SK, Millet S, Villanueva MP, Berenshteyn F, Song C, Joyner AL (2005) Morphogenetic and cellular movements that shape the mouse cerebellum; insights from genetic fate mapping. *Neuron* 45(1):27-40.

Shaham O, Menuchin Y, Farhy C, Ashery-Padan R (2012) Pax6: a multi-level regulator of ocular development. *Prog Retin Eye Res* 31(5):351-76.

Shin OH (2014) Exocytosis and synaptic vesicle function. *Compr Physiol* 4(1):149-75.

Short KM, Hopwood B, Yi Z, Cox TC (2002) MID1 and MID2 homo- and heterodimerise to tether the rapamycin- sensitive PP2A regulatory subunit, Alpha 4, to microtubules: implications for the clinical variability of X-linked Opitz GBBB syndrome and other developmental disorders. *BMC Cell Biol* 3:1.

Short KM and Cox TC (2006) Subclassification of the RBCC/TRIM superfamily reveals a novel motif necessary for microtubule binding. *J Biol Chem* 281(13):8970-80.

Silla T, Karadoulama E, Mąkosa D, Lubas M, Jensen TH (2018) The RNA exosome adaptor ZFC3H1 functionally competes with nuclear export activity to retain target transcripts. *Cell Rep* 23(7):2199-2210.

Sillitoe RV and Joyner AL (2007) Morphology, molecular codes, and circuitry produce the three-dimensional complexity of the cerebellum. *Annu Rev Cell Dev Biol* 23:549-77.

Smyth AM, Duncan RR, Rickman C (2010) Munc18-1 and syntaxin1: unraveling the interactions between the dynamic duo. *Cell Mol Neurobiol* 30(8):1309-13.

Sotelo C (2004) Cellular and genetic regulation of the development of the cerebellar system. *Prog Neurobiol* 72(5):295-339.

Stoorvogel W, Strous GJ, Geuze HJ, Oorschot V, Schwartz AL (1991) Late endosomes derive from early endosomes by maturation. *Cell* 65(3):417-27.

Sudarov A and Joyner AL (2007) Cerebellum morphogenesis: the foliation pattern is orchestrated by multi-cellular anchoring centers. *Neural Dev* 2:26.

Südhof TC (2013) Neurotransmitter release: the last millisecond in the life of a synaptic vesicle. *Neuron* 80(3):675-90.

Suzuki M, Hara Y, Takagi C, Yamamoto TS, Ueno N (2010) MID1 and MID2 are required for Xenopus neural tube closure through the regulation of microtubule organization. *Development* 137(14):2329–2339.

Tomecki R, Kristiansen MS, Lykke-Andersen S, Chlebowski A, Larsen KM, Szczesny RJ, Drazkowska K, Pastula A, Andersen JS, Stepien PP, Dziembowski A, Jensen TH (2010) The human core exosome interacts with differentially localized processive RNases: hDIS3 and hDIS3L. *EMBO J* 29(14):2342-57.

Trimble WS (1993) Analysis of the structure and expression of the VAMP family of synaptic vesicle proteins. *J Physiol Paris* 87(2):107-15.

Trockenbacher A, Suckow V, Foerster J, Winter J, Krauss S, Ropers HH, Schneider R, Schweiger S (2001) MID1, mutated in Opitz syndrome, encodes an ubiquitin ligase that targets phosphatase 2A for degradation. *Nat Genet* 29(3):287-94.

Ullrich B, Li C, Zhang JZ, McMahon H, Anderson RG, Geppert M, Südhof TC (1994) Functional properties of multiple synaptotagmins in brain. *Neuron* 13(6):1281-91.

Unterbruner K, Matthes F, Schilling J, Nalavade R, Weber S, Winter J, Krauß S (2018) MicroRNAs miR-19, miR-340, miR-374 and miR-542 regulate MID1 protein expression. *PLoS One* 13(1):e0190437.

Wan J, Yourshaw M, Mamsa H, Rudnik-Schöneborn S, Menezes MP, Hong JE, Leong DW, Senderek J, Salman MS, Chitayat D, Seeman P, von Moers A, Graul-Neumann L, Kornberg AJ, Castro-Gago M, Sobrido MJ, Sanefuji M, Shieh PB, Salamon N, Kim RC, Vinters HV, Chen Z, Zerres K, Ryan MM, Nelson SF, Jen JC (2012) Mutations in

the RNA exosome component gene EXOSC3 cause pontocerebellar hypoplasia and spinal motor neuron degeneration. *Nat Genet* 44(6):704-8.

Wang VY, Rose MF, Zoghbi HY (2005) Math1 expression redefines the rhombic lip derivatives and reveals novel lineages within the brainstem and cerebellum. *Neuron* 48(1):31-43.

Wasmuth EV and Lima CD (2012) Exo- and endoribonucleolytic activities of yeast cytoplasmic and nuclear RNA exosomes are dependent on the noncatalytic core and central channel. *Mol Cell* 48(1):133-44.

Wasmuth EV and Lima CD (2017) The Rrp6 C-terminal domain binds RNA and activates the nuclear RNA exosome. *Nucleic Acids Res* 45(2):846-860.

Watkins GR, Wang N, Mazalouskas MD, Gomez RJ, Guthrie CR, Kraemer BC, Schweiger S, Spiller BW, Wadzinski BE (2012) Monoubiquitination promotes calpain cleavage of the protein phosphatase 2A (PP2A) regulatory subunit alpha4, altering PP2A stability and microtubule-associated protein phosphorylation. *J Biol Chem* 287(29):24207-15.

Wei Y, Wang D, Jin F, Bian Z, Li L, Liang H, Li M, Shi L, Pan C, Zhu D, Chen X, Hu G, Liu Y, Zhang CY, Zen K (2017) Pyruvate kinase type M2 promotes tumour cell exosome release via phosphorylating synaptosome-associated protein 23. *Nat Commun* 8:14041.

White JJ and Sillitoe RV (2013) Development of the cerebellum: from gene expression pattern to circuit maps. *WIREs Dev Biol* 2:149–164.

Wieczorek S, Combes F, Lazar C, Giai Gianetto Q, Gatto L, Dorffer A, Hesse AM, Couté Y, Ferro M, Bruley C, Burger T (2017) DAPAR & ProStaR: software to perform statistical analyses in quantitative discovery proteomics. *Bioinformatics* 33(1):135-136.

Wingate RJ and Hatten ME (1999) The role of the rhombic lip in avian cerebellum development. *Development* 126(20):4395-404.

Winkle CC and Gupton SL (2016) Membrane trafficking in neuronal development: Ins and Outs of neural connectivity. *Int Rev Cell Mol Biol* 322:247-80.

Winter J, Lehmann T, Suckow V, Kijas Z, Kulozik A, Kalscheuer V, Hamel B, Devriendt K, Opitz J, Lenzner S, Ropers HH, Schweiger S (2003) Duplication of the MID1 first exon in a patient with Opitz G/BBB syndrome. *Hum Genet* 12(3):249-54.

Winter J, Basilicata MF, Stemmler MP, Krauss S (2016) The MID1 protein is a central player during development and in disease. *Front Biosci* 21:664-82.

Xu J, Liu Z, Ornitz DM (2000) Temporal and spatial gradients of Fgf8 and Fgf17 regulate proliferation and differentiation of midline cerebellar structures. *Development* 127(9):1833–1843.

Yamamori S, Itakura M, Sugaya D, Katsumata O, Sakagami H, Takahashi M (2011) Differential expression of SNAP-25 family proteins in the mouse brain. *J Comp Neurol* 519(5):916-32.

Yap K, Lim ZQ, Khandelia P, Friedman B, Makeyev EV (2012) Coordinated regulation of neuronal mRNA steady-state levels through developmentally controlled intron retention. *Genes Dev* 26(11):1209-23.

Zanchetta ME and Meroni G (2019) Emerging roles of the TRIM E3 ubiquitin ligases MID1 and MID2 in cytokinesis. *Front Physiol* 10:274.

Zervas M, Millet S, Ahn S, Joyner AL (2004) Cell behaviors and genetic lineages of the mesencephalon and rhombomere 1. *Neuron* 43(3):345-57.

Zhang YW, Thompson R, Zhang H, Xu H (2011) APP processing in Alzheimer's disease. *Mol Brain* 4:3.

Zinder JC, Wasmuth EV, Lima CD (2016) Nuclear RNA exosome at 3.1 Å reveals substrate specificities, RNA paths, and allosteric inhibition of Rrp44/Dis3. *Mol Cell*

64(4):734-745.

Zinder JC and Lima CD (2017) Targeting RNA for processing or destruction by the eukaryotic RNA exosome and its cofactors. *Genes Dev* 31(2):88-100.

Zuo Y and Deutscher MP (2001) Exoribonuclease superfamilies: structural analysis and phylogenetic distribution. *Nucleic Acids Res* 29(5):1017-26.